Universidad de Navarra

Facultad de Ciencias

New insights into pathogenesis of acute porphyria attacks and proof-of-concept of augmenting hepatic PBGD as etiological treatment

DANIEL JERICÓ ASENJO

Tesis Doctoral 2022

Universidad de Navarra

Facultad de Ciencias

New insights into pathogenesis of acute porphyria attacks and proof-of-concept of augmenting hepatic PBGD as etiological treatment

Memoria presentada por D. Daniel Jericó Asenjo para aspirar al Grado de Doctor por la Universidad de Navarra en el Programa de Doctorado de Medicina Aplicada y Biomedicina.

El presente trabajo ha sido realizado bajo la Dirección del Dr. Antonio Fontanellas Romá en el Departamento de Hepatología del CIMA-Universidad de Navarra y autoriza su presentación ante el tribunal que lo ha de juzgar.

Pamplona, 22 de abril de 2022

Dr. Antonio Fontanellas Romá

Esta tesis doctoral se ha llevado a cabo gracias a la concesión de la ayuda predoctoral de la Fundación Mutua Madrileña de Investigación Médica y la ayuda de la Fundación FEDER (Federación Española de Enfermedades Raras) para realizar la estancia en “L’École nationale supérieure de technologie des biomolécules de Bordeaux” en Francia.

A mis abuelas y abuelos

Mª Jesús, Ramón, Carmen y Gerardo

AGRADECIMIENTOS

Esta tesis recopila los resultados que hemos tenido durante mis años de trabajo en el laboratorio de porfiria del CIMA, pero este apartado me da la oportunidad de acordarme de todas las personas que han formado parte de ella. A todos vosotros quiero daros las gracias.

Antonio, gracias por haberme dado la oportunidad de entrar a trabajar en nuestro grupo, por tu dedicación y por seguir apostando por mí. Ana, gracias porque me has enseñado todo lo que sé hacer en un laboratorio, por haberme acogido tan bien desde el primer momento y por las mil y una anécdotas que surgen del día a día. Karol, gracias por ser una gran compañera y por los innumerables paseos hasta el animalario de CIFA que siempre han ido acompañados de grandes conversaciones y risas. Tengo suerte de pertenecer a “Cobra PAI”.

A Matías por estar siempre dispuesto a ayudar con cualquier duda. A todo el departamento de Hepatología: Eva, Sara, Roberto, Maite, Alex, JoseMari, Uxue, Iker… siempre habéis estado disponibles y me habéis facilitado el trabajo. En especial a Laura, porque a tu ayuda le tengo que añadir todo lo que nos hemos reído con chistes malos durante los cafés y comidas.

También quiero agradecer al personal del animalario, a Marga y María del PET, Manuel Alegre, María por su ayuda en las resonancias, Kepa por el proyecto de la proteína y a Lanciego y todo su equipo de neuro que nos han ayudado mucho en este proyecto y con los que hemos pasado largos ratos que se hacían más entretenidos.

I would like to thank Paolo and Lei for the production and supply of the mRNAs, it has been a pleasure to work with such a new and fashionable technique.

Merci à Gilles et Charlotte pour l'expérience professionnelle et l'opportunité de vivre dans une ville comme Bordeaux, même si ce n'est que pour quelques mois et avec des restrictions par la pandémie. Merci aussi àl 'équipe porphyrie de france qui nous a aidé dans le projet avec les lapins.

A mis compañeros del Máster, especialmente Belén y Guille, por acompañarme durante este camino y preocuparos por cómo iba avanzando el proyecto. También quiero agradecer a Jose Ignacio Riezu porque me ha hecho disfrutar la experiencia docente que hemos compartido los 3 años durante las prácticas de la universidad.

A Oscar, Pablo e Iñigo con los que me adentré en ciencias en el Grado de Bioquímica. También quiero daros las gracias a vosotros por los buenos momentos que pasamos entonces y seguimos pasando alrededor de una mesa. No puedo pasar por alto que me enseñasteis que un pHmetro con la tapa puesta no funciona.

A Víctor, Garci, Baste y Goñi, por haberos interesado por este trabajo, por vuestro apoyo y sobre todo por vuestro inagotable sentido del humor. Sois unos grandes amigos.

Gracias a mi familia por cuidarme. A mis abuelas y abuelos por vuestro interés y cariño. Aita y ama gracias por haberme ensañado todo lo demás, por vuestro ejemplo de esfuerzo. Arantxa, gracias por tu autenticidad y tu forma de ver las cosas.

Y por último gracias a ti, Sayoa. Por haberme escuchado y animado en todo momento. Por tu alegría. Por todos los momentos que hemos compartido y seguiremos sumando a nuestra colección.

¡Gracias a todos!

ABBREVIATIONS

LIST OF ABBREVIATIONS

AAV	Adeno-associated virus
ADP	ALAD deficiency porphyria
AIA	2-allyl-2-isopropylacetamide
AIP	Acute intermittent porphyria
ALA	δ-aminolevulinic acid
ALAD	δ- aminolevulinic acid dehydratase
ALAS	δ-aminolevulinic acid synthase
ALP	Alkaline phosphatase
ALT	Alanine aminotransferase
ApoAI	Apolipoprotein AI
bp	Base pairs
BV	Brain ventricle
CBF	Cerebral blood flow
cDNA	Complementary deoxyribonucleic acid
CEP	Congenital erythropoietic porphyria
CHAPS	3-((3-cholamidopropyl)dimethylammonio)-1-propanesulfona
cm	Centimeter
CNS	Central nervous system
CPO	Coproporphyrinogen oxidase
creat.	Creatinine
CT	Computed tomography
CYP450	Cytochrome P450
ρ	Density
dL	Deciliter
DNA	Deoxyribonucleic acid
DTT	Dithiothreitol

E. coli	*Escherichia coli*
EDN1	Endothelin-1
EDNRB	Endothelin receptor type B
ELISA	Enzyme-linked immunosorbent assay
EPP	Erythropoietic protoporphyria
ERT	Enzyme replacement therapies
ET	Echo time
FC	Ferrochelatase
^{18}F-FDG	18F-fluorodeoxyglucose
FOV	Field of view
FOXO1	Forkhead box (transcription factor family)
g	Gram
GABA	γ-aminobutyric acid
GMP	Good manufacturing practices
GT	Gene therapy
GTT	Glucose tolerance test
h	Hour
HCP	Hereditary coproporphyria
HDL	High-density lipoprotein
HEA	Hexylamine resin
HEP	Hepatoerythropoietic porphyria
HO	Heme oxygenase
hPBGD	Human porphobilinogen deaminase
HPLC	High performance liquid chromatography
i.p.	Intraperitoneal
iRNA	Interfering ribonucleic acid
IRT	Inversion recovery time
i.v.	Intravenous

kDa	Kilo Daltons
kg	Kilogram
L	Liter
LNPs	Lipid nanoparticles
MBq	Megabecquerel
MEP	4-mercapto-ethyl-pyridine resin
µg	Microgram
mg	Milligram
MGS	Mouse grimace scale
µl	Microliter
ml	Mililiter
µm	Micrometer
µM	Micromolar
mm	Milimeter
mM	Milimolar
MRI	Magnetic resonance imaging
mRNA	Messenger ribonucleic acid
ms	Millisecond
MT-CO1	Mitochondrial cytochrome c oxidase 1
NaBr	Sodium bromide
NHP	Non-human primates
nm	Nanometer
nmol	Nanomole
OLT	Orthotopic liver transplantation
Pb	Phenobarbital
PBG	Porphobilinogen
PBGD	Porphobilinogen deaminase
PBS	Phosphate buffer saline

PCR	Polymerase chain reaction
PCT	Porphyria cutanea tarda
PEG	Polyethylene glycol
PEPT2	Peptide transporter 2
PET	Positron emission tomography
PGC1α	PPAR-gamma coactivator-1 alpha
PPA	Phenylpropylamine resin
PPARα	Peroxisome proliferator-activated receptor-alpha
PPO	Protoporphyrinogen oxidase
PRES	Posterior reversible encephalopathy syndrome
qPCR	Quantitative polymerase chain reaction
rAAV	Recombinant adeno-associated virus
rhApoAI-PBGD	Recombinant human ApoAI linked to N-terminus of PBGD
rhPBGD	Recombinant human porphobilinogen deaminase
Rif	Rifampicin
RNA	Ribonucleic acid
RNases	Ribonucleases
RT	Repetition time
s.c.	Subcutaneous
SD	Standard deviation
SEC-MALS	Size Exclusion Chromatography with Multi-Angle Light Scattering
TCA	Tricarboxylic acid
UROD	Uroporphyrinogen III decarboxylase
UROS	Uroporphyrinogen III synthase
UTR	Untranslated region
VP	Variegate porphyria
λ	Wavelength
WB	Western-Blot

WT	Wild-type
XLP	X-linked protoporphyria

TABLE OF CONTENTS

TABLE OF CONTENTS

PREFACE

Management of rare diseases is a challenge since some of them are poorly described and, therefore, drug development is difficult to address. According to the World Health Organisation, there are about 7,000 different rare diseases affecting 6-8 % of the world's population. Despite scientific advances, less than 10 % of these patients receive treatment. Although regulatory agencies try to encourage pharmaceutical companies to investigate and develop therapeutic drugs, most of the basic research is done in universities and hospital-associated centers. The knowledge generated is of great value for a better description of the natural history of rare diseases and the design of more efficient therapies.

Acute Intermittent Porphyria (AIP) is a rare genetic disease of hepatic origin characterized by acute neurovisceral attacks. Currently, available treatments for AIP are not optimal and do not cover the entire spectrum of symptoms and presentations of the disease; thus, research for the development of more efficient drugs is essential. Patients with AIP have a deficiency of the hepatic porphobilinogen deaminase (PBGD) protein. So, our line of research, unlike approved treatments, is based on increasing protein PBGD levels in the liver as an etiological solution to the disease.

AIP affects central, autonomic and peripheral nervous system. However, many aspects of the onset and course of this disease are still unknown. Recent research led by our group, reported some alterations in the central nervous system (CNS) such as decreased cerebral blood flow (CBF) during porphyria crises and brain ventricle (BV) enlargement in patients suffering recurrent porphyria attacks. Hence, **the first aim** of this thesis was to analyze these pathological features in a well-characterized mouse model of the disease and the effect of increasing hepatic PBGD activity on these CNS implications.

In recent years, messenger RNA (mRNA) based treatments have revolutionized the approach to this type of diseases, thus the administration of human PBGD (hPBGD)

mRNA could be a promising therapeutic approach. mRNA therapy is based on modified RNA sequences that enhance their stability and translatability into therapeutic proteins, and their delivery into lipid nanoparticles (LNPs) that prevent mRNA degradation and target the liver. It is worth noting that the administration of hPBGD mRNA allows expression of the therapeutic protein as rapid as hours, a crucial feature to stop the acute attack as soon as the first symptoms appear. In addition, the LNPs can be readministered, allowing single or repeated administrations depending on the clinical status of the patient [1].

Prior to this thesis, we performed a proof-of-concept study in the AIP mouse model to demonstrate the safety and therapeutic impact of systemic hPBGD mRNA as a potential therapy for this disease [2]. In rare diseases such as AIP, recruiting patients to perform clinical trials is difficult. For this reason, additional preclinical efficacy and safety studies are required, preferably in large animal models. Thus, the therapeutic effect of hPBGD mRNA was assayed in non-human primates (NHP) and a new model of acute attack in rabbits. I actively participated in these studies and, as an extension of them, **the second aim** of this thesis was the complete biochemical and clinical characterization of the new rabbit model, as well as the efficacy results of the mRNA-based therapy.

Therapeutic protein delivery to the liver may be an alternative treatment. Our group generated a recombinant protein formed by linking Apolipoprotein AI (ApoAI) to the N-terminus of human PBGD (rhApoAI-PBGD) in order to transfer PBGD protein into liver cells. Intravenous (i.v.) or subcutaneous (s.c.) administration of rhApoAI-PBGD showed sustained efficacy in delivery PBGD to hepatocytes resulting in enhanced hepatic enzymatic activity and protection against AIP attacks in the mouse model [3]. However, large-scale production under good manufacturing practices (GMP) conditions is challenging for enzyme replacement therapies. During my final degree project, I participated in the development of an HEK293 cell line that produces rhApoAI-PBGD.

Following this line of investigation, **the third aim** of this thesis was to develop a large-scale production and purification process of rhApoAI-PBGD protein in CHO-K1SP cells, a cell line used for the production of recombinant proteins, in order to facilitate GMP procedures, reduce the cost of large-scale production process, and assay the therapeutic effect of the recombinant protein in large animals.

INTRODUCTION

1. Heme Biosynthesis Pathway

Heme is an essential component of hemoproteins involved in multiple biological processes: oxidation-reduction reactions (peroxidases and catalases), detoxification mechanisms (cytochrome P450, CYP450), transport and storage of oxygen (hemoglobin and myoglobin), and energy demands of cells through cytochromes of the mitochondrial respiratory chain. Heme is a porphyric ring composed of ferrous iron (Fe^{2+}) and protoporphyrin IX. Although, it is produced in all nucleated cells, the bone marrow and the liver are the main organs for heme synthesis producing 80 % and 15 % of total heme, respectively [4]. To underline the importance of the heme synthesis pathway and production, red blood cells and hepatocytes synthesize 2.8 x 10^9 and 5 x 10^8 molecules of heme per second, respectively [5].

The heme biosynthesis pathway is constituted by eight different enzymes. The first and limiting step is the decarboxylative condensation of non-essential amino acid glycine with succinyl-CoA coming from tricarboxylic acid (TCA) cycle (also known as Krebs cycle), which is catalyzed by the δ-aminolevulinic acid synthase (ALAS, EC 2.3.1.37) (Fig. 1) [6,7].

To maintain an appropriate intracellular heme level is crucial since its excess is toxic and its deficiency is detrimental for cell metabolism. ALAS tightly regulates heme biosynthesis pathway. It requires of cofactor pyridoxal 5'-phosphate, the active form of vitamin B6 to perform is function [8]. There are two isoforms of this rate limiting enzyme: ALAS1, that executes its function in the liver and non-erythroid tissues; and ALAS2, that acts in erythroid tissue [9]. The *ALAS2* gene is regulated by erythroid-specific transcription factors and iron availability during the exponential production of hemoglobin in the erythroblast. In the liver, where hemoproteins are rapidly turned over in response to metabolic needs, *ALAS1* can be highly upregulated by the administration of certain drugs such as barbiturates, sulphonamides or rifampicin (Rif)

among others. These drugs are metabolized by the CYP450 that enhances transcription of both *CYP450* and *ALAS1* genes through binding of nuclear receptors to a cis-acting regulatory drug-responsive element sequence located upstream of the promoter of such genes [10]. Likewise, *ALAS1* can be down-regulated by negative feedback of heme in cases of high availability of regulatory free heme [11,12]. Fasting also induces direct transcriptional upregulation of *ALAS1* via the nuclear receptor peroxisome proliferator-activated receptor-alpha (PPARα) and the PPAR-gamma coactivator-1 alpha (PGC1α) [13,14]. Heme also decreases the stability of *ALAS1* mRNA [15], inhibits uptake of pre-ALAS1 into the mitochondria [16], and produces the breakdown of ALAS1 protein via heme-mediated induction of the protease Lon peptidase 1 [17].

Intermediate metabolites in the heme synthesis pathway include porphyrin precursors, which are δ-aminolevulinic acid (ALA) and porphobilinogen (PBG), and a linear tetrapyrrole (hydroxymethylbilane) that is promptly converted to cyclic tetrapyrroles known as porphyrinogens, the reduced form of porphyrins (Fig. 1) [18].

Under physiological conditions, there is small excretion of porphyrin precursors and porphyrins, as the heme pathway is tightly regulated and most of them are used to synthesize heme. ALA, PBG and highly carboxylated porphyrins are water-soluble being predominantly excreted in urine. This is the case of the octocarboxylated uroporphyrin III, hepta-, hexa- and pentacarboxylated porphyrins that appear in the stepwise decarboxylation of uroporphyrinogen to coproporphyrinogen. Whereas low carboxylated porphyrins, as dicarboxylated protoporphyrin IX, are only excreted via the hepatobiliary route. Tetracarboxylated coproporphyrin has an intermediate number of carboxylic acid side chains and can be excreted both in the bile or urine. Hydroxymethylbilane can also spontaneously (nonenzymatic) form the isomer uroporphyrinogen I that leads to coproporphyrinogen I formation and is as well

excreted via the hepatobiliary route or urine [18]. Only isomer III is involved in the final synthesis of the heme molecule.

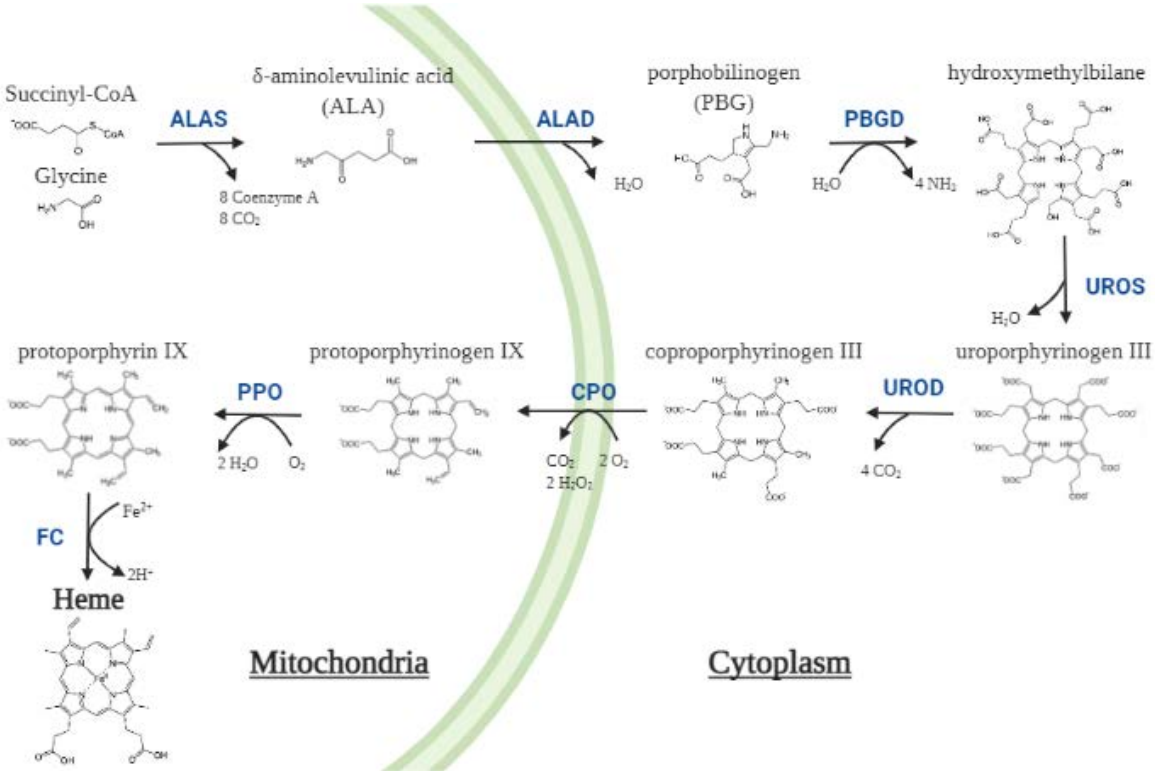

Figure 1. Heme biosynthesis pathway in mammalian cells. The pathway consists of eight enzymes, four of them located in the cytoplasm and the other four in the mitochondria. Eight ALA molecules are required to synthesize four PBG molecules that, subsequently, are used for the synthesis of a single hydroxymethylbilane molecule and finally to a heme prosthetic group. Adapted from Franken et al [19].

Heme catabolism is regulated by heme oxygenase (HO, EC 1.14.14.18). HO produces carbon monoxide and biliverdin, which is subsequently reduced to bilirubin by cytosolic biliverdin reductase. Carbon monoxide is a strong vasodilatory, anti-inflammatory and immunomodulatory agent and both biliverdin and bilirubin are efficient scavengers of reactive oxygen species and reduce the formation of peroxidation products [20]. Among three different HO isoforms, HO-1 is expressed in liver, spleen, brain and testicles, and is considered to be of keen research interest as its expression level is induced during various physiological and pathological conditions [21].

2. Porphyrias

Porphyrias are a heterogeneous group of metabolic diseases caused by altered activity in any of the eight enzymes of the heme synthesis pathway (Table 1) [20]. They are characterized by loss-of-function mutations in any of the last seven enzymes, except X-linked Protoporphyria, which is associated with gain-of-function mutations in *ALAS2*. On the contrary, ALAS2 deficient activity is associated with X-linked sideroblastic anemia (OMIM 300751) [22,23]. No pathogenic mutations in the *ALAS1* gene have been described.

Table 1. Type of porphyria associated with the alteration of specific enzyme in the heme synthesis pathway. Hepatoerythropoietic porphyria refers to homozygous form of PCT, which shows childhood onset. GoF, gain-of-function mutation. LoF, loss-of-function mutation.

Enzyme	Mutation	Disease	OMIM
δ-Aminolevulinic acid synthase 2 (ALAS2, EC 2.3.1.37)	GoF	X-linked Protoporphyria (XLP)	300752
δ-Aminolevulinic acid dehydratase (ALAD, EC 4.2.1.24)	LoF	ALAD Deficiency Porphyria (ADP)	612740
Porphobilinogen deaminase (PBGD, EC 2.5.1.61)	LoF	Acute Intermittent Porphyria (AIP)	176000
Uroporphyrinogen III synthase (UROS, EC 4.2.1.75)	LoF	Congenital Erythropoietic Porphyria (CEP)	263700
Uroporphyrinogen III decarboxylase (UROD, EC 4.1.1.37)	LoF	Porphyria Cutanea Tarda (PCT) Hepatoerythropoietic porphyria (HEP)	176100
Coproporphyrinogen oxidase (CPO, EC 1.3.3.3)	LoF	Hereditary Coproporphyria (HCP)	121300
Protoporphyrinogen oxidase (PPO, EC 1.3.3.4)	LoF	Variegate Porphyria (VP)	176200
Ferrochelatase (FC, EC 4.99.1.1)	LoF	Erythropoietic Protoporphyria (EPP)	177000

Depending on which step of the heme synthesis pathway the enzyme failure occurs, ALA and PBG, porphyrins or both would be accumulated. Porphyrias can be classified according to the tissue in which high production of porphyrins and/or porphyrin precursors happens. Erythropoietic ones include XLP, CEP and EPP; whereas ADP, AIP, PCT, HCP and VP are classified as hepatic porphyrias. HEP involves increased porphyrin production in both erythropoietic and liver tissues.

Clinically, porphyrias can be classified into photocutaneous porphyrias or acute hepatic porphyrias [6,7]:

- Cutaneous porphyrias (PCT, CEP, EPP and XLP) show photosensitivity and skin lesions after light exposure (wavelength (λ) around 400 nm) in body regions where porphyrins are accumulated [24].

- Acute hepatic porphyrias are characterized by neurovisceral attacks, which are associated with porphyrin precursors accumulation [25]. While only ALA is increased in ADP, both ALA and PBG accumulation are observed in AIP, VP and HCP. VP and HCP may also present photosensitivity due to porphyrin accumulation, and for that reason both used to be classified as mixed porphyrias [26]. A deep description of the acute neurovisceral attacks is detailed in the following section.

2.1. Acute Neurovisceral Attacks

Symptoms of acute neurovisceral attacks are very heterogeneous and include autonomous (severe abdominal pain, hypertension, tachycardia, nausea, vomiting, diarrhea/constipation), central (anxiety, depression, insomnia, hallucinations, among others) and peripheral (muscle weakness and pain, fatigue, paraplegia) nervous system affectations among others. Severe neurological complications may cause death due to respiratory and bulbar paralysis [25–27].

Two major hypothesis have been proposed for the physiological origin of the acute attacks: heme deficiency leads to decreased hemoprotein function [28] and energy production in the mitochondria; and a second hypothesis suggests a potential neurotoxicity of ALA and/or PBG. This last hypothesis is the most accepted as the onset of acute attacks has always been associated with porphyrin precursors accumulation. Specifically, symptomatology has been attributed to ALA because I) patients with other diseases such as ADP, hereditary tyrosinemia type I (OMIM 276700) or lead poisoning only accumulate ALA and show neurological pathology similar to acute attacks; II) *in vitro* assays confirm the association of ALA with oxidative stress; and III) ALA selectively competes for the binding of γ-aminobutyric acid (GABA) associated with synaptic GABA receptors in CNS membranes [29]. In addition, some authors suggest that polymorphisms in the peptide transporter 2 (*PEPT2*), in particular *PEPT2*1*1*, highly increases serum ALA affinity that could be related to the passage of toxic ALA to the brain through the choroid plexus and to an increased susceptibility to suffer neuropsychiatric symptoms [30]. Renal damage is also associated with chronic accumulation of this porphyrin precursor [31]. In the proximal tubular cells of the kidney, PEPT2 promotes ALA reabsorption, and patients with PEPT2*1*1 variant showed worse renal function than those with the low affinity PEPT2*2*2 variant [32]. Chronic accumulation of ALA and PBG is also related with high incidence in the development of hepatocellular carcinoma [33]. Besides, orthotopic liver transplantation (OLT) has proven to cure severely affected patients with acute hepatic porphyrias [34,35], and transplantation of a porphyric liver into a non-porphyric receptor developed acute attacks [36] thus, supporting the liver as the major etiologic site of pathology. Despite all this, the relationship between porphyrin precursors levels and the prodrome symptoms is still unclear.

Porphyria acute attacks can be triggered by endogenous or exogenous factors such as medications/chemicals, excess alcohol intake, smoke, steroid hormones (estrogens

and progesterone), stress, infection, acute illness, physical exhaustion, caloric deprivation or rapid weight loss [6,7]. Symptoms are more common in women due to the role of reproductive hormones. In fact, acute attacks commonly happen in women of fertile age and are unusual after menopause [37]. All these triggering factors have in common the induction of hepatic *ALAS1* mRNA expression either directly via PGC1α (e.g. fasting) [13]; or by positive feedback caused by excessive heme consumption to form hemoproteins (e.g. CYP450) or by increasing its degradation through HO-1 [11,12].

Patients can be classified according to whether they suffer from sporadic acute attacks (1-3 per year) or recurrent acute attacks (> 3 per year). About 5 % of patients with acute porphyrias suffer recurrent attacks, which has a major impact on their quality of life [38,39]. These patients usually require hospitalization and strong analgesic treatment. Chronic opiates therapy is often needed to control pain [40]. AIP and VP are the most prevalent acute hepatic porphyrias and in them, symptoms are associated with intermittent neurovisceral attacks

3. Variegate Porphyria (VP)

VP is an autosomal dominant metabolic disease caused by the hepatic deficiency of mitochondrial PPO, the seventh enzyme of the heme biosynthesis pathway. It catalyzes the oxidation of protoporphyrinogen IX to protoporphyrin IX. Human *PPO* gene is located on the long arm of chromosome 1, in locus 23.3 (1q23.3). It compromises 13 exons and encodes a 477 amino acid protein with a molecular mass of 51 kDa. More than 140 different *PPO* pathogenic variants have been identified causing VP (Source: Human Gene Mutation Database at the Institute of Medical Genetics in Cardiff). VP prevalence in Europe is 7 per 1,000,000 inhabitants while in

the South African white population is 1.2-3 per 1,000 people [18]. This high prevalence is due to the founder mutation R59W (the change from arginine to tryptophan in codon 59) in Afrikaner population, a South African ethnic group descended from predominantly Dutch settlers [41].

Approximately 50 % of normal enzyme activity is observed in patients with VP, which comes mainly from the normal allele. In patients with biallelic mutations, at least one of the mutant alleles must produce residual PPO enzyme activity. These are rare cases in which clinical onset manifestations begin in childhood [42].

Patients with VP are biochemically characterized by elevated protoporphyrin in stool, and high ALA, PBG and porphyrins urinary accumulation during the acute attack. Besides, plasma fluorescence scanning is useful in the diagnosis of porphyria; patients with VP have a distinct fluorescence emission peak around 626 nm corresponding to a mixture of porphyrins rather than a specific porphyrin [18]. For correct diagnosis, the identification of deleterious mutations in the *PPO* gene must be genetically confirmed [42].

Patients with VP suffer cutaneous blistering lesions, milia, scarring, and areas of decreased and increased pigmentation. The protoporphyrinogen IX that is accumulated undergoes chemical oxidation and is related to the phototoxic lesions affecting sunlight-exposed areas of the skin. Avoiding sunlight exposure is the only solution for the cutaneous pathology as no treatment is yet available [43].

Neurovisceral acute attacks, associated with high porphyrin precursors accumulation, are also included among the symptoms. Although, it has been suggested that protoporphyrinogen produced allosteric inhibition of PBGD, leading to ALA and PBG accumulation in VP [44], the origin of these precursors accumulation in VP has not been clarified. The management of acute attacks in patients with VP is the same as that applied for AIP (will be discussed below).

4. Acute Intermittent Porphyria (AIP)

AIP is an autosomal dominant disease caused by hepatic deficiency of PBGD, the third enzyme of the heme biosynthesis pathway, also known as hydroxymethylbilane synthase. Human *PBGD* gene is located on the long arm of chromosome 11 in locus 23.3 (11q23.3). It compromises 15 exons and encodes a 361 amino acid protein with a molecular mass of 42 kDa. There have been described over 400 different mutations of this gene, most of them are missense/nonsense mutations (Source: Human Gene Mutation Database at the Institute of Medical Genetics in Cardiff).

Most patients suffer AIP due to the inheritance of one copy of a mutated allele resulting in an enzyme activity deficiency of approximately 50 %. Prevalence of pathogenic mutations in *PBGD* gene is 1 per 1,700 inhabitants, but clinical penetrance is very low (≤ 1 %, 6 per million inhabitants) [45]. Remarkably, prevalence is higher in Sweden and two valleys of the Spanish region of Murcia due to founder effect.

PBGD catalyzes the condensation of 4 monopyrrole PBG molecules into a single linear tetrapyrrole hydroxymethylbilane molecule in the cytosol of hepatocytes. The active enzyme uses a dipyrromethane as cofactor that is covalently bind by a thioether bond to an invariant cysteine residue (Cys261) of the PBGD catalytic site [46]. The dipyrromethane is produced by the formation of an hexapyrrole that is subsequently cleavage by hydrolysis of the thioether bond into hydroxymethylbilane (linear tetrapyrrole, Fig. 1) and the dipyrromethane [47]. The PBGD works optimally at a pH of 8.2 (being inactive with pH < 6) and is very thermostable (being inactive with temperature < 20 ºC) [48].

In situations in which *ALAS1* is induced, PBGD deficiency results in a partial blockage of the heme synthesis pathway leading to high levels of ALA and PBG in plasma and urine. This can trigger acute neurovisceral attacks in patients with AIP. Thus, in

addition to clinical manifestations it is important to measure the urine ALA and PBG levels for the diagnosis of AIP. The presence of PBG in urine can be rapidly determined by the Hoesch test. The plasma fluorescence emission peak of AIP is 620 nm, the same as HCP and therefore does not allow discriminatory diagnosis as in the case of VP. To identify genetic mutations in the *PBGD* gene is required to confirm the diagnosis.

4.1. Current Treatments

Current approved treatments for AIP and the new innovative therapies that are being evaluated are presented in Figure 2. The first-line therapeutic approach for acute attacks relies on carbohydrate loading and hemin infusions (Panhematin® in the United States, Normosang® in the European Union, Recordati, Milan, Italy) to down-regulate hepatic *ALAS1* transcription and thus, reduce heme precursors production and excretion.

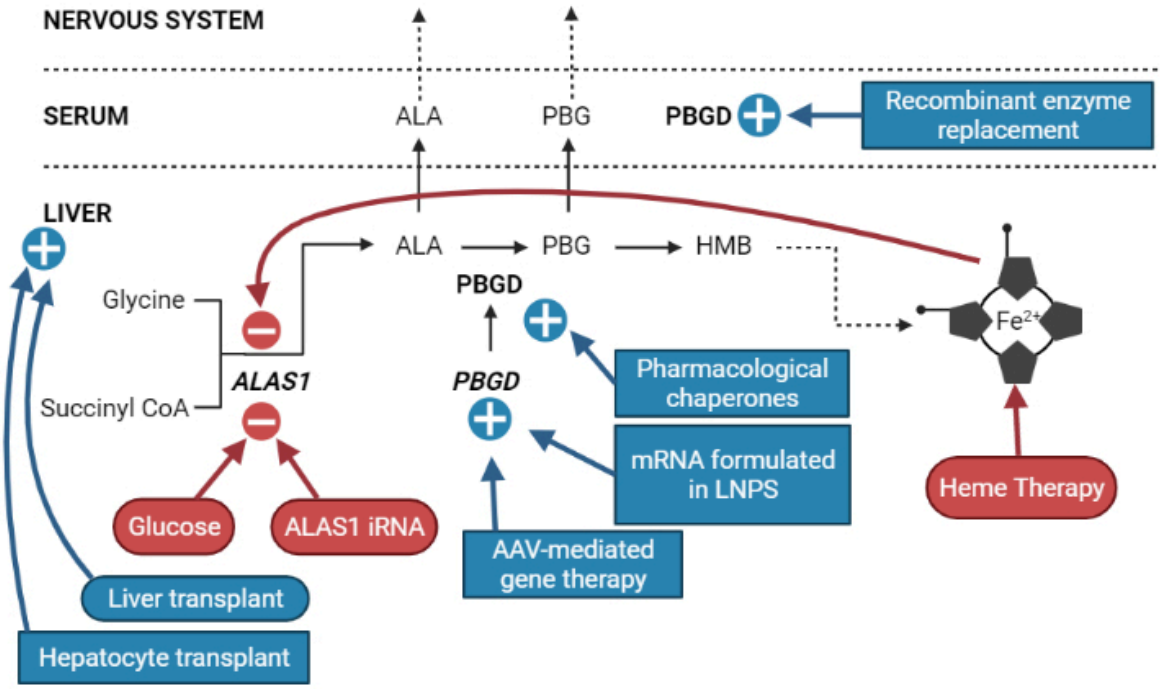

Figure 2. Sites of action of current and innovative therapeutic options for AIP. Current approved therapies are represented in round outlines; Innovative therapies are represented in square outlines. Red colour is for therapies that inhibit *ALAS1*; blue colour is for therapies that increase PBGD activity.

4.1.1. Carbohydrate loading

This treatment is recommended for patients that present sporadic acute attacks with mild pain and no paresis.

Fasting situations induces *ALAS1* transcription [13,49,50] by means of the PGC1α and Forkhead box transcription factor (FOXO1) binding together with the insulin responsive element site or with the nuclear respiratory factor-1 site on the *ALAS1* gene promoter. Carbohydrate loading therapy is based on oral or i.v. glucose infusions (300-500 g/day), which produces subsequent insulin increase that promotes FOXO1 phosphorylation through PI3-K/Akt system. Thus, the FOXO1/PGC1α is disrupted and *ALAS1* transcription repressed (Fig. 3) [13,49,50]. Nevertheless, recent studies have

not shown a clear preventive effect [51,52] and frequent glucose infusions may raise the risk of hyponatremia [53].

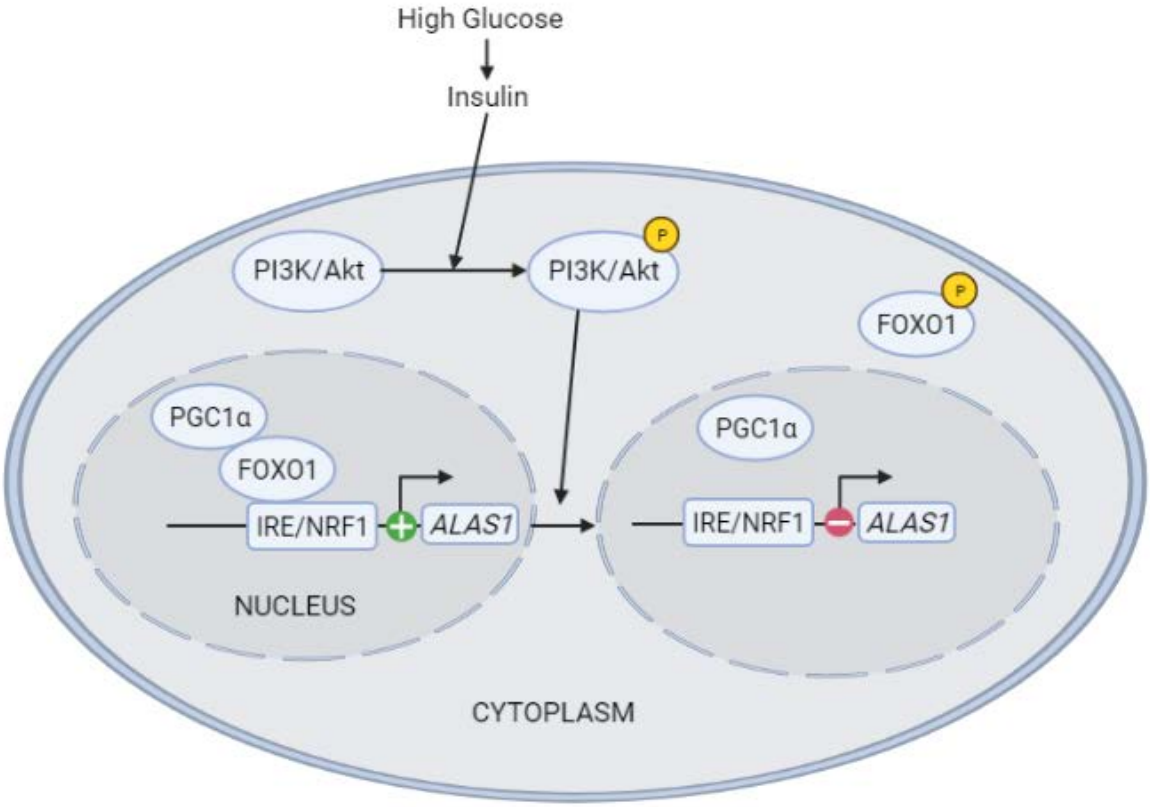

Figure 3. *ALAS1* regulation by glucose therapy. IRE, Insulin Responsive Element. NRF1, Nuclear Respiratory Factor 1. PI3K/Akt, Phosphoinositide 3-kinases/Protein kinase B. P, represents phosphorylation. +, represents induced *ALAS1* transcription. -, represents repressed *ALAS1* transcription.

4.1.2. Hemin

Hemin replacement therapy consists in the restoration of the hepatic heme pool, therefore suppressing *ALAS1* by inhibitory feedback. It is more effective than glucose therapy but it is also more expensive and can only be i.v. given. Another problem associated with hemin administration is the high instability of the molecule in solution.

Standard dose of hemin therapy in clinical practice is 3-4 mg/kg of hemin per day for 3-4 days of i.v. administration until ALA and PBG levels are normalized and symptoms

are relieved [54]. This treatment is recommended for patients whose disease presents in form of sporadic severe attacks (85 % of total sporadic cases), and suffer from abdominal pain, fatigue, muscle pain and peripheral neuropathy. The efficacy of hemin therapy depends on the early initiation of its i.v. administration [55].

Prophylactic application of hemin is an off-label use of hemin offered by many health facilities for patients suffering recurrent attacks, although this treatment does not reverse an established neuropathy [56]. In patients that have four or more acute attacks per year and that show high ALA and PBG levels in urine during non-acute phases, hemin has been used to prevent acute attacks. Despite there are no reports showing efficacy as a preventive treatment, its prophylactic application appears to be beneficial in patients as concluded in an audit reported by The National Acute Porphyria Service in England [54]. However, repeated hemin administrations typically cause side effects such as thrombophlebitis at the peripheral vein infusion site, requiring the administration through a central vein. Recurrent hemin doses can also increase serum ferritin levels, suggesting hepatic iron overload [57]. In addition, it can also produce loss of effectiveness due to maintained *HO-1* induction that reduces regulatory heme pool levels and consequently upregulates heme synthesis, thus, increasing the risk of acute attacks recurrence [11,58]. Finally, hemin therapy is usually not recommended for renal compromised patients since administration of large amounts of hemin has been associated with transitory renal failure [59].

4.1.3. ALAS1-directed short interfering RNA

Recently, givosiran (Givlaari™, Alnylam Pharmaceuticals, Cambridge, MA, USA) has been approved by the FDA (https://www.fda.gov/drugs/resources-information-approved-drugs/fda-approves-givosiran-acute-hepatic-porphyria) and the EMA (https://www.ema.europa.eu/en/medicines/human/EPAR/givlaari) for the prevention of recurrent acute attacks in patients with acute hepatic porphyrias [60]. Givosiran is a

small interfering RNA against ALAS1 mRNA (ALAS1 iRNA) which prevents *ALAS1* activation. It showed promising results in a Phase 3 clinical trial (NCT03338816) reducing up to 74 % of acute attacks and reducing porphyrin precursors accumulation. Besides, it reduces the use of analgesics and hemin in patients, avoiding the potential side effects of recurrent hemin administration [61]. One of the main advantages of this therapeutic drug is that it can be s.c. administered, opening up the possibility for an easy and fast administration.

Nevertheless, more adverse events were observed in the treated group than in the placebo group during the Phase 3 clinical trial, such as nausea, fatigue, elevation of serum alanine aminotransferases levels (ALT), or increased serum creatinine (creat.) and decreased estimated glomerular filtration rate that suggest kidney function issues [61]. Few patients showed severe adverse effects such as pulmonary embolism and one died from acute pancreatitis. Recently, another adverse event associated with ALAS1 iRNA was reported revealing crosstalk with the one-carbon metabolism. Although hypermethioninemia and hyperhomocysteinemia (HHcy) had been previously reported in patients with AIP receiving hemin therapy, givosiran induced an aggravation of this dysregulation [62,63], which is associated with increased cardiovascular risk [64]. The high prevalence of adverse events emphasizes the importance of restricting the treatment to severe AIP, decreasing the frequency of dosing and administering the minimum effective dose for each patient without compromising treatment efficacy [65].

4.1.4. Liver transplantation

OLT or combined kidney/liver transplantation is the last therapeutic option for patients with severe and recurrent life-threatening attacks [34,66]. However, OLT procedure presents limitations such as life-long immunosuppression regimen, limited availability of donors, and high rate of hepatic artery thrombosis and mortality/morbidity associated

with the procedure [67]. Moreover, transplantation does not improve previous neurological damages, which are irreversible.

4.2. Innovative Therapies

Key opinion leaders and experts in this field suggest the need for innovative therapies with less adverse effects than can be applied to all groups of patients with acute porphyria regardless of their kidney function or frequency of acute attacks. For that purpose, different strategies have been developed (Fig. 2).

4.2.1. Cell Therapy

One of these approaches is the wild-type (WT) hepatocytes transplantation into a *PBGD* deficient liver. Experimental studies showed that hepatocytes transplantation reduce by 50 % the ALA and PBG plasma accumulation in an acute attack induced in AIP mice by recurrent phenobarbital (Pb) administrations [68]. These data support the fact that only a fraction of corrected hepatocytes may improve AIP symptoms [69]. Although it could be a less invasive and less expensive strategy than liver transplantation, transplanted hepatocytes have a short half-life (about three months) and long-term improvement requires further investigation [69].

4.2.2. Chaperones

Pharmacological chaperones bind to unstable or misfolded proteins for protecting them from early degradation. This binding is able to increase half-life of a mutated protein and thus, enhancing its cellular activity. One of the advantages of this therapeutic strategy is the capacity to be orally administered; by contrary, it could only be effective in those patients whose mutation produces a partially active protein. Currently, this approach is only at the preclinical stage [70].

4.2.3. Gene therapy using viral vectors

Gene therapy (GT) consists in the introduction of genetic material into the nucleus of target cells. Liver directed GT has been proposed as a therapeutic option for many different inborn errors of metabolism, and for patients with AIP that suffer severe and recurrent acute attacks.

Recombinant adeno-associated virus (rAAV) carrying human *PBGD* (*hPBGD*) complementary DNA (cDNA) driven by liver-specific promoters were developed and a proof-of-concept study was validated in a mouse model of the disease [71,72]. Safety profile of this rAAV was also assayed in NHP [73]. However, the administration of a rAAV2/5 expressing *PBGD* did not reduce porphyrin precursors accumulation in 8 patients with severe AIP in a phase 1 open-label clinical trial (NCT02082860) [74]. The lack of efficacy in the clinical trial may be related to the selected doses (from 5×10^{11} to 1.8×10^{13} genome copies/kg) which would result in insufficient hepatic transduction to achieve biochemical correction and clinical benefit [74].

Currently, new generations of AAV vectors are more efficient at transducing the liver but still present some limitations for its use in AIP. The therapeutic efficacy of non-integrative viral vectors, as is the case of AAVs, would be diluted due to natural hepatocyte proliferation (every 4 months in humans), and could only be administered once as they induce strong immune reaction after the first exposure. Actually, pre-existing neutralising antibodies may also reduce the efficacy of its first dose. Recently, an increased risk of insertional mutagenesis in livers with high propensity to develop a tumorigenic process has been described in experimental models [75]. Finally, AAV vectors require to achieve nuclear localization before producing the messenger that generates the transgenic protein. Thus, AAV-based GT are not an optimal therapeutic choice for AIP with sporadic presentations as gene expressions would not be rapidly produced. Altogether, this therapeutic strategy should only be considered for patients

with severe and frequent acute attacks that do not show symptoms and signs of hepatocellular carcinoma [75].

4.2.4. Molecular therapies using non-viral vectors

Johansson et al. assayed GT for the first time to address the treatment of AIP using non-viral vectors carrying the murine *Pbgd* cDNA sequence [76]. In particular, they studied naked DNA, DNA complexed to cationic liposomes, free cationic polymer polyethylenimine or galactose-conjugated as delivery systems. All of them showed no efficacy in increasing hepatic PBGD activity in AIP mice [77].

New non-viral vectors generation has improved hepatic delivery. In fact, our group performed a preclinical study that provided proof-of-concept for systemic hPBGD mRNA as a potential therapy for AIP [2]. mRNA was formulated in LNPs to protect it from the ubiquitous presence of RNases [78], and uridine was globally replaced with 1-methylpseudouridine to increase stability and reduce mRNA immunogenicity. LNPs encapsulating mRNA are taken up by hepatocytes through apolipoprotein E receptor-mediated endocytosis [79–81]. Due to the lipid nature of the nanoparticles, mRNA escapes from the endosome leading to its release into the cytoplasm, where it is translated into functional PBGD protein by the ribosome [82] (Fig. 4).

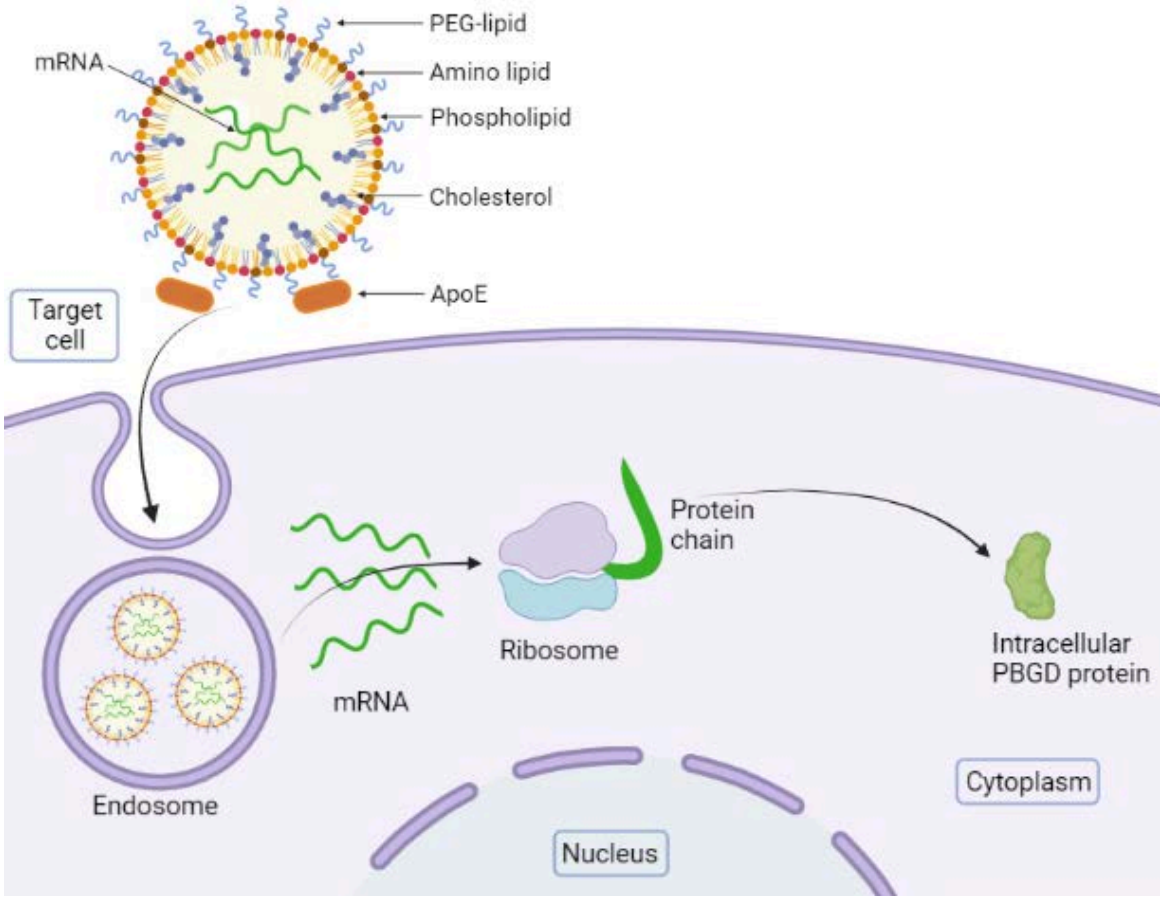

Figure 4. LNPs-mediated delivery and release of mRNA into the cytoplasm of hepatocytes for exogenous PBGD protein production. ApoE, Apolipoprotein E. Adapted from Córdoba et al. [1].

LNPs are multi-component spherical vesicles (~ 100 nm) consisting of phospholipids, cholesterol, polyethylene glycol (PEG)-conjugated lipids, and mainly of amino lipids [83–85]. Intracellular delivery and endosomal escape are the main challenges for the success of therapeutic mRNA, and, together with tolerability, are addressed by the amino lipids [80]. Phospholipids also assist endosomal escape and mRNA release into the hepatocyte cytosol by providing fusogenicity with the target cell membranes [80]. Cholesterol enhances particle stability by modulating membrane integrity and stiffness, and PEG inhibits interactions with plasma proteins allowing increased LNPs circulation time and scape from phagocytic cells [86]. The natural tropism of these LNPs for the LDL receptor has facilitated applications focused on the liver [87].

In our preclinical study, hPBGD mRNA formulated in LNPs systemic administration (0.5 mg/kg) showed optimal characteristics for the treatment of AIP. It produced hepatic hPBGD protein activity 2 h after the injection in AIP mice, rapid action capability is crucial for sporadic presentations of the disease [2]. The increased of PBGD activity in the liver of AIP mice lasted for 10 days, with the duration of acute attacks in patients with AIP being between 5 and 7 days [39]. A single 0.5 mg/kg dose of hPBGD mRNA was able to prevent and reduce high porphyrin precursors accumulation in ongoing attack [2]. Furthermore, hPBGD mRNA protected against *Alas1* induction, pain symptoms, hypertension and motor disturbances that appear in the AIP mice after Pb administration for 4 consecutive days [2]. Therapeutic efficacy without evidence of hepatotoxicity was also confirmed after 3 consecutives i.v. administration of hPBGD mRNA in Pb-challenged AIP mice [2].

Multiple administration of 0.5 mg/kg of hPBGD mRNA in larger animals confirmed safety and translatability. A model showing high porphyrin precursors excretion was generated in rabbits by joint administration of the porphyrinogenic drugs 2-allyl-2-isopropylacetamide (AIA) and Rif. Therapeutic efficacy against AIA and Rif induced accumulation of porphyrin precursors was achieved within 24 h after the administration of a single i.v. dose of 0.5 mg/kg of hPBGD mRNA. The study was repeated up to 3 times without any loss of efficacy [2]. Finally, 5 consecutive hPBGD mRNA administrations over 4 months in NHP maintained hepatic PBGD activity over therapeutic levels and was well tolerated. No neutralizing antibodies were detected, which is a crucial feature for the treatment of patients with recurrent attack episodes [2].

4.2.5. Recombinant enzyme replacement

Direct administration of the functional protein in patients with defective or missing protein is known as enzyme replacement therapy (ERT) and has been assayed as an

alternative approach for the treatment of AIP. A recombinant human PBGD (rhPBGD) protein administration, both i.v. or s.c., was assayed as a therapeutic option to reduce porphyrin precursors during an acute attack in the AIP mouse model [88]. However, s.c. administration of the rhPBGD (Porphozym®, Zymenex) in a phase I clinical trial was discontinued due to short half-life of the protein in circulation (about 2 h) and lack of effectiveness to protect against acute attacks [89].

The inability to enter target cells or to do so in a therapeutic amount is a limiting factor for most recombinant proteins. Thus, ERT is mainly restricted to secreted proteins [87]. To avoid this limitation and improve recombinant protein uptake into hepatocytes, our group has developed a recombinant protein formed by ApoAI linked to the N-terminus of human PBGD (rhApoAI-PBGD) [3]. ApoAI is the main component of high-density lipoprotein (HDL) and is internalized into hepatocytes during the centripetal transport of cholesterol [90,91]. ApoAI receptor, SR-B1, is highly expressed in hepatocytes leading to HDL endocytosis. SR-B1 is also present in the cerebral microvasculature, allowing transcytosis of HDL into the CNS [92,93]. Preclinical data showed that rhApoAI-PBGD had a longer half-life in the blood circulation than the rhPBGD (9.9 h vs. 0.75 h) and that it could penetrate into hepatocytes, increasing PBGD activity in the liver of AIP mice. Consistently, its i.v. or s.c. administration efficiently prevented and abrogated Pb-induce acute attacks in AIP mice [3]. Remarkably, the s.c. administration route could be a substantial advantage for patients as it would allow easy and rapid administration of the drug without requiring hospitalization, which would alleviate the acute attack symptoms in early stages.

An important limitation of ERT is the immunologic activation and consequently antibodies formation. Although preclinical data only showed neutralizing antibodies formation in 1 of 5 mice weekly injected with 7 doses of rhApoAI-PBGD, none of the mice developed antidrug antibodies against either PBGD or ApoAI when the recombinant protein was injected with the murine sequence [3]. Nevertheless, the main

limitation for translating the recombinant conjugated ApoAI proteins into the clinical area might emerge with large-scale production; of note, rhApoAI-PBGD production was performed in *Escherichia coli* (*E. coli*) as described in Córdoba et al. [3]. Thus, further optimization of the production process should be carefully considered.

HYPOTHESIS AND OBJECTIVES

Hypothesis

Our working **hypothesis** is that increasing hepatic PBGD levels either by GT (rAAV2/5-*PBGD*), mRNA formulated in LNPs (hPBGD mRNA) or ERT (rhApoAI-PBGD) is able to normalize high urinary ALA and PBG levels and counteract symptoms and biochemical features associated with the acute attacks in animal models of hepatic porphyria.

Objectives

General Objectives

The main objective is to use animal models of acute porphyria to explore the effect of hepatic PBGD augmentation against poorly described disease features associated with acute hepatic porphyrias.

Neuroradiological studies performed by our group showed significant enlargement of the BV in seven of eight severely affected patients with AIP. Indeed, decreased brain perfusion was observed during the acute attack in two of these patients. Thus, the **first aim** of this thesis was to analyze brain alterations in the AIP mouse model that recapitulates biochemical features of acute attacks after Pb challenge.

Larger animal models would be useful for an extensive analysis of the clinical manifestations associated with acute attacks and the effect of increased hepatic PBGD levels. Previous work has shown that the administration of the porphyrinogenic drugs AIA and Rif in rabbits induced heme biosynthesis pathway leading to large accumulation of porphyrin precursors. However, further characterization of this pharmacological acute porphyria model is required. Thus, the **second aim** was to characterize this new rabbit model of acute porphyria from a biochemical and clinical perspective. Besides, the therapeutic effect of hPBGD mRNA would be also assayed.

A long-lasting therapeutic effect of rhApoAI-PBGD was observed after either i.v. or s.c. administration in AIP mice challenge with Pb [3]. However, GMP procedures for large-scale production and purification of recombinant proteins are challenging. Thus, the **third aim** was to assayed rhApoAI-PBGD production in the CHO-K1SP eukaryotic cell line in order to facilitate large-scale production and subsequent purification.

Specific Objectives

1. To evaluate the morphological CNS changes and brain perfusion in AIP mice.
   a. Effect of increased PBGD activity by rAAV2/5-*PBGD* administration in the CNS of AIP mice.

2. To develop a new animal model of acute porphyria in rabbits.
   a. Biochemical characterization and clinical features of the new chemically induced porphyria model in rabbits.
   b. Efficacy study and safety profile of hPBGD mRNA compared to hemin treatment.

3. To produce and purify rhApoAI-PBGD in an eukaryotic cell line.
   a. Selection of the optimal conditions and medium of culture for the production of rhApoAI-PBGD in CHO-K1SP cell line.
   b. Purification of the produced rhApoAI-PBGD.
   c. Evaluation of its presence in the lipoprotein fraction and pharmacodynamic studies after i.v. administration in AIP mice.
   d. Advantages of ApoAI-PBGD conjugation after intrahepatic expression.

MATERIALS AND METHODS

1. mRNA production and formulation

Production of LNPs containing modified mRNA encoding hPBGD and hApoAI-PBGD was performed by Moderna Inc. (Cambridge, MA, USA) under the supervision of PhD. Lei Jiang and PhD. Paolo G.V. Martini.

Codon-optimized mRNA encoding hPBGD and hApoAI-PBGD was synthesized *in vitro* by T7 RNA polymerase-mediated transcription. The mRNA was initiated with a cap, followed by a 5′ untranslated region (UTR), an open reading frame encoding hPBGD or hApoAI-PBGD, a 3′ UTR, and a polyadenylated tail. Uridine was globally replaced with 1-methylpseudouridine. For *in vivo* i.v. delivery, LNPs formulations were generated containing mRNA and lipids at a molar ratio of 3:1 (mRNA / lipids). Lipids include ionisable cationic lipid, fusogenic lipid, structural lipid, and PEG lipid at a molar ratio of 30/30/38.5/1.5, respectively. mRNA-loaded nanoparticles were exchanged into final storage buffer and had particle sizes of 80-100 nm, > 80 % encapsulation of the mRNA as measured by a RiboGreen assay, and < 10 endotoxin units per ml.

2. AIP mouse model

Lindberg et al. described a mouse model of AIP generated by crossbreeding T1 (C57BL/6$^{Pbgdtm1(neo)Uam}$) and T2 (C57BL/6$^{Pbgdtm2(neo)Uam}$) mouse strains [94]. Compound heterozygote T1/T2 mice (AIP) exhibit 30 % of the WT PBGD activity and a slightly increased urinary porphyrin precursors excretion [94]. T1 and T2 mice with heterozygous mutations do not develop the disease but the biallelic model replicates the drug-precipitated biochemical abnormalities of acute porphyria in humans [71]. Porphyrin precursors accumulation can be exacerbated by Pb (porphyrinogenic drug according to “The Drug Database for Acute Porphyria”; https://www.drugs-

porphyria.org/) administration reproducing pain and motor neuropathy that characterize acute porphyrias. Experimental protocol (CEEA 050-16) was performed according to European Council Guidelines and approved by the local Animal Ethics Committee.

2.1. Study design for central nervous system studies in AIP mice

Morphological CNS changes and brain perfusion were analyzed in WT and AIP mice. To evaluate the role of hepatic PBGD deficiency in CNS involvement, half of the AIP received a single dose of 5×10^{12} gc/kg of rAAV2/5-*PBGD* vector for enhancing hepatic PBGD activity. Finally, to overload the deficient enzymatic step and biochemically imitate severe human AIP, half of the animals in each group received 16 Pb challenges (doses of 75, 80, 85 and 90 mg/kg per day administered intraperitoneal (i.p.) for each challenge) distributed every two weeks for 8 months. Therefore, animals were 4-month-old at the beginning of the Pb challenges and 1-year-old at the time of the CNS studies. Liver-targeted GT was performed in 8- to 12-week-old mice, one month before the onset of the Pb challenges. Mice distribution was as follows: AIP, n = 4; AIP+Pb, n = 3; AIP-GT, n = 4; AIP-GT+Pb, n = 3; WT, n = 5; and WT+Pb, n = 5.

At the end of the study, mice were housed in metabolic cages and 24 h urine samples were collected. Urinary PBG and ALA levels were determined by ion-exchange chromatography (M11017c-0509, BioSystems, Barcelona, Spain) according to the manufacturer's instructions. PBG can be non-enzymatically converted to porphyrins, so it is important to protect urine from light and store it at 4 ºC [18].

At sacrifice, PBGD enzymatic activity was determined in liver homogenates by measuring the conversion of PBG to uroporphyrin. Firstly, 1 g of tissue was homogenized at 4 ºC in 0.8 ml of lysis buffer (sodium phosphate 1 mM pH 7.6 with dithiothreitol (DTT) 1 mM, Cl_2Mg 1 mM and Triton X-100 0.05 %). The homogenate

was centrifuged at 12,000 rpm at 4 ºC for 20 minutes and the clear supernatant without any cellular debris was used the same day for protein determination (Bradford using an albumin standard) and PBGD activity. The supernatant samples were diluted with the lysis buffer to adjust the protein amount of the reaction to 0.5 mg; and 50 µl of this mixture were pre-incubated with 0.9 ml of Tris-HCl 0.1 M with DTT 0.1 mM (incubation buffer, pH 8.1) for 3 min at 37 ºC. Next, 250 µl PBG substrate 1 mM were added to the mixture and it was incubated in the dark at 37 ºC for 1 h. The reaction was stopped with 175 µl cold trichloroacetic acid 40 % (T9159, Sigma-Aldrich, Saint Louis, MO, USA) and the uroporphyrinogen formed was oxidized to uroporphyrin after light exposure. Uroporphyrins were measured quantitatively in a spectrofluorometer with an excitation λ at 405 nm and window emission λ values between 550-660 nm. PBGD activity was expressed in terms of pmol uroporphyrin/mg protein/h using appropriate standards.

2.2. Magnetic resonance imaging studies in the brain of AIP mice

BV size was measured by brain magnetic resonance imaging studies (MRI) in the 1-year-old mice. MRI studies were performed in a Bruker Biospec 70/20 scanner using a combination of a linear coil (for transmission) with a mouse head phase array coil (for reception). Animals were anesthetized with sevoflurane (5 % for induction and 3 % for maintenance) and placed in an MRI-adapted stereotaxic holder with a water circulating blanket to maintain body temperature. Respiration and body temperature were continuously monitored. As an anatomical reference, we acquired a T2-weighted axial sequence (Repetition Time (RT) = 4200 ms; Echo Time (ET), 33 ms; α = 180◦; field of view (FOV) = 1.8 × 1.8 cm; matrix = 256 × 256; slice thickness = 0.5 mm, number of slices = 28).

CBF measurements were also registered at the end of the study using arterial spin labelling [95,96]. CBF maps were calculated using a Flow-sensitive alternating inversion recovery echo planar imaging (also known as FAIR-EPI) sequence using selective and global inversion (RT: 15 000 ms, ET: 16.4 ms, α = 90◦; FOV = 1.8 × 1.8 cm; matrix = 80 × 64; slice thickness = 1mm, inversion recovery time (IRT) = 25 ms, number of IRT values = 22, number of slices = 1). The value of CBF was calculated according to the formula:

$$\mathrm{CBF} = \theta\left(\frac{1}{T1,\mathrm{sel}} - \frac{1}{T1,\mathrm{nosel}}\right),$$

θ represents the blood/brain distribution coefficient (0.9 ml/g) [97].

2.3. Structural studies in the brain of AIP mice assessed by brain histology

5-months-old WT (n = 2) and AIP (n = 2) female mice received three Pb challenges on alternate weeks. Two weeks after the last challenge, animals were perfused with 4 % paraformaldehyde. Then, brains were immersed in para-formaldehyde overnight and, finally, in a mixture of 20 % Glycerol + 2 % dimethyl sulfoxide for 48 h. Classical histological analyses were performed with Nissl stain for cells or Fibers. The hippocampus sections of mouse brain slices were immunostained for endothelin receptor type B (Ednrb, UniProtKB - A0A2S1UF14) and glial fibrillary acidic (Gfap, UniProtKB - P03995) protein using different rabbit polyclonal antibodies (ab117529, Abcam, Cambridge, UK; Z0334, DakoCytomation, Glostrup, Denmark, respectively).

2.4. Measurement of plasma Endothelin-1 and gene expression of *endothelin receptor type B* and *alas1*

Plasma Endothelin-1 (Edn1, UniProtKB – Q6FH53) measurements in WT (n = 5), AIP (n = 4) and AIP treated with GT (n = 4) mice were made using a quantitative enzyme-linked immunosorbent assay (ELISA) (DET100, R&D systems, Minneapolis, MN, USA).

Gene expression of *Ednrb* (MGI:MGI:102720) and *Alas1* was measured by quantitative PCR (qPCR) with an iCycler IQ real-time PCR thermal cycler (170-8740, Bio-Rad, Hercules, CA, USA) using iQ SYBR Green supermix (1708880, Bio-Rad, Hercules, CA, USA). Briefly, mRNA was extracted from liver tissues using Maxwell RSC simplyRNA Tissue (Promega Biotech, Madrid, Spain) and then converted into cDNA by reverse-transcriptase PCR.

qPCR was performed using the following specific primers:

- *Ednrb*. Forward primer: 5'-AAGAATGCCCAAGAGAAAAC-3', reverse primer: 5'-AAAAAGGAAGGAAGGAAAATC-3', product length of 239 base pairs (bp).

- *Alas1*. Forward primer: 5'-CAAAGAAACCCCTCCAGCCAATGA-3', reverse primer: 5'-GCTGTGTGCCGTCTGGAGTCTGTG-3', product length of 104 bp.

The amount of gene transcripts was calculated as the n-fold difference relative to the control mouse using the *β-actin* gene as an internal control.

- *β-actin*. Forward primer: 5'-CGCGTCCACCCGCGAG-3', reverse primer: 5'-CCTGGTGCCTAGGGCG-3', product length of 194 bp.

Results are expressed according to the formula $2^{\Delta Ct(actin)-\Delta Ct(gene)}$, where ΔCt represents the difference in threshold cycle between genes.

3. Chemically induced VP rabbit model

3.1. Experimental study design

Thirteen female WT New Zealand rabbits (Granja de San Bernardo, Tulebras, Spain) were s.c. injected with 350 mg/kg AIA in the morning and i.p. with 200 mg/kg Rif in the afternoon. A total of 11 AIA and 12 Rif doses were administered during 20 days in three different challenges that were days 1–3 (D1), days 8-10 (D8) and days 15-19 (D15). An additional dose of Rif was administered on day 20, 16 h before sacrifice. Three of these rabbits received a single i.v. dose of 0.5 mg/kg hPBGD mRNA on day 16, and four of them were injected with four hemin doses of 8 mg/kg i.p. (Normosang, Recordati, Puteaux, France) from day 15 to 18. The hemin dose administered in rabbits is twice the highest “standard dose” used in human acute porphyria patients (4 mg/kg), given that i.p. administration of 8 mg/kg in mice reproduces the effects of i.v. hemin infusion in humans [2,11]. We used i.p. administration to preserve auditory pinna veins in the rabbits to carry out the glucose tolerance test (GTT). Seven non-injected rabbits were used as a reference group. Experimental protocols were approved by the Ethics Committee of the University of Navarra (CEEA142-16) and the Institute of Public Health of Navarra, Spain (Doc: 2017/50445) according to European Council Guidelines.

3.2. Biochemical and molecular parameters measured in the VP rabbit

Rabbits were housed in individual cages, and 24 h urine samples were collected daily over the three challenges. Urinary PBG and ALA levels were determined by ion-exchange chromatography (M11017c-0509, BioSystems, Barcelona, Spain) according to the manufacturer’s instructions. Serum ALA and PBG were quantified by liquid chromatography-mass spectrometry using a Waters XBridge BEH C18 column

(2.5 µm, 2.1 × 50 mm). Calibration standards were prepared by adding diluted solutions of ALA (A3785-500MG, Merck, Darmstadt, Germany), ALA-13C5 (711187, Merck, Darmstadt, Germany), PBG (P226-10MG, Frontier Scientific, Newark, NJ, USA), and C13-PBG (P41393, Inochem, Carnforth, UK) in acetonitrile/water (50/50) internal standard solution (100 µM) to blank serum. Standards were then purified using an OASIS PRiME HLB µElution plate (186008052, Waters Chromatography Europe B.V., Etten-Leur, The Netherlands). The recoveries calculated for PBG and ALA in rabbit serum were between 88 % and 98 % and between 87 % and 100 %, respectively. ALA and PBG in the cerebrospinal fluid were measured by liquid chromatography coupled to a triple-quadrupole mass spectrometry system (Xevo TQMS, Waters Chromatography Europe B.V., Etten-Leur, Nederland) following a metabolite derivatization process (AccQTag, Waters Chromatography Europe B.V., Etten-Leur, Nederland).

Porphyrins were quantified in a PerkinElmer LS50B spectrofluorometer (excitation λ of 409; emission λ of 600 nm; PerkinElmer, Waltham, MA, USA) after oxidation with Lugol's iodine [98]. Total urinary porphyrins were determined by spectrophotometry (UV 1800, Shimadzu Corporation, Kyoto, Japan) between 350 and 450 nm after acidification, according to the method of Elder et al [99]. The different urinary porphyrins were separated by reverse-phase high performance liquid chromatography (HPLC) with fluorometric detection (Ultimate 3000, Thermo Fisher Scientific, Whaltham, MA, USA). Plasma porphyrins were measured by dilution of the plasma in phosphate buffer as already described [100]. The solution was compared with a standard by scanning the fluorescence emission λ from 570 to 750 nm (excitation λ at 405 nm), using a RF6000 spectrofluorometer (Shimadzu Corporation, Kyoto, Japan) fitted with a red-sensitive photomultiplier. Total fecal porphyrins were determined by spectrophotometry (UV 1800, Shimadzu Corporation, Kyoto, Japan) after hydrochloric acid extraction in the presence of ether [101]. The fractionation of fecal porphyrins was

performed after formation of methyl ester porphyrins, which were then extracted with chloroform and finally separated by normal-phase HPLC with fluorometric detection [102].

Lipid peroxidation was determined using the TBARS kit (KGE013, R&D Systems, Minneapolis, MA, USA) according to the manufacturer's instructions. Briefly, a colorimetric product formed by the reaction of malondialdehyde (end product of polyunsaturated lipids oxidation) with thiobarbituric acid was measured at λ of 532 nm in a Multiskan Ascent 96 plate reader photometer (Thermo Fisher Scientific, Waltham, MA, USA). Urinary parameter data were normalized per creat. excretion rate. Creat. levels were measured in a Cobas Hitachi c311 Analyzer (Roche Diagnostics International, Mannheim, Germany).

At sacrifice, rabbits were exsanguinated by intracardiac perfusion at room temperature before organ removal. Serum samples were stored at −20°C until analyzed. Liver status (ALT and alkaline phosphatase, ALP) was analyzed in a Cobas Hitachi c311 Analyzer (Roche Diagnostics International, Mannheim, Germany). PBGD enzymatic activity was determined as described in previous AIP mouse model section in fresh liver homogenates. Liver tissue samples were also stored at −80 °C for further analysis as follows:

A) Enzyme activities were determined in homogenates from a mix of liver lobes. ALAD activity was performed as previously described [103]. UROS activity was determined by an enzyme-coupled assay as described [104]. For UROD activity measurement, pentacarboxylporphyrinogen III was used as the substrate and its decarboxylation was quantified by HPLC as coproporphyrinogen III formation [105]. CPO activities were determined as already described [106]. PPO activities were quantified as described [100], and FC activities were measured fluorometrically by zinc-mesoporphyrin formation according to Li et al [107]. Activities of the respiratory chain

were measured in isolated liver mitochondria according to previously described methods for spectrophotometric assays [108], using between 6 and 30 µg of mitochondrial protein.

B) Total heme levels were measured in liver homogenates using a heme assay kit (MAK316, Sigma-Aldrich, Saint Louis, MO, USA). Mitochondrial heme A levels were measured using a colorimetric method. For mitochondria extraction, liver samples were homogenized in 1.8 ml Buffer A (compound of Mannitol 225 mM, Sucrose 75 mM, EGTA 0.1 mM, Fatty Acids-free BSA 1 mg/ml and Hepes-NaOH 10 mM, pH 7.4) using a Glashomogenizer Potter (853202, B. Braun, Melsungen, Germany) and centrifuged at 700 g for 10 min at 4 ºC. The collected supernatant was again centrifuged at 10,000 g for 10 min at 4 ºC. Then, the pellet was resuspended (500 and 250 µl of Buffer A) and centrifuged 2 times under the same previous conditions. Finally, the isolated mitochondria were resuspended in 100 µl of Buffer B (compound of Sucrose 395 mM, EGTA 0.1 mM and Hepes-NaOH 10 mM, pH 7.4). Briefly, 900 µg from isolated liver mitochondrial proteins were incubated on ice for 30 min with sodium phosphate buffer solution (23.8 mM final, pH 7.4) with 1.9 % Triton X-100 (T9284, Sigma-Aldrich, Saint Louis, MO, USA). Absorbance was measured at 445 nm in a Multiskan Ascent 96 plate reader photometer (Thermo Fisher Scientific, Waltham, MA, USA) at baseline (oxidized condition), and after adding 10 mg of ascorbic acid (reduced condition) (50-81-7, Sigma-Aldrich, Saint Louis, MO, USA). Mitochondrial heme A levels were calculated by the absorbance increase between the reduced and oxidized condition considering the molar extinction coefficient (ε_{445nm}, 164 mM^{-1} cm^{-1}).

C) Gene expression was measured by qPCR as previously described in AIP mouse model using the following specific rabbit primers:

- *Alas1*. Forward primer: 5'-GCAGCAGTGTCGTCCGCAAA-3', reverse primer: 5'-CGGAGAGGACCCCAGTGGAC-3', product length of 141 bp.

- *Alad*. Forward primer: 5'-CTACCCCATCTTCGTCACGG-3', reverse primer: 5'-GCCTGGAATGCTCCGTTTTC-3', product length of 333 bp.

- *Pbgd*. Forward primer: 5'-AGCCCCAGGATGAGAGTGAT-3', reverse primer: 5'-GCTGGTTCCCACTACACTCC-3', product length of 396 bp.

- *Uros*. Forward primer: 5'-GCCAGGATCCATACGTCAGG-3', reverse primer: 5'-GCAGGCCGATTCTACTCACT-3', product length of 294 bp.

- *Urod*. Forward primer: 5'-GCCTGCTGTGAACTGACTCT-3', reverse primer: 5'-ATGTCATCAGAGTCCACGGG-3', product length of 301 bp.

- *Cpo*. Forward primer: 5'-GTGGGAGAGGAAGGAAGGAG-3', reverse primer: 5'-GGATAGTGGGAGCATGAGGA-3', product length of 236 bp.

- *Ppo*. Forward primer: 5'-TCTGGCTCGTGTCCTGAGTA-3', reverse primer: 5'-TGGCTCCTTCAGTCCTAGCT-3', product length of 316 bp.

- *Fc*. Forward primer: 5'-AGCACTATTGACAGGTGGCC-3', reverse primer: 5'-GCATGCGCACATACAGTCAG-3', product length of 511 bp.

- *Ho-1*. Forward primer: 5'-AACCCGGTCTACGCCCCGCT-3', reverse primer: 5'-CCATCCCCTACACGCCGGCC-3', product length of 120 bp.

- *Hepcidin*. Forward primer: 5'-GTTCTCCAGCAGCAGACACA-3', reverse primer: 5'-TCAAAATGTGGGATCTGCTG-3', product length of 170 bp.

- *Hsp70*. Forward primer: 5'-TGGTGCTGACGAAGATGAAG-3', reverse primer: 5'-AGGTCGAAGATGAGCACGTT-3', product length of 235 bp.

The amount of gene transcripts was calculated as the n-fold difference relative to the control mouse using the *β-actin* gene as an internal control.

- *β-actin*. Forward primer: 5'-CTGGAACGGTGAAGGTGACA-3', reverse primer: 5'-AAAGTTCTGCAATGTGGCCG-3', product length of 73 bp.

Results are expressed according to the formula $2^{\Delta Ct(actin)-\Delta Ct(gene)}$, where ΔCt represents the difference in threshold cycle between genes.

D) For the western-blot (WB) assay, 50 mg of liver samples were homogenized in RIPA lysis buffer containing protease inhibitors and sodium orthovanadate, and sonicated for protein extraction. 30 µg of protein was diluted with Laemmli sample buffer (#1610747, Bio-Rad, Hercules, CA, USA) and loaded for a room temperature electrophoresis procedure in precast gels (Mini-PROTEAN TGX #4561085, Bio-Rad, Hercules, CA, USA) at constant 120 V in running buffer (192 mM glycine, 25 mM Tris, and 0.1 % SDS). Then, separated proteins were transferred onto a nitrocellulose 0.45 µm or polyvinylidene fluoride membrane by a 4°C electrophoretic transfer at constant 120 V in a transfer buffer (192 mM glycine, 25 mM Tris, and 20 % methanol). The primary antibodies used were as follows: anti-ALAS1 antibody (ab84962, dilution 1:750, Abcam, Cambridge, UK), total OXPHOS rodent WB antibody cocktail (ab110413, dilution 1:500, Abcam, Cambridge, UK), and anti-actin antibody (A2066, dilution 1:4,000, Sigma-Aldrich, Saint Louis, MO, USA). Anti-mouse (A0168, 1:10,000, Sigma-Aldrich, Saint Louis, MO, USA) and anti-rabbit (7074, 1:10,000, Cell Signaling Technology, Danvers, MA, USA) were used as secondary antibodies. Primary antibodies were incubated overnight at 4 °C and secondary antibodies for 1 h at room temperature. Signals were detected using a Western Lightning Plus ECL kit (NEL103E001EA, PerkinElmer, Waltham, MA, USA) in a ChemiDoc MP imaging system (Bio-Rad). Specific WB signals for each OXPHOS complex were quantified with Imagen Lab software 6.01 (Bio-Rad, Hercules, CA, USA) using actin protein for loading normalization.

Liver samples were also taken for histological and immunohistochemistry analysis on the same liver sections. Hematoxylin-eosin staining was performed in formalin-fixed liver sections. Mitochondrial immunostaining was also performed in formalin-fixed liver sections using anti-mitochondrial cytochrome c oxidase 1 (MT-CO1) antibody (1D6E1A8, Abcam, Cambridge, UK) according to the manufacturer's instructions.

3.3. Physiological parameters measured in the VP rabbit

Blood pressure was measured at baseline (day −4) and on days 10 and 18, and the GTT was performed on fasted animals 1 day later each time. Blood pressure was determined by a non-invasive leg-cuff system in awake animals using a Hewlett-Packard M1165A model 56S apparatus. For the GTT assay, serum glucose levels (mg/dL) were measured at 0, 5, 10, 20, 30, 45, 60, 75, and 90 min after i.v. injection of 0.5 g/kg of glucose solution (0.5 mg/ml) using a Accu-Chek AVIVA apparatus (Accu-Chek, Mannheim, Germany).

Brain and heart glucose uptake and electrophysiological studies were performed under inhaled isoflurane anesthesia at the end of the second and the third challenge (days 11 and 20, respectively). *In vivo* 18F-fluorodeoxyglucose (^{18}F-FDG) uptake in the brain was determined by positron emission tomography (PET) after a fasting period of 16 h [109]. Rabbits were injected i.v. with 18.4 ± 0.1 MBq of ^{18}F-FDG. After a conscious uptake period of 45 min, animals were analyzed in a microPET (Mosaic, Philips, Amsterdam, The Netherlands) tomograph (with 2 mm resolution, 11.9 cm axial FOV and 12.8 cm transaxial FOV), and a computed tomography (CT) Biograph Duo PET/CT (Siemens Healthineers, Knoxville, TN, USA).

Motor-evoked potentials in the sciatic nerve were recorded in anesthetized rabbits (0.3 ml/kg intramuscular ketamine). The electrical stimuli were delivered using pairs of

needles placed s.c. near the exit point of the sciatic nerve at the hip, with a separation of 0.5 mm and the cathode located distally. Stimuli were delivered by a Grass S180 stimulator (Grass-AstroMed, West Worwick, RI, USA). Motor potentials were recorded using steel needle electrodes (Viasys Healthcare, Conshohocken, PA, USA) located at the center of the tibialis anterior muscle, midway between the ankle and the knee (active electrode), and at the dorsum of the foot (reference electrode). The responses were amplified by a Grass P511 amplifier (Grass-AstroMed, West Worwick, RI, USA), digitized using a CED power 1401 A/D converter (Cambridge Electronic Design, Cambridge, UK), and stored in a PC using Signal 3 software (Cambridge Electronic Design, Cambridge, UK). Stimulation intensity was increased gradually to ensure the maximal response amplitude. The largest response out of 10 biphasic negative-positive potentials was selected for analysis.

4. rhApoAI-PBGD protein produced in CHO-K1SP cells

4.1. Production of rhApoAI-PBGD protein in CHO-K1SP

Previously in our group, the sequence of rhApoAI-PBGD (Fig. 5) was synthetized and subcloned in a pGenHT1.0 plasmid (sequence under trade secret, GenScript Biotech, Piscataway, NJ, USA) with a signal peptide in the 5' terminal position of ApoAI to allow protein secretion into the supernatant. The signal peptide splits off during the maturation process and it is not in the secreted protein. The plasmid was transfected into CHO-K1SP eukaryotic cells. 48 h post-transfection, the expression level was higher than 0.080 mg/L as measured by ELISA test (Human ApoAI ELISA^{PRO} Kit, 3710-1HP-2, Mabtech, Nacka Strand, Sweden). Afterwards, the cell pools with the highest expression were subjected to single clone screening using the limiting dilution method, followed by single clone batch in 6-well plates. The top 10 clones were selected for fed-

batch culture. The highest shaking flask fed-batch titer of single clone reached to 40.46mg/L determined by ELISA test. Finally, the Top 3 clones (Clone 8, 11 and 45 with the titer of 24.42 mg/L, 34.73 mg/L and 40.46 mg/L respectively in shaking flask fed-batch) were selected for further studies. The plasmid is owned by GenScript and the selection process for these three clones was carried out at their facility. The following studies and techniques described in this thesis were carried out by the doctoral student at the CIMA facility or at the "École nationale supérieure de technologie des biomolecules de Bordeaux" (ENSTBB), France.

DEPPQSPWDRVKDLATVYVDVLKDSGRDYVSQFEGSALGKQLNLKLLDNWDSVTST
FSKLREQLGPVTQEFWDNLEKETEGLRQEMSKDLEEVKAKVQPYLDDFQKKWQEEM
ELYRQKVEPLRAELQEGARQKLHELQEKLSPLGEEMRDRARAHVDALRTHLAPYSDE
LRQRLAARLEALKENGGARLAEYHAKATEHLSTLSEKAKPALEDLRQGLLPVLESFKV
SFLSALEEYTKKLNTQ**SGNGNAAATAEENSPKMRVIRVGTRKSQLARIQTDSVVATL**
KASYPGLQFEIIAMSTTGDKILDTALSKIGEKSLFTKELEHALEKNEVDLVVHSLKDLP
TVLPPGFTIGAICKRENPHDAVVFHPKFVGKTLETLPEKSVVGTSSLRRAAQLQRKF
PHLEFRSIRGNLNTRLRKLDEQQEFSAIILATAGLQRMGWHNRVGQILHPEECMYAV
GQGALGVEVRAKDQDILDLVGVLHDPETLLRCIAERAFLRHLEGGCSVPVAVHTAM
KDGQLYLTGGVWSLDGSDSIQETMQATIHVPAQHEDGPEDDPQLVGITARNIPRGP
QLAAQNLGISLANLLLSKGAKNILDVARQLNDAH

Figure 5. rhApoAI-PBGD amino acid sequence. ApoAI sequence is represented in green letters, PBGD sequence is represented in bold font and blue letters, and the yellow box indicates the Cys261 of the active center of the enzyme. Domain 3 of the PBGD (underline) covers residues from 241 (highlighted in purple) to the end.

4.2. Selection of the optimal conditions for the production of rhApoAI-PBGD in CHO-K1SP cell line

Different conditions were assayed for incubation of clones 8, 11 and 45 in DYNAMIS AGT synthetic medium (a2617501, Gibco, Thermo Fisher Scientific, Whaltham, MA, USA) that do not contain fetal bovine serum, avoiding prions infections or other contaminating elements. The synthetic medium was supplemented with Feed B (a2503004, Gibco, Thermo Fisher Scientific, Whaltham, MA, USA) 8 % of total volume on days 4, 6, 8, 10 and 12 of culture. Glucose and lactate were measured every day (Enzytec™ *Liquid* D-Glucose E8140 and L-Lactic acid E8260, respectively, R-Biopharm, Darmstadt, Germany) to maintain levels between 4-6 g/L of glucose and low lactate cell production. Cells were incubated in agitation (120 rpm) at 32 ºC or 37 ºC in 125 ml Flask, at 8 % CO_2. Cell counting was performed with Malassez chamber to check cell viability. The production of rhApoAI-PBGD protein in CHO-K1SP cells was confirmed by enzymatic PBGD measurement and WB analysis. PBGD activity was measured as previously described in AIP mouse model section in 50 µl of cell supernatant. The fluorimeter lecture was done under the same conditions in an Infinite F200 fluorimeter (TECAN, Männedorf, Switzerland). WB was performed as already described in rabbit section loading 20 µl of cell supernatant (the maximum quantity that fit in the wells) and using a rabbit monoclonal antibody against PBGD diluted 1:1,000 (ab129092, Abcam, Cambridge, UK) or a goat polyclonal antibody against ApoAI diluted 1:2,000 (AF3664, R&D Systems, Minneapolis, MN, USA) as primary antibodies. An anti-rabbit (7074, Cell Signaling, Danvers, MA, USA) or anti-goat (HAF109, R&D Systems, Minneapolis, MN, USA) immunoglobulin G diluted 1:10,000 were respectively used as secondary antibodies.

For rhApoAI-PBGD mass analysis, the different protein fractions separated on precast gels (Mini-PROTEAN TGX #4561085, Bio-Rad, Hercules, CA, USA) were sent to Proteomic Platform of the University of Bordeaux for trypsin digestion and recognition

of sequence-specific peptides in a LTQ ORBITRAP XL mass spectrometer (Lumos, Wyatt Technology, Santa Bárbara, CA, USA).

In other experiments, supernatant of clone 45 at day 8 (in which the complete form of the protein stands out over the truncated one) was incubated at 32 ºC or 37 ºC (depending on their origin conditions) with or without 1:100 anti-proteases cocktail (Protease Inhibitor Cocktail, P8340, Sigma-Aldrich, Saint Louis, MO, USA). In addition, cells were incubated with the anti-proteases cocktail at 1:800 concentrations to improve production performance. Higher concentrations of the antiproteases cocktail (1:100 and 1:400) inhibited cell growth and generated toxicity and cellular death in CHO-K1SP cells.

4.3. Purification assays of rhApoAI-PBGD protein

4.3.1. Purification experiments by resins

A screening was carried out to select a resin on which the protein could be purified. 4-mercapto-ethyl-pyridine (MEP), hexylamine (HEA) and phenylpropylamine (PPA) resins were assayed in a 96 wells microplate (AcroPrep™ Screen Expert Plates 96WP3MIXM50, Pall, Port Washington, NY, USA). Firstly, resins were equilibrated twice with 100 µl phosphate buffer saline (PBS) pH 7 mixed at 1,100 rpm during 1 min before adding the cell supernatant containing the rhApoAI-PBGD (also, mixed at 1,100 rpm during 1 h). After adding the protein, the microplate was washed twice with 100 µl PBS pH 7 (1,100 rpm, 1 min), and the attached protein was eluted with sodium acetate 25 mM buffer pH 5 (1,100 rpm, 1 min). Immunoblot against PBGD and ApoAI, and enzymatic activity analysis were performed as explained above to check for rhApoAI-PBGD protein in the elution fractions. SEC-MALS analysis (Size Exclusion Chromatography with Multi-Angle Light Scattering) on a HPLC for SEC coupled with

miniDAWN and Optilab for light scattering and refractometer (Wyatt technology, Santa Bárbara, CA, USA) was performed to check for protein aggregates in the elution fraction with high protein concentration.

4.3.2. Purification experiments by Size-Exclusion Chromatography

In order to disaggregate the rhApoAI-PBGD molecules, 50 ml of Retained fraction 2 were incubated with DTT 20 mM + CHAPS 4 % for 1 h at room temperature and eluted in 1 L SEC column with PBS pH 7 as elution buffer. WB analysis against PBGD and ApoAI were performed as detailed in point 3.2 of Materials and Methods. Quantification of the rhApoAI-PBGD protein was performed by an ELISA test against ApoAI (Human ApoAI ELISA^{PRO} Kit, 3710-1HP-2, Mabtech, Nacka Strand, Sweden) and enzymatic PBGD activity in different eluted fractions. SEC-MALS analysis was performed to check for rhApoAI-PBGD aggregates in the elution fractions. Those aliquots with higher amount of rhApoAI-PBGD and enzymatic activity were selected for further *in vivo* studies.

4.4. Detection of rhApoAI-PBGD protein in serum lipoprotein fractions

In order to analyze wether rhApoAI-PBGD protein circulates bound to serum lipoproteins, 60 nmol/kg of the recombinant protein was i.v. injected in three T1 mice via tail vein injection. Blood sample was collected 72 h post-injection, and different lipoprotein fractions were extracted from the serum. Firstly, 400 µL of serum were mixed with 1,100 µL of sodium bromide (NaBr) buffer at a density (ρ) of 1.006 g/L. Samples were centrifuged at 301,000 x g for 2 h at 4 ºC, and serum lipoproteins were distributed on a density gradient. VLDL fraction was collected at the top. Then, a new NaBr buffer (ρ = 1.4 g/L) was added, adjusting the final ρ to 1.04 g/L. A second centrifugation (301,000 x g, 2.5 h) distributes the LDL fraction to the top. Finally,

another centrifugation (301,000 x g, 3 h) after the addition of NaBr buffer (ρ = 1.4 g/L, adjusting the final density to 1.21 g/L) was performed which shifted the HDL fraction to the top. The presence of rhApoAI-PBGD protein in each of the fractions was determined by immunoblot using the anti-PBGD and anti-ApoAI primary antibodies for protein detection in each fraction.

4.5. Pharmacodynamics studies of rhApoAI-PBGD protein

To assay the therapeutic effect male AIP mice were i.v. administered with 60 nmol/kg of the purified rhApoAI-PBGD (n = 4). Another 9 animals were i.v. administered with 60 nmol/kg of rhApoAI-PBGD from *E. coli* origin. Besides, 5 animals were included as control group. These mice were challenged with 4 consecutive doses of Pb (75, 80, 85 and 90 mg/kg administered i.p.). ALA and PBG excretion levels were measured in 24 h urine samples. The Mouse Grimace Scale (MGS) (Fig. 6) was performed at the end of the Pb challenge (4 h after the last Pb injection) to evaluate pain behaviour. The following day, animals received an extra dose of 90 mg/kg of Pb and were euthanized 20 mins after. Hepatic PBGD activity was performed in fresh liver samples.

Figure 6. The MGS is a tool to score pain behaviour during acute porphyria attacks [110,111]**.**

5. Intracellular stability of the hApoAI-PBGD protein

To get further insight regarding the intracellular stability of the conjugated protein, we expressed in the liver of male AIP mice human PBGD or ApoAI-PBGD proteins using the technology of mRNA formulated in lipid nanoparticles. In a pharmacokinetic assay, several animals were sacrificed 24 hours after mRNA administration at different doses (0.5 or 2.5 mg/kg) to confirm that hepatic PBGD activity was similar in both groups.

To assay the therapeutic effect of the hApoAI-PBGD mRNA, male AIP mice received 2 challenges of 4 consecutive doses of Pb (75, 80, 85 and 90 mg/kg administered i.p.) on days 0 to 3 and 12 to 15. On day 1, AIP mice were i.v. administered with 2.5 mg/kg hApoAI-PBGD mRNA (n = 2), 0.5 mg/kg of hPBGD mRNA (n = 5) or luciferase mRNA (n = 5). Mice were placed in metabolic cages over the Pb challenge to collect urine 24 h samples and measure daily porphyrin precursors excretion. Pain measurement using the MGS [110,111] was performed at the end of the second Pb challenge (day 15, 4 h after the last Pb injection). Animals were euthanized on day 16, and hepatic enzymatic activity was performed on liver homogenates. Experimental protocol CEEA050-16 was performed according to European Council Guidelines and approved by the local Animal Ethics Committee.

6. Statistical analysis

Statistical analyses were performed using GraphPad Prism v6.01. Before statistical analysis, data were transformed using the formula log (1 + x) to normalize the variances. Comparisons between two groups were made by two-sided Student's t tests. In the case of comparisons between more than two groups, data were analyzed using a one- or two-way ANOVA, and pairwise comparisons were made using Bonferroni's Multiple Comparison tests. The statistical significance of differences was

tested with two-tailed t-tests and p values of < 0.05 indicated statistically significant differences. Data are means ± standard deviation (SD). Confidence intervals were constructed as the normal-based 95 % CI: mean ± 2 SD.

RESULTS

1. CNS alterations in the AIP mouse model

1.1. Brain ventricular enlargement in AIP mice

In baseline situation, AIP mice exhibit slightly elevated urine ALA and PBG levels unless a barbiturate (e.g. Pb) is administered (Fig. 7A-B). We analyzed structural changes in one-year-old AIP mice that never received barbiturates or were exposed to any other triggering factor inducing an acute attack. Given that AIP mice showed BV widening when compared to WT animals (Fig. 7C-D), these data suggest that this feature is associated to low levels of porphyrin precursors accumulation. Of note, we observed that recurrent Pb-induced acute attacks on alternate weeks for 8 months further exacerbated BV enlargement in AIP mice (Fig. 7D). This could not be attributed to any direct toxic effect of Pb since repeated administration of this drug did not significantly modify BV volume in WT animals (Fig. 7D). Importantly, recurrent Pb administration failed to increase the size of BV in animals treated with rAAV2/5-*PBGD* aiming to restore PBGD hepatic levels (Fig. 7D). Indeed, the administration of a single dose of rAAV2/5-*PBGD* one month before the onset of recurrent attacks protected AIP mice against hepatic *ALAS1* over-expression (Fig. 7E) and the consequent accumulation of heme precursors (Fig. 7A-B). These data indicate a relationship between high hepatic production of heme precursors and BV enlargement and suggest that the increased of hepatic PBGD activity levels by rAAV2/5-*PBGD* administration (Fig. 7F) restored the heme synthesis pathway regulation in the liver and protect against morphological consequences in the brain of AIP mice.

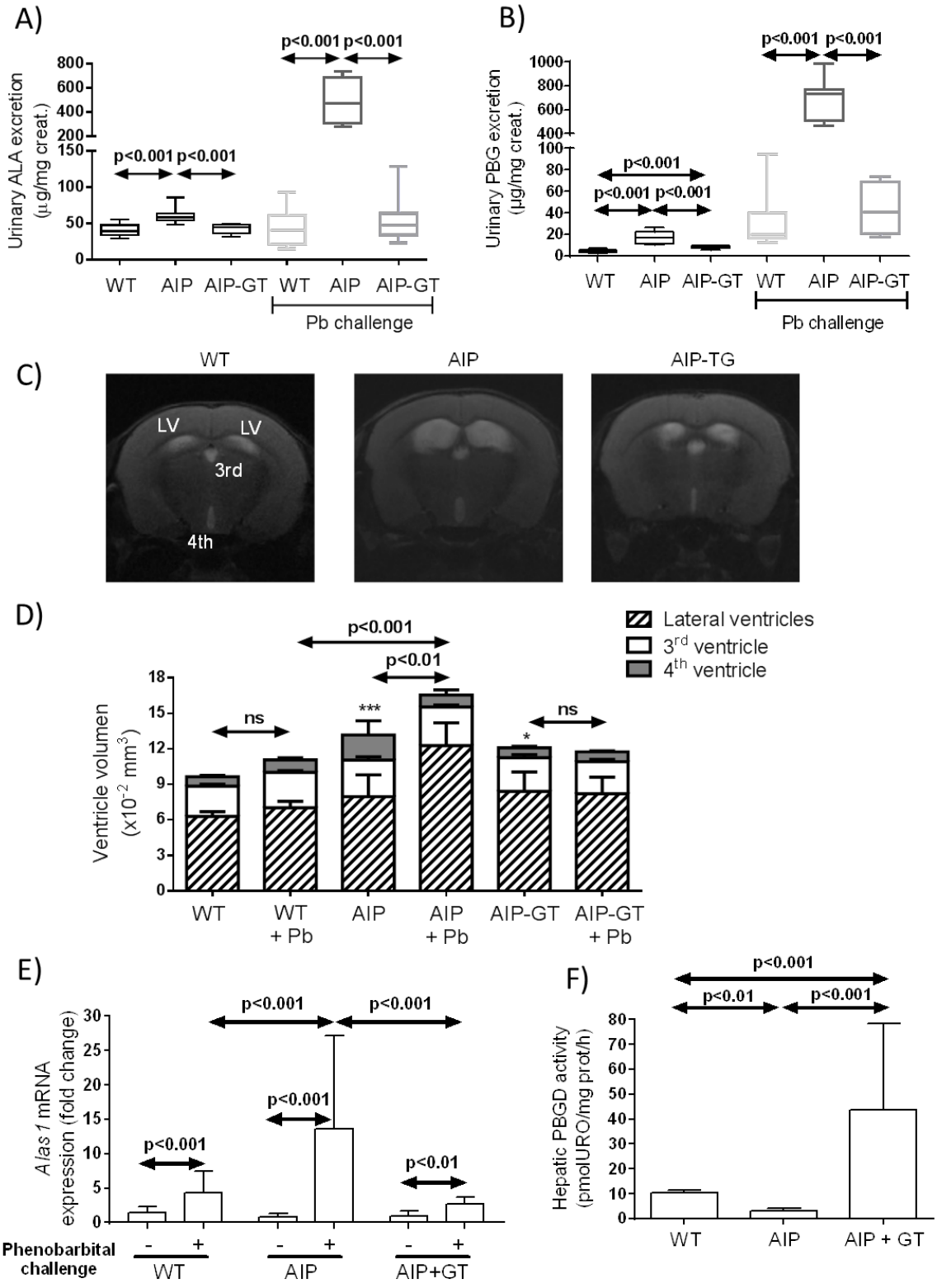

Figure 7. Biochemical parameters and BV enlargement in one-year-old WT and AIP mice with or without rAAV2/5-*PBGD* liver GT. Urinary A) ALA and B) PBG excretion in WT, AIP and AIP treated with rAAV2/5-*PBGD* GT (AIP-GT) male mice receiving or not Pb challenge every two weeks for 8 months. C) Representative T2-weight MRI of one animal corresponding to WT, AIP and AIP-GT groups. D) Volume measurements of 3rd, 4th and lateral ventricles in

WT, AIP and AIP-GT mice receiving or not recurrent Pb challenges. E) Hepatic *Alas1* expression before and after the last 4-days period of Pb challenge in WT and AIP mice groups. Those animals exposed to Pb challenge received an additional Pb dose after the fourth dose and were euthanized 20 min later to study the induction of hepatic expression of *Alas1.* F) Hepatic PBGD activity at sacrifice. Data are mean ± SD *, $p < 0.05$; ***, $p < 0.001$ vs WT group.

Histological examination of brain slices was performed in a new cohort of 6- to 7-month-old mice receiving three consecutive Pb challenges (every two weeks). Brain from these animals did not show any evidence of ischemic areas or neuronal damage or death (Fig. 8A–D). In the grey matter of AIP mice, we observed a denser neurofilament pattern in layers located in the periventricular areas, but no changes in neuronal cellularity or abnormalities in neural fibre structures (Fig. 8E–H). These data suggest that the enlarged BV size found in AIP mice cannot be related to brain atrophy or neuronal cell loss.

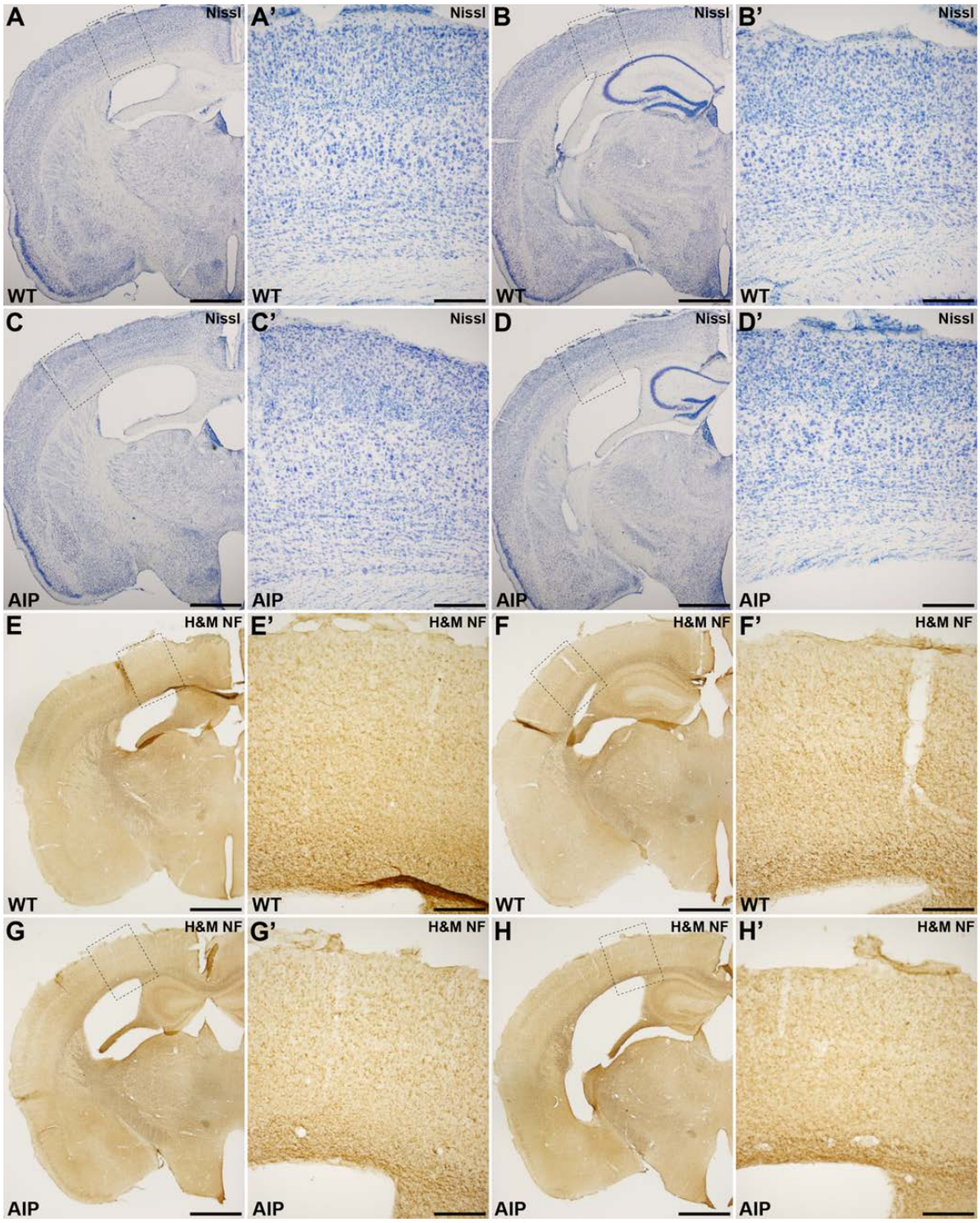

Figure 8. Brain histological analysis in consecutive coronal sections of WT and AIP mice to determine neuronal damage. Classical histological analysis to label neuronal populations and identify the basic neuronal structure (Nissl staining) was performed in two WT (A,A´ and B,B´) and two AIP (C,C´ and D,D´) mice (6– to 7–month-old at sacrifice) after three consecutive Pb challenges (every two weeks). High and medium molecular weight neurofilaments were stained by immunohistochemistry in these WT (E, E´ and F, F´) and AIP (G, G´ and H, H´) mice in consecutive coronal sections. BV atrophy and a narrowing of neurofilament layers were

observed in the nearest region of the BV in the brain of AIP mice. Scale bar: 1000 μm in A-H panels and 200 μm in A´-H´ panels.

1.2. Decreased brain perfusion in AIP mice

In addition to the augmented size of BV, AIP mice showed a 39 % reduction in brain perfusion as compared to WT animals (Fig. 9A). Importantly, CBF showed normal levels in AIP mice treated with rAAV2/5-*PBGD* recalling the improvement of brain perfusion that occurs in patients after reducing strong heme precursors accumulation associated with their acute attacks [112]. In mice undergoing recurrent Pb-induced attacks, CBF measurement performed 24 h after the last challenge showed a reduction in both WT and AIP animals (Fig. 9A). Thus, Pb masked the effect of the acute porphyria attack on CBF parameter in mice.

Unlike what was observed in patients, plasma EDN1 in WT and AIP mice with or without rAAV2/5-*PBGD* showed similar levels (Fig. 9B). Pb challenge increased its plasma concentration similarly in all three groups (Fig. 9B). Given that EDNRB plays a major role in the clearance of circulating EDN1 [113], we also measured the expression of this receptor in the liver and different brain regions (Fig. 9C–F). In the liver, the expression levels of *Ednrb* gene were lower in AIP mice than in WT and AIP mice treated with rAAV2/5-*PBGD*, although the differences only reached statistical significance in the last group (Fig. 9C). Indeed, while the administration of Pb did not modify its liver expression in AIP mice, it caused an increase in those mice that received liver-directed GT (Fig. 9C).

An interesting finding was that AIP mice exhibited an increase of EDNRB in the CA1 hypothalamus region, which is located adjacent to the BV space in the mouse brain (Fig. 10A-A´ and B-B´). In AIP mice, the *Ednrb* gene showed higher expression levels in the hippocampus (Fig. 9D) and hypothalamus (Fig. 9E) brain regions than WT mice,

but similar expression levels in the brain cortex of both WT and AIP mice (Fig. 9F). These data indicate that changes in *Ednrb* expression were limited to specific regions of the AIP mice brain. Of interest, *Ednrb* over-expression in the CA1 hypothalamus was reversed in animals treated with liver-directed GT (Fig. 9E and Fig. 10C-C'). Given that Pb greatly alters cerebral perfusion, none of these animals received barbiturates.

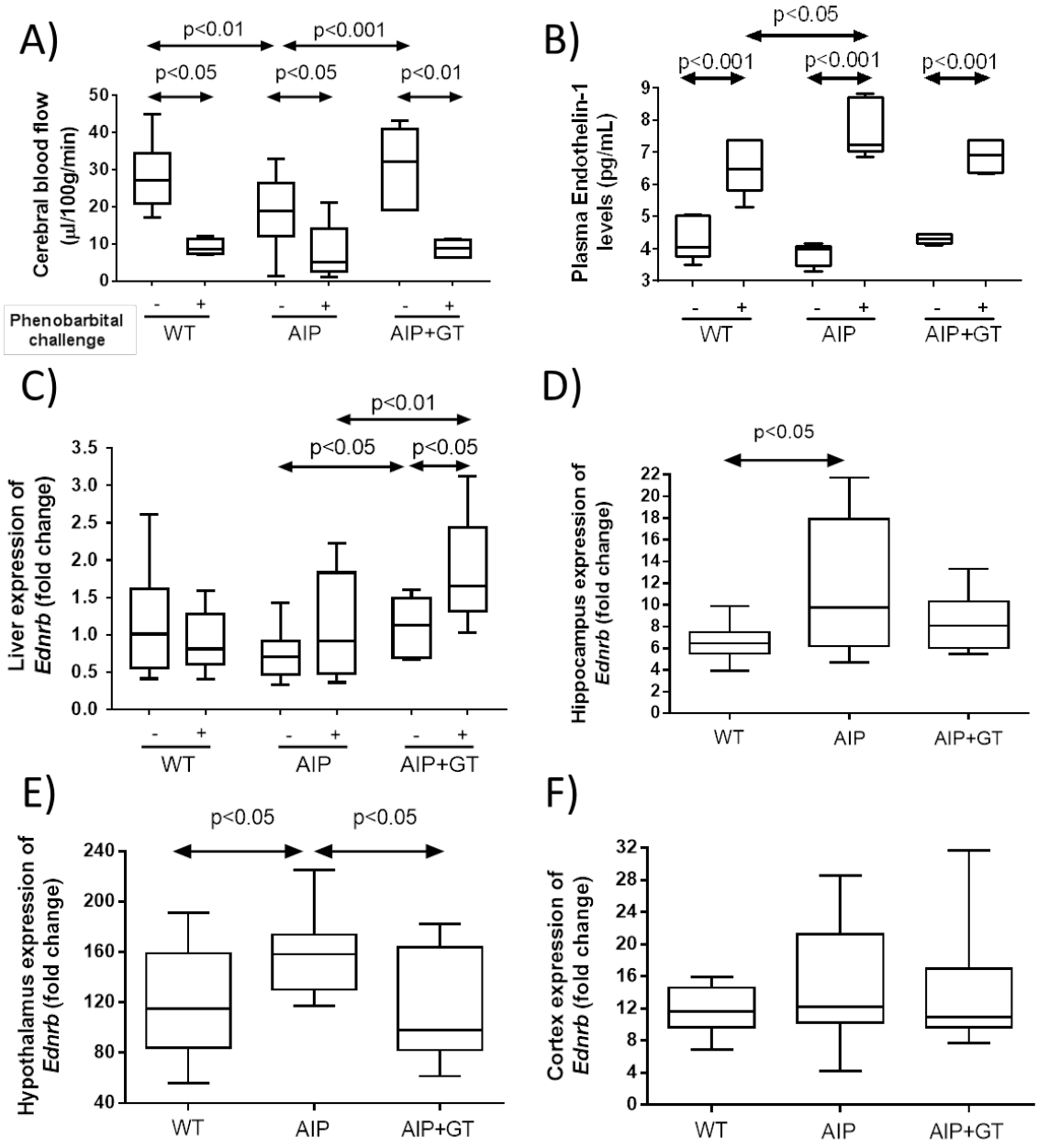

Figure 9. CBF, plasma EDN1 levels and the expression of *Ednrb* in WT and AIP mice receiving or not a single dose of rAAV2/5-*PBGD*. A) CBF was measured by arterial spin

labelling. B) Plasma EDN1 levels was determined by ELISA immunoassay in WT and AIP mice treated or not with PBGD-liver GT. C) Hepatic expression of *Endrb* gene before and after a 4-day period of Pb challenge in the indicated groups of animals. Endrb expression was also measured in D) hippocampal, E) hypothalamus, and F) cortex brain regions in the indicated groups of mice that never received Pb. Data are mean ± SD.

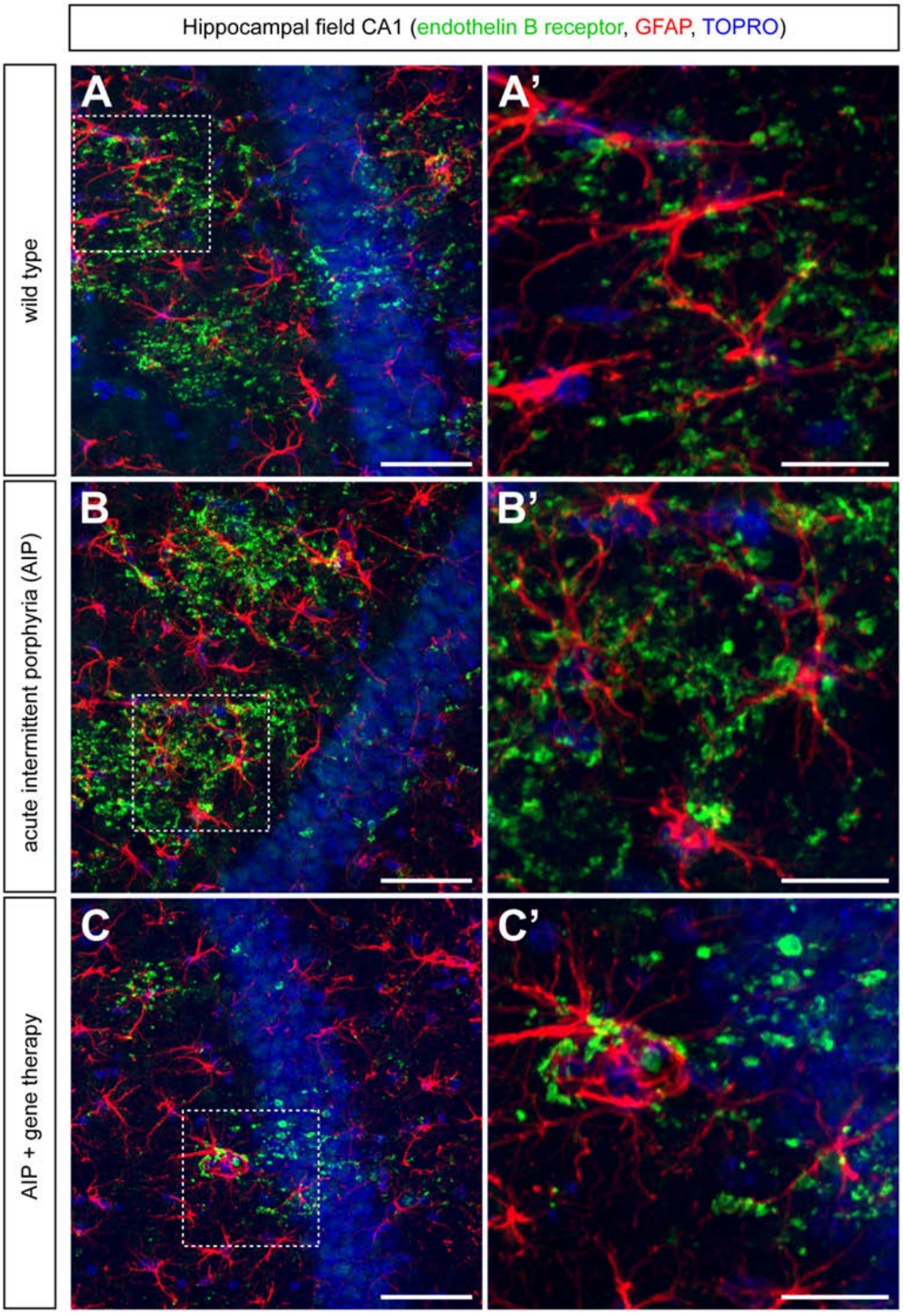

Figure 10. ENDRB and glial fibrillary acidic protein (GFAP) in hippocampus. Representative hippocampus sections of A) a WT, B) an AIP and C) an AIP mouse treated with liver-directed GT. Paraformaldehyde-fixed mouse brains from animals presented in Fig. 8 were

immunostained for EDNRB and GFAP. Alexa Fluor-labelled secondary antibody TOPRO-3 was used for nuclear staining. Scale bar: 650 µm in A, B and C panels and 20 µm in A', B′ and C′ panels.

Overall, our findings suggest that small vessel dysfunction might cause an imbalance in CBF and BV enlargement. Of interest, augmenting hepatic PBGD levels protect against porphyrin precursors accumulation, corrected CBF and prevented the progressive BV enlargement occurring in AIP mice subjected to repeated acute attacks.

2. mRNA-based therapy in a rabbit model of VP offers new insights into the pathogenesis of acute attacks

2.1. Biochemical characterization of a novel rabbit model of VP

Combined administrations of eleven doses of AIA (350 mg/kg, s.c.) and twelve doses of Rif (200 mg/kg, i.p.) in rabbits during 20 days strongly induced *Alas1* and *Ho-1* gene expression in the liver (Fig. 11A-B), the rate-limiting enzymes of heme synthesis and its catabolism, respectively. Besides the induced hepatic *Alas1* gene expression (Fig. 11A), an increased ALAS1 protein level was also observed by immunoblot (Fig. 11C). While recurrent co-administration of AIA and Rif induced both gene expression and activity of the hepatic ALAD enzyme (Fig. 11D, left and right panels, respectively), the other cytoplasmic enzymes of the pathway, that is, PBGD, UROS, and UROD, remained unchanged (Fig. 11E-G).

Finally, a significant inhibition was observed in the activity of the three mitochondrial enzymes that catalyse the last steps of heme synthesis; that is, CPO, PPO, and FC (Fig. 11H-J, right panels). However, the expression of their respective genes was repressed, unchanged, and induced, respectively (Fig. 11H-J, left panels). These data

suggest that metabolites derived from AIA and Rif directly interfere with the activity of the last three enzymes of the pathway, mainly PPO, and greatly activate heme synthesis and catabolism pathway.

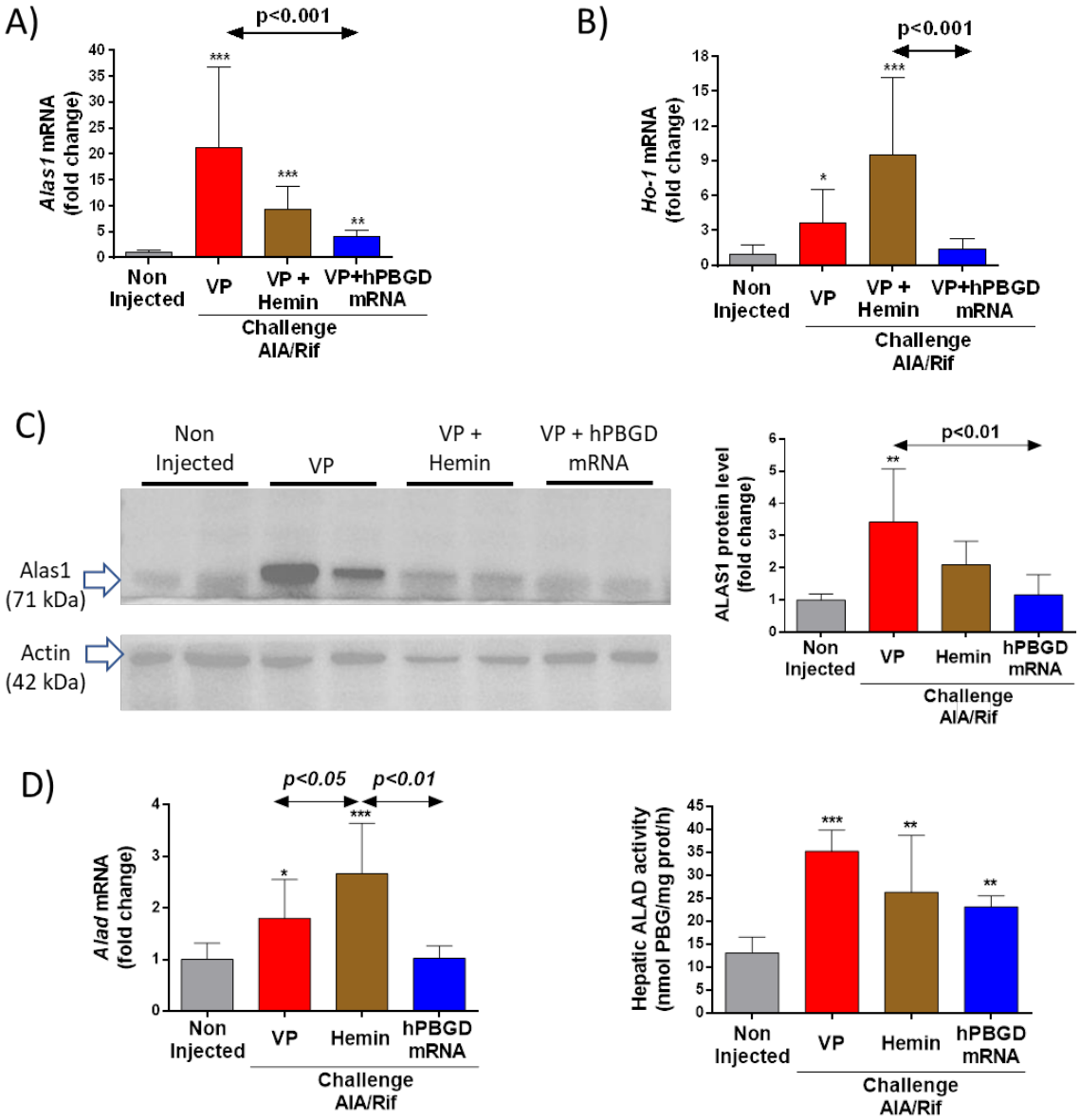

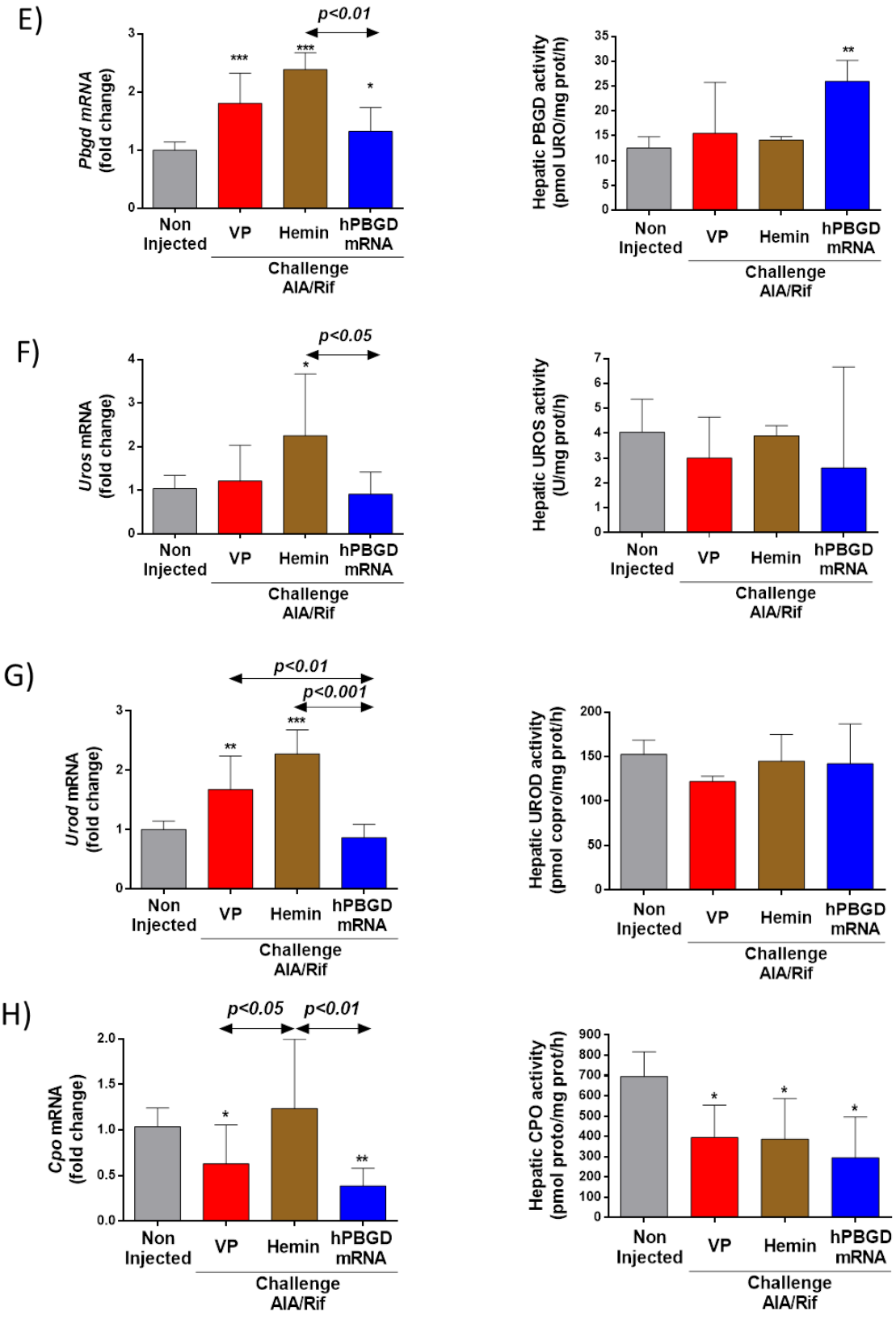
E)
p<0.01
Pbgd mRNA (fold change)
Hepatic PBGD activity (pmol URO/mg prot/h)
F)
p<0.05
Uros mRNA (fold change)
Hepatic UROS activity (U/mg prot/h)
G)
p<0.01
p<0.001
Urod mRNA (fold change)
Hepatic UROD activity (pmol copro/mg prot/h)
H)
p<0.05
p<0.01
Cpo mRNA (fold change)
Hepatic CPO activity (pmol proto/mg prot/h)
Non Injected
VP
Hemin
hPBGD mRNA
Challenge AIA/Rif

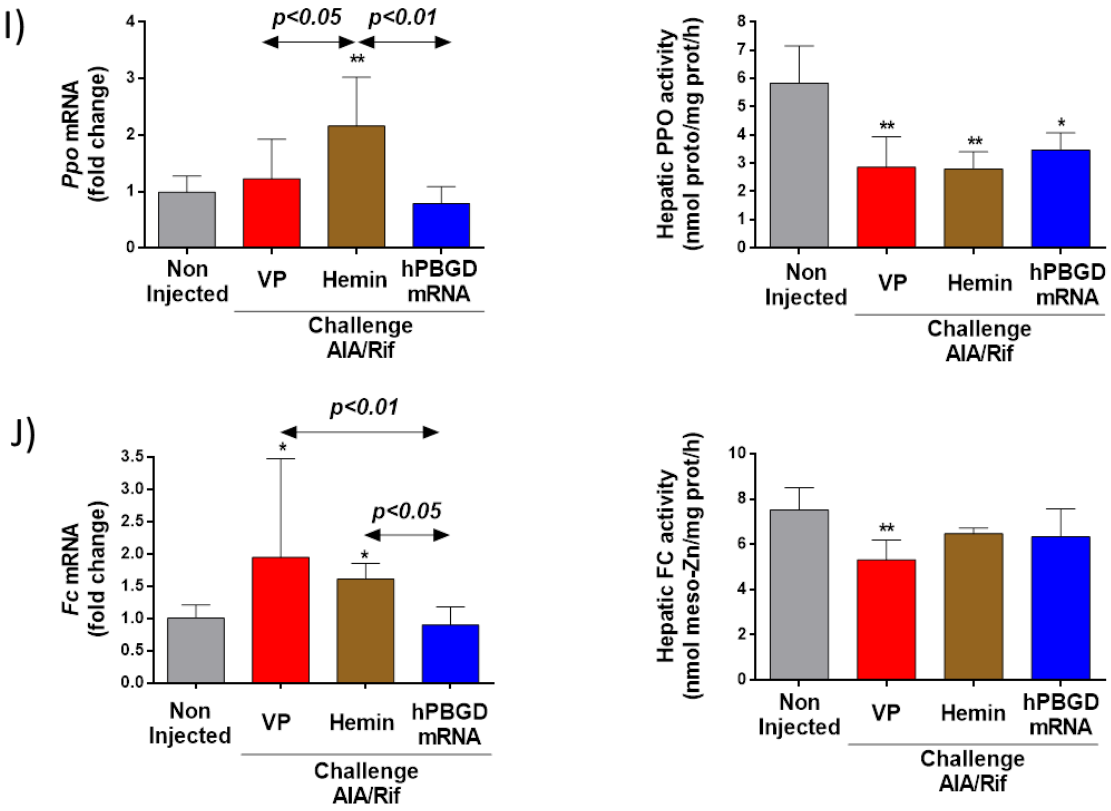

Figure 11. Gene expression and biochemical status of the heme biosynthesis pathway in the liver of VP rabbits and the effects of hemin and hPBGD mRNA administration. All measurements were performed in liver samples at sacrifice. Gene expression of A) *Alas1* and B) *Ho-1*. C) Immunoblot detection of Alas1 protein. β-actin was used as protein loading control. Quantification of bands was performed using the Image J program in a total of 4 different WB. Gene expression measurements of D) ALAD, E) PBGD, F) UROS, G) UROD, H) CPO, I) PPO and J) FC enzymes of the heme biosynthetic pathway. Data are mean ± SD. *, $p < 0.05$; **, $p < 0.01$; ***, $p < 0.001$ vs non-injected rabbits.

As a consequence of the heme synthesis and catabolism pathways alterations, high levels of PBG (Fig. 12A-B) and porphyrins (Fig. 12C) were measured throughout the study in urine samples. Indeed, total urinary excretion of heme precursors on the last day of the study increased by 80-fold in challenged rabbits when expressed as moles of ALA (2 mol of ALA are required to form 1 mol of PBG and 8 mol of ALA form one porphyrin) (Fig. 12D).

No significant increase of urinary ALA levels (Fig. 12E) occurred until the third challenge (D15), which was the longest (5 days of challenge). The elevated PBG/ALA ratio in the urine samples may be due to highly increase of the hepatic ALAD activity (nearly 3-fold) in the challenged rabbits compared with non-injected animals (Fig. 11D, right panel). Of note, porphyrin precursor determination in cerebrospinal fluid extracted on day 20 did not show ALA accumulation (< 0.05 mM), but high PBG levels were detected in the two rabbits treated with AIA and Rif (0.47 ± 0.28 mM versus < 0.05 mM in control rabbits, n = 2) in which non-blood-contaminated cerebrospinal fluid samples could be extracted. Thus, the accumulation of the ALA metabolite requires an extended induction of the heme synthesis pathway in this model.

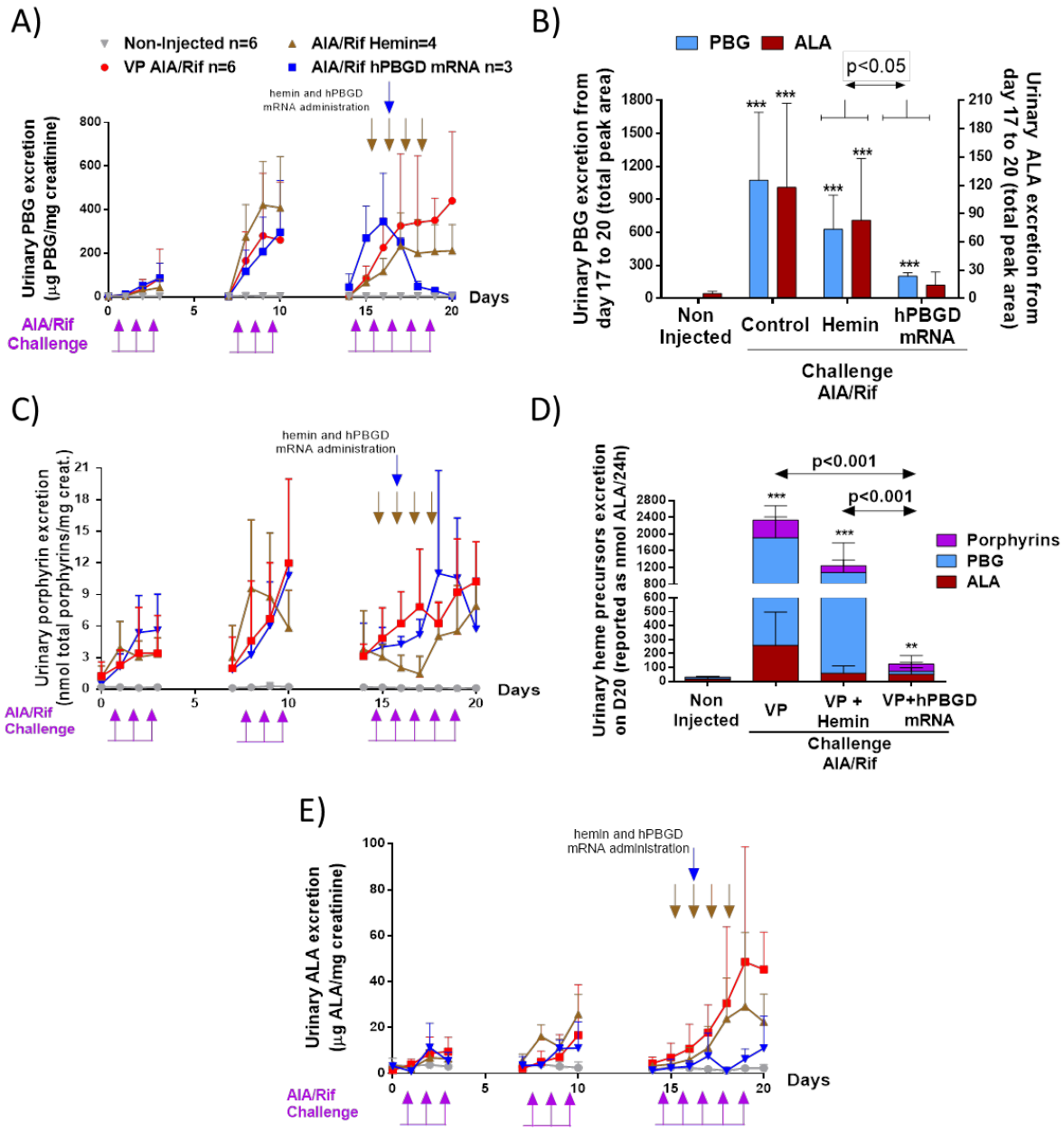

Figure 12. Biochemical characterization of the VP model in rabbits and protection effects of hemin and hPBGD mRNA against porphyrin precursors and porphyrin accumulation. Thirteen female New Zealand rabbits were challenged with AIA and Rif during 20 days. Of these, hemin (8 mg/kg) was i.p. injected into 4 animals on days 15–18 (brown arrows) and hPBGD mRNA (0.5 mg/kg) was i.v. administered on day 16 (blue arrow) in 3 rabbits. A) Urinary PBG excretion over time. B) Quantification of the total peak area of the urinary PBG and ALA excretion between days 17 and 20. C) Urinary porphyrin excretion over time. D) Total urinary accumulation of heme precursors on day 20 reported as nmol ALA per 24 h (two ALA molecules are required to synthesize a PBG monopyrrole, and eight ALA molecules are required to synthesize one porphyrin). E) Urinary ALA excretion over time. Data are mean ± SD. *, $p < 0.05$; **, $p < 0.01$; ***, $p < 0.001$ against the non-injected group.

Highly carboxylated porphyrins, that is, the octocarboxylated uroporphyrin and heptacarboxylporphyrin fractions, predominated in urine samples when compared to tetracarboxylated coproporphyrin and pentacarboxylporphyrin (Fig. 13A). Plasma porphyrin levels were also very high (Fig. 13B), with a specific plasma fluorometric emission maximum around 623 nm for most of the samples. In VP patients, plasma fluorescence emission maximum λ are characteristically around 626 nm, whereas they are around 620 nm in AIP patients [6,114]. After protein precipitation in plasma samples from two animals challenged with AIA and Rif, porphyrin concentrations dropped by a half (from 2,276 ± 234 nmol/L total porphyrin to 1,057 ± 59 nmol/L free porphyrin), which suggests a major accumulation of protoporphyrinogen bound to proteins.

Finally, repeated administration of AIA and Rif increased fecal porphyrin excretion (132 ± 74 nmol/g, n = 2; normal values < 30 nmol/g). Fecal porphyrin fractionation showed a major peak of dicarboxylic protoporphyrin (84 % protoporphyrin, 2.6 % harderoporphyrin, 7.9 % coproporphyrin, 1.5 % isocoprophyrin, 3.0 % pentaporphyrin, 0.2 % hexaporphyrin, 0.1 % heptaporphyrin, and 0.6 % uroporphyrin) (Fig. 13C). Tetracarboxylic coproporphyrin can be excreted in both urine and feces. Preferential urinary excretion of the coproporphyrin in this model (31.6 % ± 16.8 % in urine versus 9.4 % ± 4 % in feces, $p < 0.03$) may be due to energy metabolism saving compared to the biliary secretion, which is energetically more expensive.

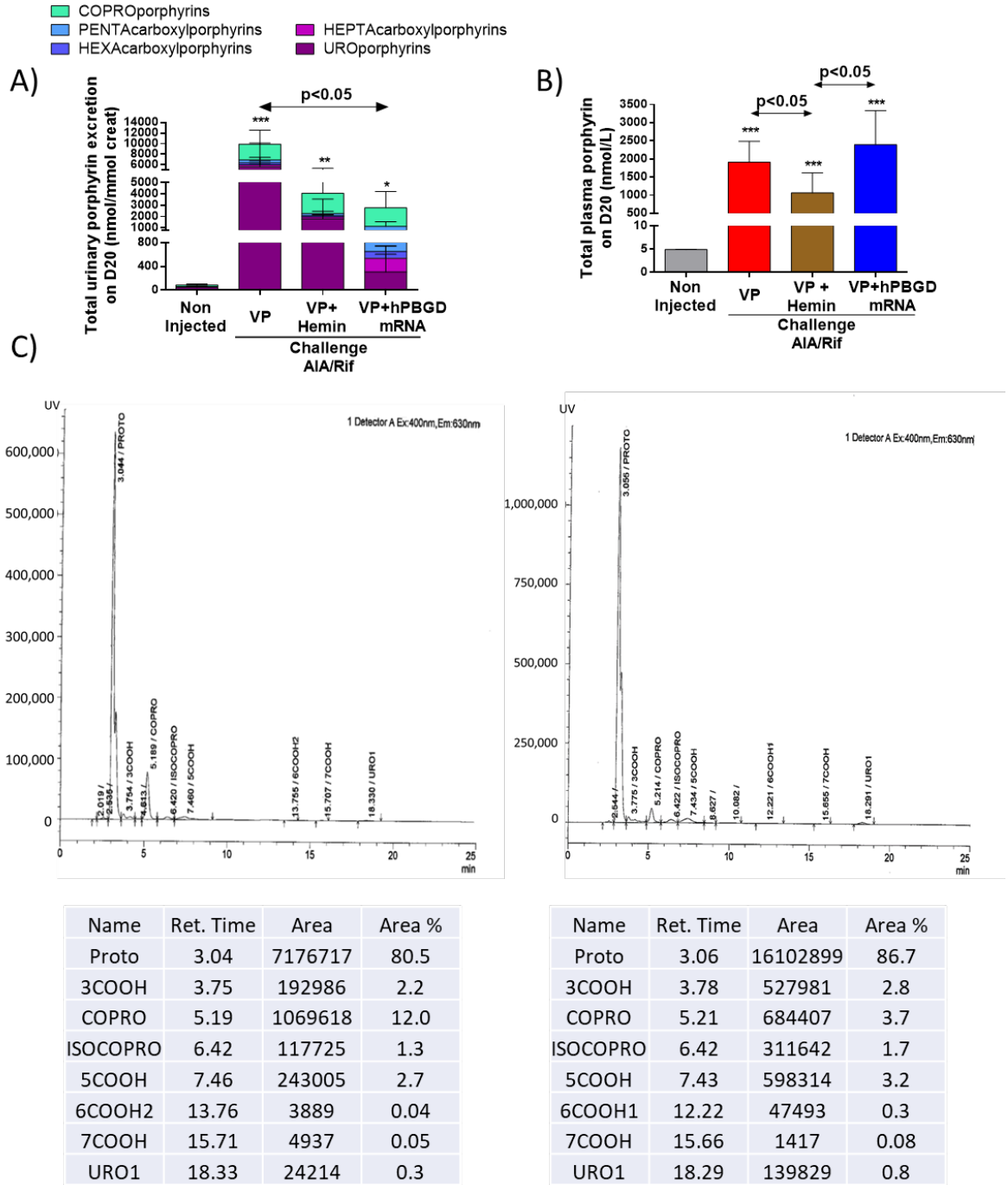

Name	Ret. Time	Area	Area %
Proto	3.04	7176717	80.5
3COOH	3.75	192986	2.2
COPRO	5.19	1069618	12.0
ISOCOPRO	6.42	117725	1.3
5COOH	7.46	243005	2.7
6COOH2	13.76	3889	0.04
7COOH	15.71	4937	0.05
URO1	18.33	24214	0.3

Name	Ret. Time	Area	Area %
Proto	3.06	16102899	86.7
3COOH	3.78	527981	2.8
COPRO	5.21	684407	3.7
ISOCOPRO	6.42	311642	1.7
5COOH	7.43	598314	3.2
6COOH1	12.22	47493	0.3
7COOH	15.66	1417	0.08
URO1	18.29	139829	0.8

Figure 13. Porphyrin accumulation in urine, plasma and stool samples. A) Urinary excretion of individual porphyrins and B) total plasma porphyrin levels on day 20. C) Porphyrin chromatograms in stool samples corresponding to a non-injected rabbit (left) and a rabbit challenged with AIA and Rif (right) on day 20. Data are mean ± SD. *, $p < 0.05$; **, $p < 0.01$; ***, $p < 0.001$ against the non-injected group.

Overall, this model recapitulates high porphyrin and porphyrin precursor accumulation in a pattern similar to patients with VP. About 50% inhibition of normal PPO activity and

high induction in regulatory enzymes of the heme synthesis and catabolism suggest that this model reproduces the severe form of VP in humans.

2.2. Effect of hemin and hPBGD mRNA administration on heme precursors accumulation

The administration of four doses of hemin, the current standard of care for acute attacks in humans, only showed a slight reduction in hepatic *Alas1* gene expression (Fig. 11A) and protein level (Fig. 11C), but further increased *Ho-1* expression (Fig. 11B). For the rest of the enzymes of the heme synthesis, their hepatic activity was not modified, although their expression increased after hemin administration (Fig. 11D-J). As a result of the hemin treatment, the urinary excretion of porphyrin precursors (Fig. 12A-B and D-E) and porphyrins (Fig. 12C-D and Fig. 13A), as well as plasma porphyrin levels (Fig. 13B), were only slightly reduced.

Although this model showed significant PBG accumulation, recurrent challenges with AIA and Rif did not modify hepatic PBGD activity (Fig. 11E). Of note, the administration of a single dose of hPBGD mRNA on day 16 (D15 challenge) increased hepatic PBGD activity 2-fold, as measured on day 20 (Fig. 11E). As a result, PBG excretion was normalized (Fig. 12A-B), and the increase in urinary ALA excretion that occurred in the VP group on day 17 was not observed (Fig. 12B and E). The administration of hPBGD mRNA increased urinary porphyrin levels during the 2 days post-injection (Fig. 12C). This is likely due to the monopyrrole PBG being rapidly metabolized by exogenous PBGD to form tetrapyrrole porphyrins. On day 20, 4 days after hPBGD mRNA administration, the liver of treated rabbits showed normal expression levels of the key regulatory enzymes of heme synthesis (*Alas1*, Fig. 11A) and catabolism (*Ho-1*, Fig. 11B), which correlated with the normal urinary excretion of heme precursors observed (Fig. 12D).

In a separate acute treatment study, hPBGD mRNA was administered when high urinary concentrations of both PBG and ALA were observed (2 h after the third AIA dose in a 4 day AIA/Rif challenge). The administration of a single hPBGD mRNA dose (0.5 mg/kg, i.v.) significantly reduced serum accumulation of PBG (Fig. 14A) and ALA (Fig. 14B) within 8 h, and rabbits recovered normal serum levels of these two precursors by 22 h post-injection.

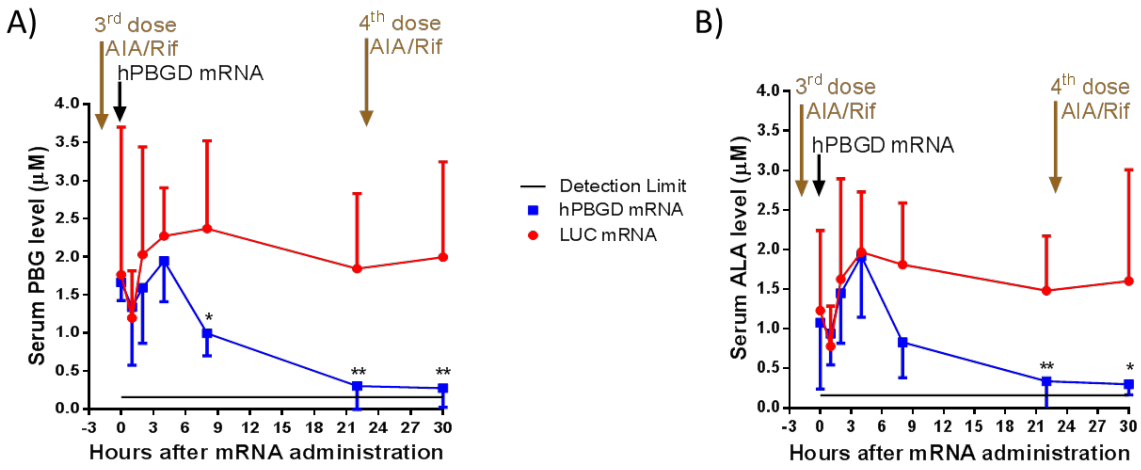

Figure 14. Serum A) PBG and B) ALA accumulation. Serum metabolites were measured just before 1, 2, 4, 8, 22 and 30 h post-injection of a single i.v. 0.5 mg/kg of hPBGD mRNA. The mRNA-based treatment (n = 5) was administered 2 h after the third AIA in a 4 day AIA/Rif challenge. The control group (n = 5) were treated with 0.5 mg/kg of luciferase (LUC) mRNA. Data are mean ± SD. *, $p < 0.05$; **, $p < 0.01$ vs Luc mRNA group.

2.3. Liver status and functionality of hepatic hemoproteins

The liver of VP rabbits showed normal weight (93.9 ± 5.3 g versus 88.2 ± 7.3 g in the control group) and normal histology after hematoxylin-eosin staining for microscopy evaluation (Fig. 15A-B). However, liver tissue immunostaining for MT-CO1 of the respiratory complex IV showed an abnormal distribution on the periphery of hepatocytes (Fig. 15C).

A) Non-injected rabbit

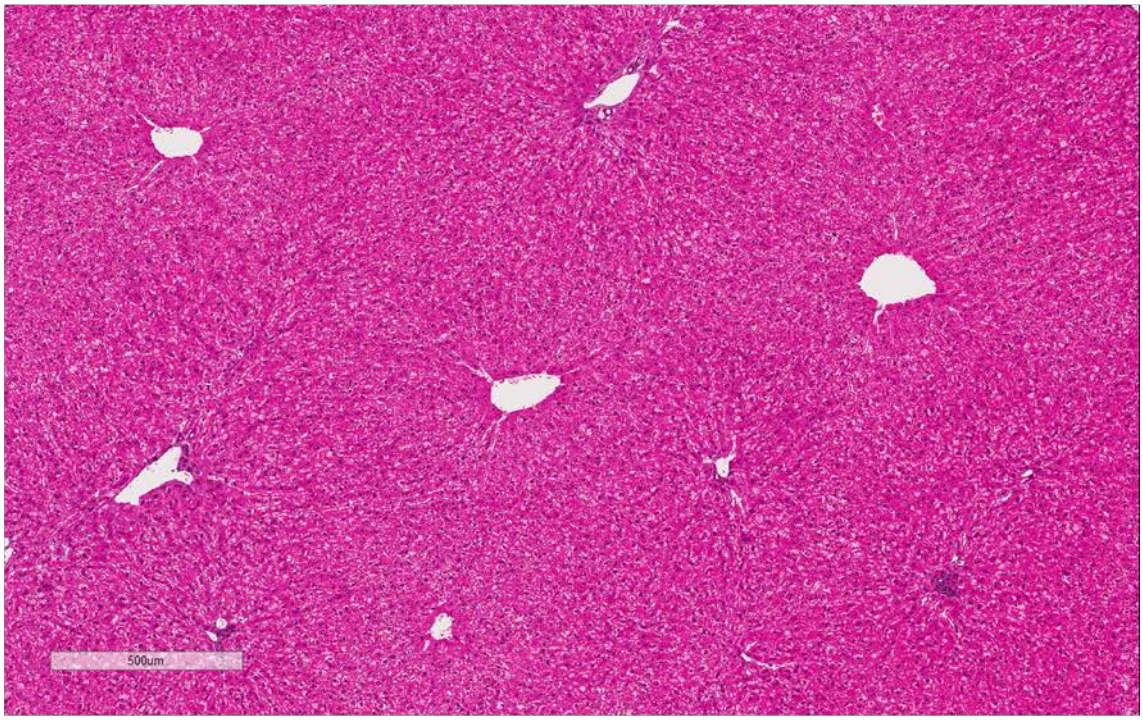

B) AIA/Rif challenged rabbit

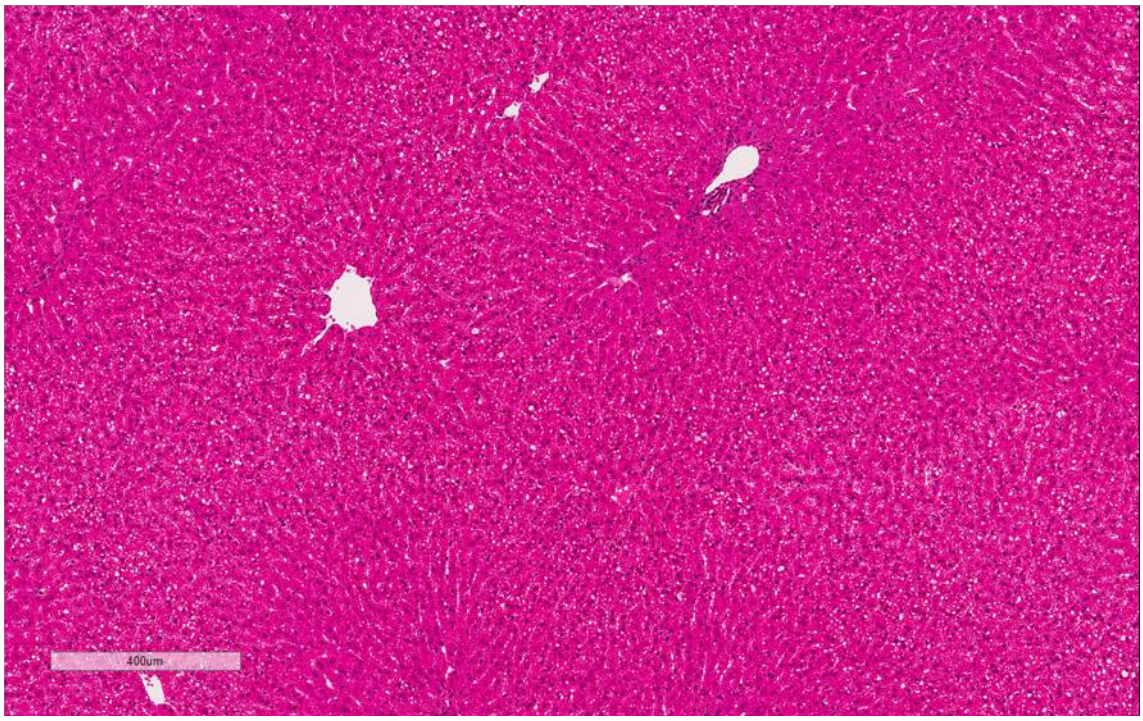

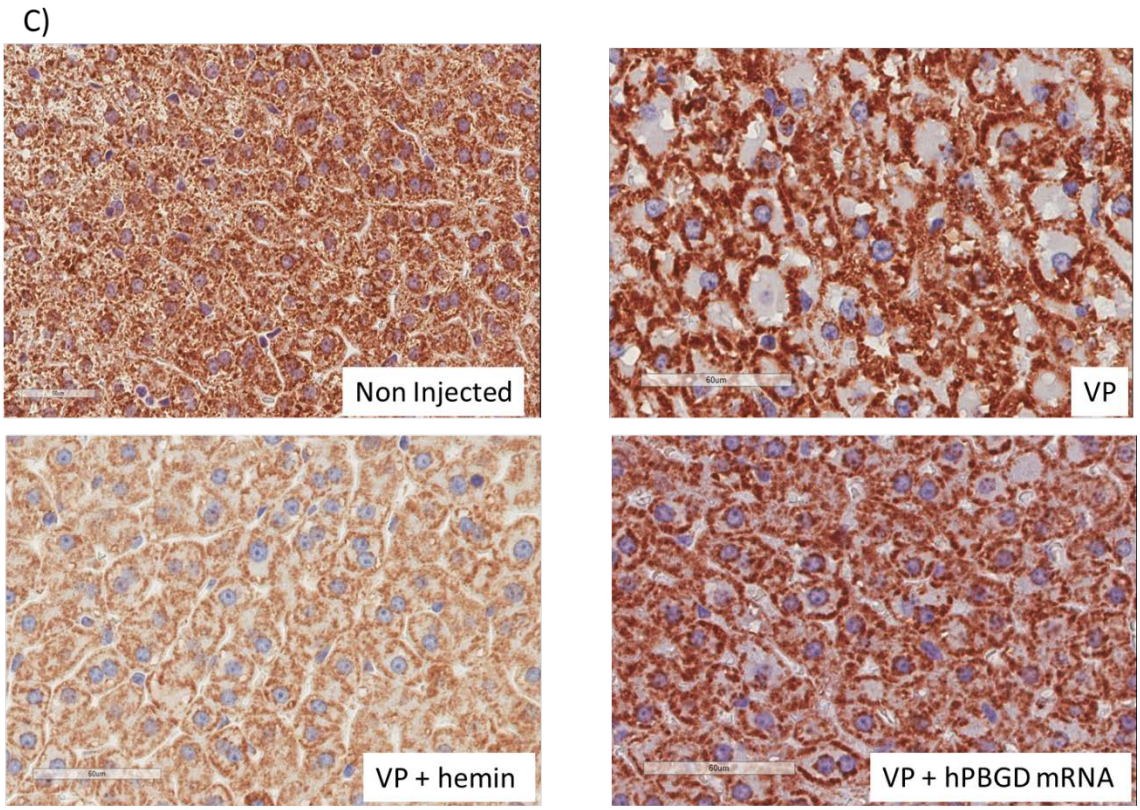

Figure 15. Representative microscopy images of liver sections from A) a non-injected rabbit and B) an AIA/Rif challenge rabbit after hematoxylin-eosin staining for the histological evaluation and C) anti-MTCO-1 immunostaining for mitochondria detection. Scale bar: A) 500 µm, B) 400 µm and C) 60 µm.

Regarding liver functional status, serum ALP levels were normal (Fig. 16A), while a slight increase in liver ALT was observed on day 20 (Fig. 16B).

Mitochondrial energy metabolism was examined in mitochondria isolated from the liver of VP rabbits by determining the activity of the mitochondrial oxidative phosphorylation (OXPHOS) complexes I–IV and the analysis of the complex protein levels, using an OXPHOS antibody cocktail. The activities were measured at the maximum enzymatic rate with saturation of substrates and were therefore independent of the contribution of the TCA cycle. Our results suggest that mitochondrial complex I, II, III, and IV enzyme activities are markedly reduced in VP rabbits (Fig. 16C), although only the protein levels of complex IV showed a significant decrease (Fig. 16D-E). These data suggest a

malfunction of the first three mitochondrial respiratory chain complexes combined with expression inhibition of complex IV.

Of note, complex IV contains heme A, whereas complex II has type B, and both heme B and C are present in complex III. Type B and C are similar to protoheme and they are not chemically modified before assimilation into the corresponding apoprotein. In contrast, heme A needs further modifications by addition of farnesyl and formyl groups to protoheme [115]. In the VP rabbits, the administration of AIA and Rif greatly increased hepatic heme (Fig. 16F) and mitochondrial hepatic heme A (Fig. 16G) levels. Of interest, animals that received hPBGD mRNA further increased heme A levels (Fig. 16G), displayed normal complex IV protein levels (Fig. 16D), and partially reversed the activity deficiency of the four mitochondrial complexes (Fig. 16C). Hemin (ferric chloride heme) administration failed to normalize either the amount of protein in complex IV (Fig. 16D) or the activity of complexes I–IV (Fig. 16C).

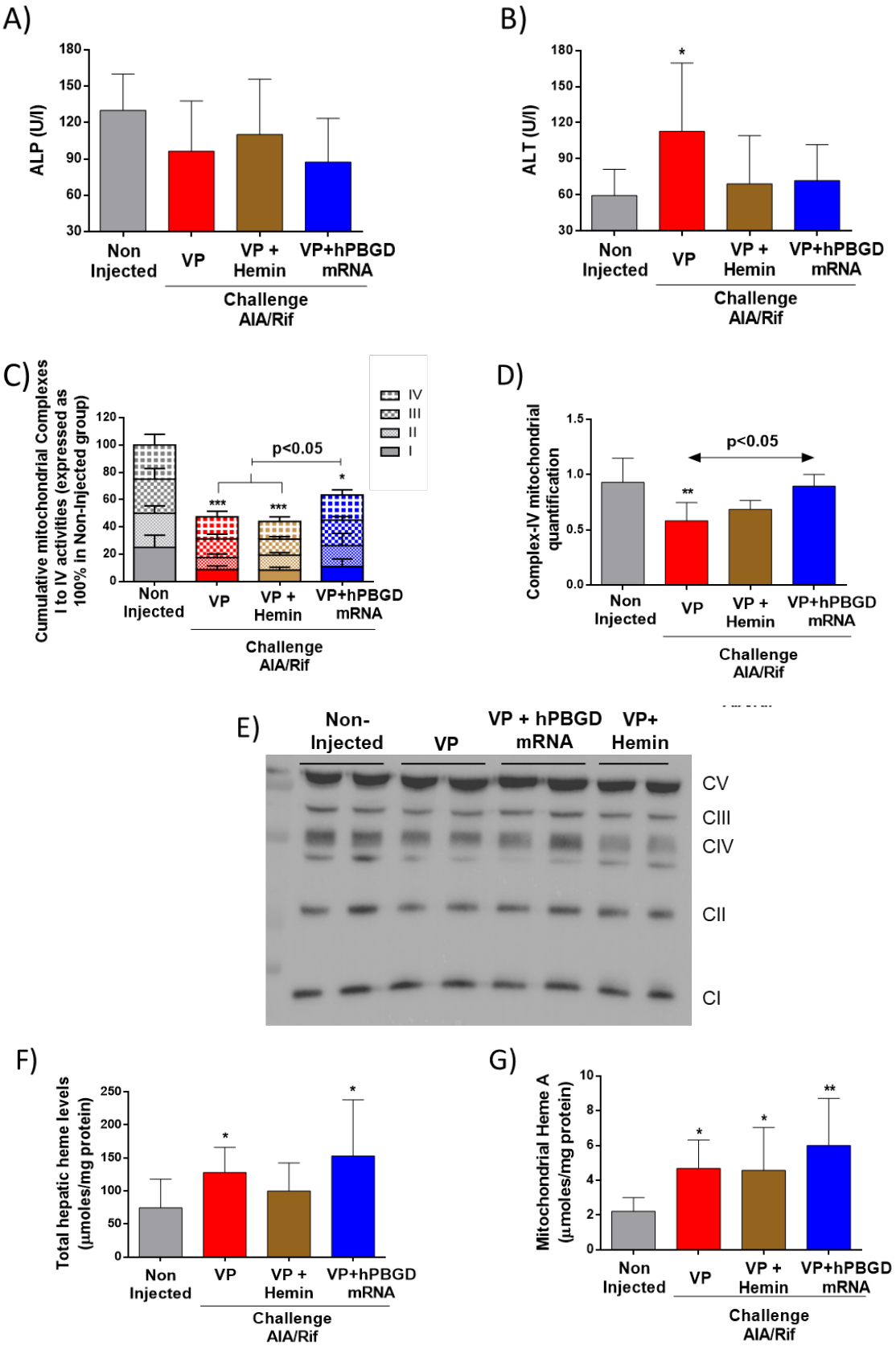

Figure 16. Liver status and function in rabbits challenged with AIA and Rif and the effects of the administration of hemin and hPBGD mRNA. Serum A) ALP and B) ALT levels from

cardiac-puncture blood samples taken at sacrifice (day 20). C) Cumulative activity of the mitochondrial respiratory complexes I–IV. D) Mitochondrial complex IV content as quantified by WB from liver samples. E) Representative image of immunoblot against OXPHOS antibody. The mitochondrial respiratory complex V is the ATP synthase. F) Total heme and G) mitochondrial heme A content measured in liver samples. Data are mean ± SD. *, $p < 0.05$; **, $p < 0.01$; ***, $p < 0.001$ against non-injected group.

Dysregulation of the mitochondrial respiratory chain and a high accumulation of porphyrin precursors are related to the induction of oxidative stress. The expression of the hepatic *Hepcidin* gene, a peptide hormone involved in iron homeostasis and used as a biomarker of oxidative stress and inflammation [116], was strongly induced in rabbits injected with AIA and Rif (Fig. 17A). Another biomarker of oxidative stress is the *Hsp70* gene, which was also overexpressed in rabbits challenged with AIA and Rif (Fig. 17B). Finally, AIA and Rif challenges induced a progressive increase of urinary thiobarbituric acid-reactive substance (TBARS) excretion (Fig. 17C), a biomarker of lipid peroxidation [117]. It is noteworthy that the highest TBARS values were obtained in the D15 challenge (Fig. 17D) concomitant with the rise in ALA excretion (Fig. 12E). Urinary excretion of TBARS and ALA showed a remarkably high correlation (Fig. 17E; $r = 0.914$, $p < 0.001$). The administration of hemin slightly reduced ALA excretion (Fig. 12E) and protected against urinary TBARS accumulation (Fig. 17C-D) but failed to reduce hepatic *Hepcidin* expression (Fig. 17A) and further increased the expression of *Hsp70* (Fig. 17B). Rabbits treated with hPBGD mRNA showed hepatic *Hepcidin* expression (Fig. 17A), *Hsp70* expression (Fig. 17B), and urinary TBARS levels (Fig. 17C-D) within the normal range determined in the non-injected control group.

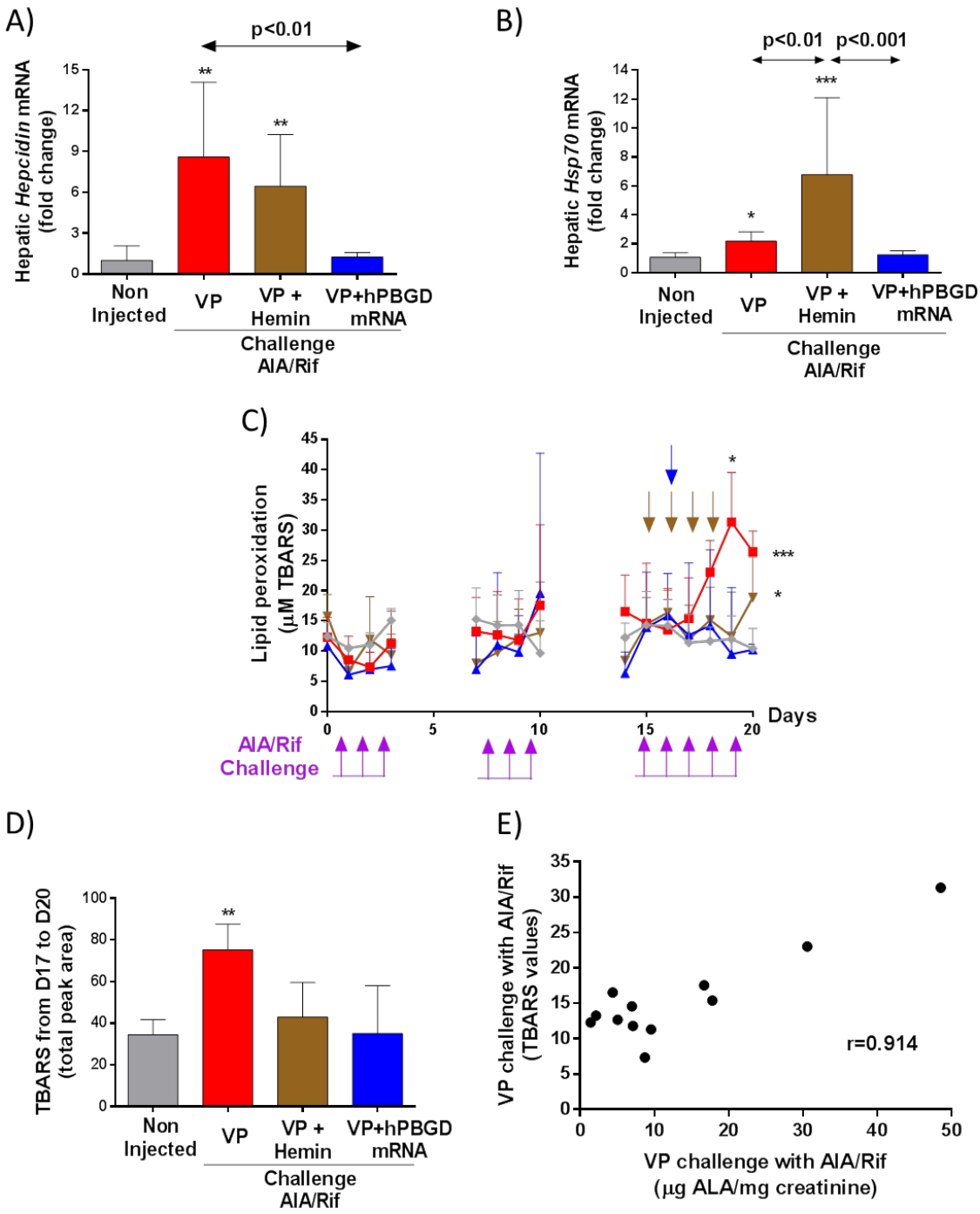

Figure 17. Protective efficacy of a single i.v. administration of hPBGD mRNA on hepatic oxidative stress and inflammation in a chemically induced rabbit model of VP. Fold change expression levels of A) *Hepcidin* and B) *Hsp70* genes determined by qPCR in the livers of VP rabbits. Protective efficacy of hPBGD mRNA against lipid peroxidation was determined by C) urine TBARS excretion over time and D) quantification of the total peak area of urinary TBARS levels on days from 17 to 20. E) Correlation between TBARS values and ALA urinary excretion, r was calculated with the Pearson correlation coefficient. Data are means ± SD. *, $p < 0.05$; **, $p < 0.01$; ***, $p < 0.001$ against non-injected group.

2.4. Clinical features of a VP model in rabbits

Systolic blood pressure in rabbits during the days 8–10 (D8) challenge (Fig. 18A) was outside the normal range calculated with results obtained from the non-injected group and significantly increased as compared with the corresponding baseline values in each animal (Fig. 18A). Both hemin and hPBGD mRNA protected these rabbits against hypertension in the D15 challenge (measured on day 18) (Fig. 18B).

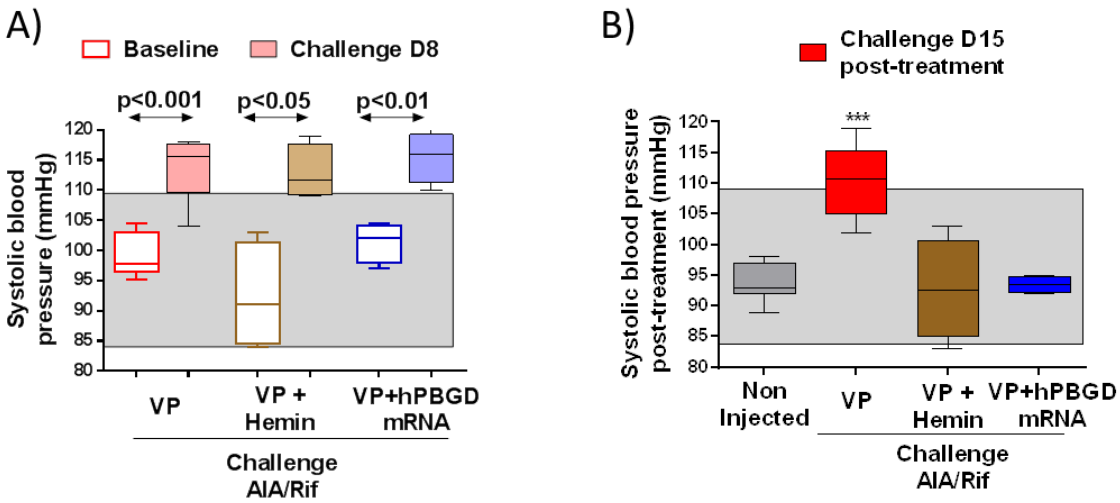

Figure 18. Systolic blood pressure. Values obtained at A) baseline (empty boxes) and D8 AIA/Rif challenge (full boxes) values. B) D15 challenge values after treatment with hemin or hPBGD mRNA. Data are mean ± SD. ***, $p < 0.001$ vs non-injected group.

Challenge with AIA and Rif induced transient motor disturbances as measured by gait difficulties (Appendix, Video 1) and abnormalities in potential evoked in the sciatic nerve (Fig. 19). Whereas the administration of four doses of hemin only partially protected against gait abnormalities, rabbits injected with a single dose of hPBGD mRNA showed normal gait (Appendix, Video 2) and amplitude values in the normal range (Fig. 19).

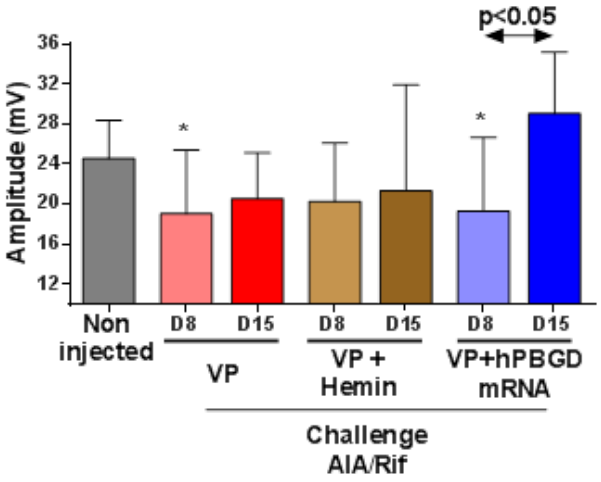

Figure 19. Amplitude of sciatic nerve in an electrophysiological nerve conduction velocity study. Study performed at the end of D8 challenge (without treatment) and D15 (after treatment). Data are mean ± SD. *, $p < 0.05$ vs non-injected group.

Finally, rabbits challenged with AIA and Rif yielded abnormal GTT results (Fig. 20A-B) and reduced tissue uptake of glucose after fasting, as measured by biodistribution of the glucose analogue ^{18}F-FDG in PET/CT imaging (Fig. 20C-D). Specific quantification of ^{18}F-FDG uptake in the brain (Fig. 20D-E) confirmed significant reduction of glucose uptake in fasted VP rabbits when compared to the non-injected control group (D8 challenge). In the D15 challenge, while hemin treatment failed to protect against these alterations, a single administration of hPBGD mRNA fully normalized GTT, measured by the time at which glucose is cleared from the blood (Fig. 20A) and total peak area (Fig. 20B) following glucose challenge. hPBGD mRNA also restored brain glucose uptake (Fig. 20D-E).

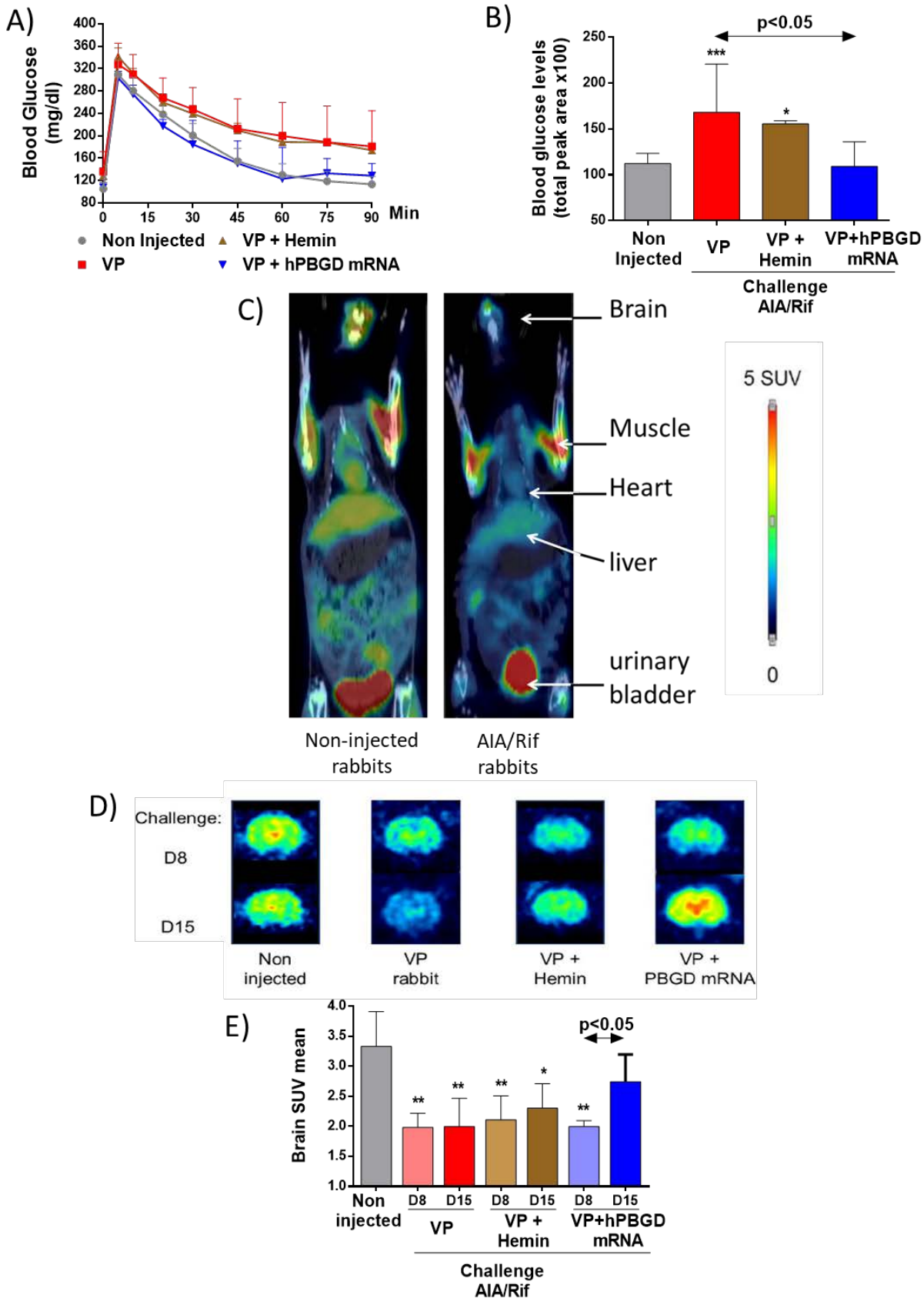

Figure 20. Glucose metabolism. A) GTT in fasted rabbits. B) Quantification of the total peak area of the GTT. Representative images of the C) body and D) brain glucose uptakes (^{18}F-FDG) in a fasted non-injected rabbit and an AIA/Rif challenged rabbit. E) Brain ^{18}F-FDG uptake in 16

h fasted rabbits performed at the end of D8 and D15 challenges. Data are mean ± SD. *, $p < 0.05$; **, $p < 0.01$; ***, $p < 0.001$ vs non-injected group.

Recurrent AIA and Rif challenge in rabbits reproduced some symptoms associated with acute porphyria attacks. Altered glucose homeostasis, liver oxidative stress, motor discoordination and changes in compound muscle action potential were associated with high accumulation of the early heme precursors upstream of the PBGD enzyme, mainly PBG. Blood pressure and the function of important hepatic hemoproteins were closely associated with heme availability. Of interest, i.v. administration of hPBGD mRNA improved all these pathological accumulation of biological molecules and behavioural disturbances associated with acute attacks, indicating that PBGD, and not PPO, was the critical enzyme for hepatic heme synthesis in VP rabbits.

3. rhApoAI-PBGD production and purification in CHO-K1SP cell line

Correction of enzymatic deficits in hepatocytes by simple systemic administration of a recombinant protein is also a desired therapeutic goal for hepatic enzymopenic disorders such as AIP. Results obtained by our research group indicate that PBGD linked to ApoAI, but not unconjugated PBGD, increases hepatic PBGD levels and abrogates acute porphyric attacks in AIP mice. Our ultimate goal was to produce and purify this conjugated protein on a large scale to undertake efficacy studies in small and large animal models described in this thesis in order to be used in preclinical trials.

Upscale production is challenging for ERT. In previous studies, we assayed the production of rhApoAI-PBGD in *E. coli* and HEK293 cell line as prokaryotic and eukaryotic host, respectively. Both approaches failed to achieve large-scale production

of rhApoAI-PBGD. Thus, our aim was to develop a new eukaryotic host for up-scale rhApoAI-PBGD protein production.

3.1. Production of rhApoAI-PBGD in CHO-K1SP cells

The biotech company GenScript subcloned our sequence of the rhApoAI-PBGD gene into the mammalian pGenHT1.0 expression plasmid. This vector has been designed to display a high capacity for expression of the therapeutic protein without resistance to antibiotics in the CHO-K1SP cell line.

The produced protein incorporates a signal peptide that allows protein secretion into the supernatant of the cell culture. This fact facilitates the purification process as the producer cells would be easily separated from the rhApoAI-PBGD by simple centrifugation or decantation. GenScript selected CHO-K1SP clones 8, 11 and 45 as the clones that constitutively overexpress rhApoAI-PBGD and had the highest productive ratios, with a titer of 24.4, 37.7 and 40.5 mg of protein/L respectively, measured by a commercial ELISA kit for ApoAI quantification.

Our first stage consisted of optimising the production of selected clones in synthetic culture medium. First, the growth ratio of each clones at two different incubation temperatures (37 ºC and 32 ºC) and 8 % CO_2 was assayed. Clone 8 showed the highest growth rate of the three selected clones and reached stationary phase of cell culture on day 7 in DYNAMIS synthetic medium supplemented with FEED B at 37 ºC (Fig. 21A-B). Although the active protein produced per day is quite similar at both tested temperatures, 32 ºC incubation allowed extending the production for three more days (Fig. 21C). Clone 45 showed the highest viability and number of CHO-K1SP cells in culture (Fig. 21A-B), and produced the highest amount of active protein at 37 ºC on day 10 of culture as measured by enzymatic PBGD activity (Fig. 21C). Of note, clone

45 incubated at 32 ºC reached those activity peak levels 2-3 days later (Fig. 21C). Both CHO-K1SP clones 8 and 45 reached the highest number of cells on day 7, regardless the culture temperature, but cells were viable during more days when incubated at 32 ºC (Fig. 21A-B). Finally, clone 11 presented a slower growth rate and was only incubated at 37 ºC (Fig. 21A-B); besides, it produced less protein than clones 8 and 45 at both temperatures, as measured by enzymatic activity (Fig. 21C). These results suggest that low incubation temperature increase cell viability without compromising the production of the rhApoAI-PBGD protein.

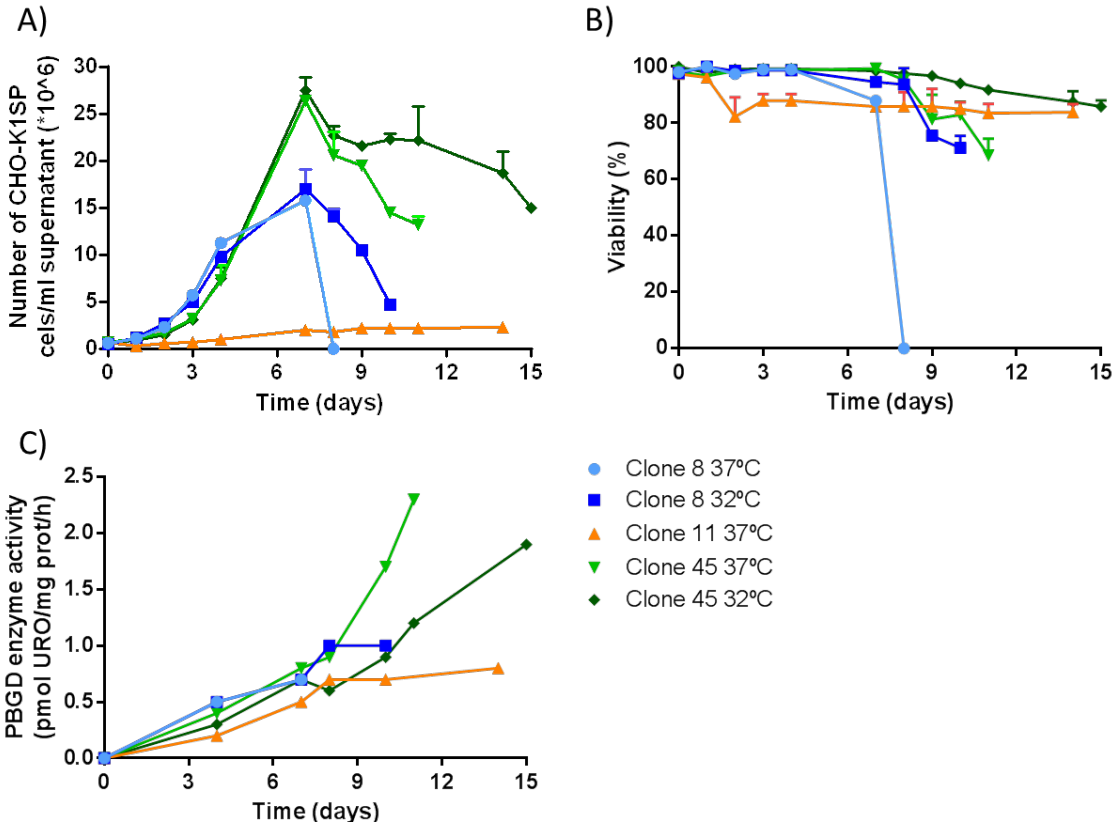

Figure 21. Growth kinetic over time of clones 8, 11 and 45 of CHO-K1SP cell line. A) Cell growth expressed as number of CHO-K1SP cells (10^6) per ml of supernatant. Cell counting was performed with Malassez chamber. B) Cell viability expressed as the % of living cells per total number of cells (living + death). C) Enzymatic activity was performed on supernatants from days 0, 4, 7, 8, 10, 11, 14 or 15.

Truncated fractions of the recombinant protein were detected in cell supernatants at both 37 ºC and 32 ºC temperatures in all three tested clones. Immunoblots against ApoAI and PBGD showed a 68 kDa protein corresponding to the full sequence of the rhApoAI-PBGD protein, and different protein fraction of 55 and 35 kDa which seem to appear over the course of days after reaching the stationary phase (Fig. 22A-B). In addition, another 20 kDa protein fraction was only detected using the anti-ApoAI antibody (Fig. 22A-C).

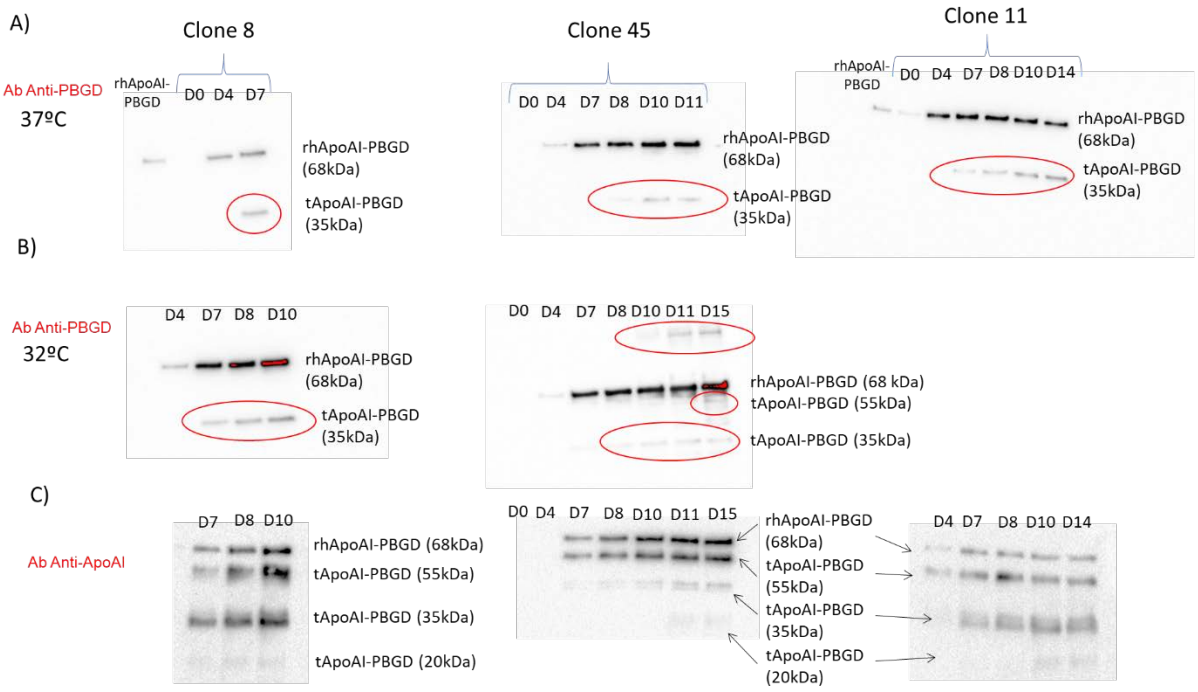

Figure 22. Supernatant of CHO-K1SP clones 8, 11 and 45 producers of the rhApoAI-PBGD protein. Representative images of immunoblots against PBGD proteins in cell supernatants from the selected clones incubated A) at 37 ºC and B) at 32 ºC. C) Immunoblot assay with an antibody against ApoAI in cells supernatants from clones 8 and 45 at 32 ºC, and clone 11 at 37 ºC. Supernatants were collected at the indicated days. tApoAI-PBGD, truncated forms of the rhApoAI-PBGD proteins.

These protein fractions were analyzed by Liquid Chromatography-Mass Spectrometry for the detection of the rhApoAI-PBGD sequence. The sequence analysis showed that

the 55 and 35 kDa protein fractions have lost the final 3' region of the domain 3 of rhApoAI-PBGD (Fig. 5), which is involved in the substrate presentation to the PBGD catalytic centre. Finally, protein sequence corresponding to the 20 kDa fraction could not be analyzed due to an insufficient amount of the extracted material. However, we suggest that it corresponds to truncated ApoAI sequence as it was only observed when using an antibody against ApoAI immunoblot detection (Fig. 22). All these data suggest that the truncated proteins have little or no PBGD catalytic activity.

In order to check whether the cleavage is due to the presence of proteases in the culture medium, supernatant from clone 45 collected on day 8 was incubated for two days at 37 ºC or 32 ºC without or with antiproteases cocktail (concentration 1:100). Our results showed no differences between addition or non-addition of the antiproteases treatment (Fig. 23A). In a new assay, we observed that cell incubation for seven days with low concentration of the antiproteases cocktail (1:800) did not reduce the appearance of the truncated forms (Fig. 23B). Therefore, we suggested that the rhApoAI-PBGD is already synthesized with a truncated form or that cutting occurs during maturation in the Golgi or Endoplasmic Reticulum compartments (just before secretion to the supernatant).

Finally, the supernatant of the rhApoAI-PBGD produced by HEK293 cell line was also analyzed by immunoblot against ApoAI and it confirmed a different degradation pattern when compared with CHO-K1SP cell line (Fig. 23C). Overall, these data suggest specific digestion associated with each cell type or that, following the cloning process and selection, different truncated sequences of the rhApoAI-PBGD protein may be inserted into the genome of the produced cell. In both cases, anti-protease treatment is ineffective in eliminating or reducing the truncated forms.

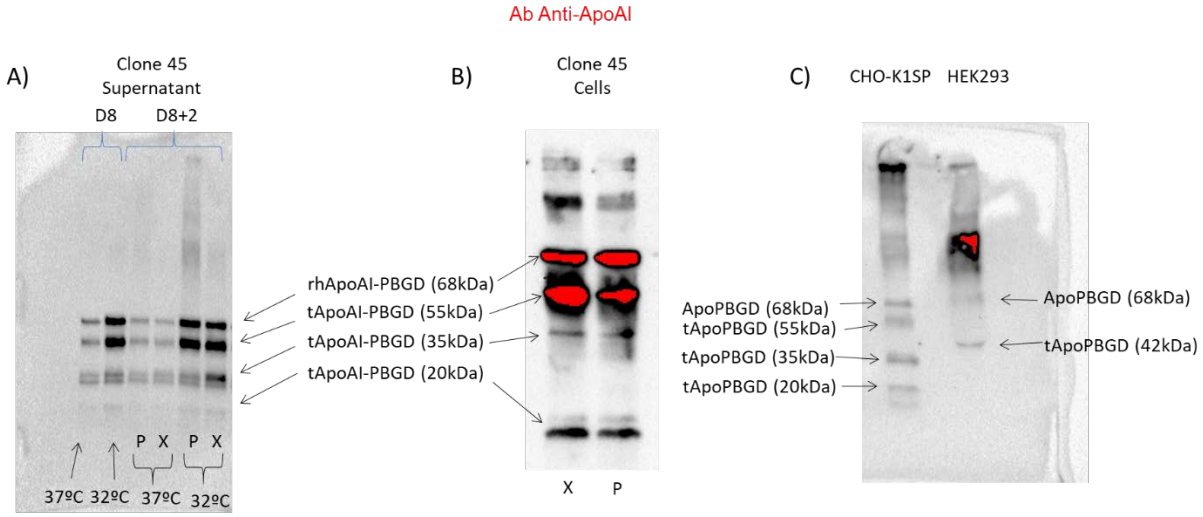

Figure 23. Ineffective effect of the anti-proteases treatment in rhApoAI-PBGD protein produced in CHO-K1SP clone 45 cell culture. A) Representative image of an anti-ApoAI immunoblot of clone 45 supernatant harvest on day 8 performed under reducing conditions. Samples were incubated for 2 days with antiproteases cocktail (P) or without it (X) at 32 ºC or 37 ºC temperatures. B) Immunoblot with an anti-ApoAI antibody performed on CHO-K1SP cells after 7 days of antiproteases treatment (P) or without it (X). C) Immunoblot anti-ApoAI performed on supernatant of CHO-K1SP clone 45 and HEK293 cells producer of the rhApoAI-PBGD protein.

3.2. Purification assays of the rhApoAI-PBGD protein from the supernatant of CHO-K1SP cells

Higher amount of aggregated protein, with molecular weights larger than 100kDa were detected in non-reducing immunoblot (Fig. 24A, right), that are not distinguished under reducing conditions (Fig. 24A, left). Culture temperature did not affect aggregate formation (Fig. 24A). Aggregate size and molar mass of the proteins from clone 45 CHO-K1SP supernatant were analyzed by SEC-MALS system. The analysis showed protein aggregates with a molecular mass from 100 to 2,000 kDa (Fig. 24B), that is, from dimers up to clusters of 30 or more rhApoAI-PBGD molecules.

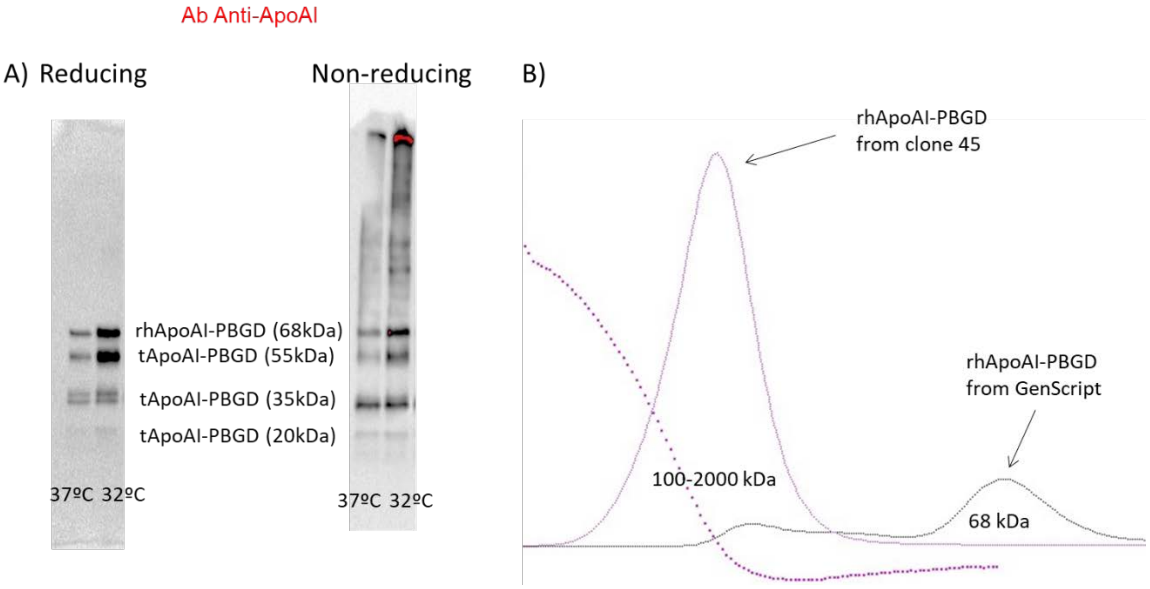

Figure 24. Characterization of rhApoAI-PBGD protein aggregates produced by CHO-K1SP cells. A) Immunoblot anti-ApoAI of the supernatant from clone 45 incubated at 37 ºC or 32 ºC performed under reducing conditions (with DTT pre-treatment) or under non-reducing conditions (without DTT pre-treatment). B) SEC-MALS analysis of rhApoAI-PBGD produced by clone 45 CHO-K1SP cells compared against rhApoAI-PBGD produced by *E. coli* by GenScript.

In order to eliminate aggregated proteins, we screened three different resins (MEP, HEA and PPA) to test which of them showed optimal interaction with the fraction of non-aggregated rhApoAI-PBGD protein. Supernatant were incubated with two DTT concentrations (10 or 100 mM) for 1h at RT. However, no protein was attached to any of the resins tested (Fig. 25). Probably, the presence of these aggregates prevents rhApoAI-PBGD from adhering to the resins, avoiding its purification.

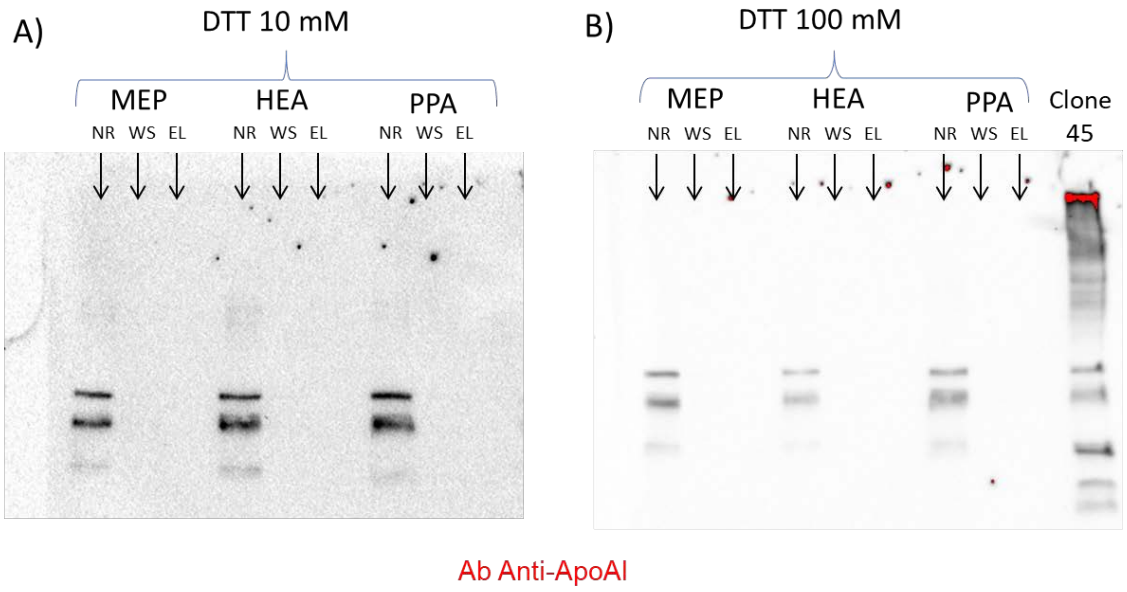

Figure 25. rhApoAI-PBGD purification assay in resins MEP, HEA and PPA. Supernatant of clone 45 was pre-treated with DTT 10 mM or 100 mM. Representative anti-ApoAI immunoblot image of the different purified fractions: NR, no retained; WS, washed fraction with PBS pH 7; EL, eluted fraction with sodium acetate buffer pH 5. WS and EL correspond to the first wash and eluted fraction.

In the following study, supernatant was treated with DTT 20 mM and CHAPS 4 % and eluted on a SEC column in order to separate by size the rhApoAI-PBGD free protein from aggregates and truncated forms (Fig. 26A). Immunoblotting detection with an anti-ApoAI antibody of the different eluted fractions revealed the presence of the rhApoAI-PBGD protein in fractions around B7 (Fig. 26B), while truncated fractions were detected in D11 and E2 fractions (Fig. 26B). However, SEC-MALS analysis of selected fraction B7 confirmed that the protein was mostly in the form of aggregates of 2000 kDa corresponding to a cluster of more than 30 rhApoAI-PBGD molecules (Fig. 26C).

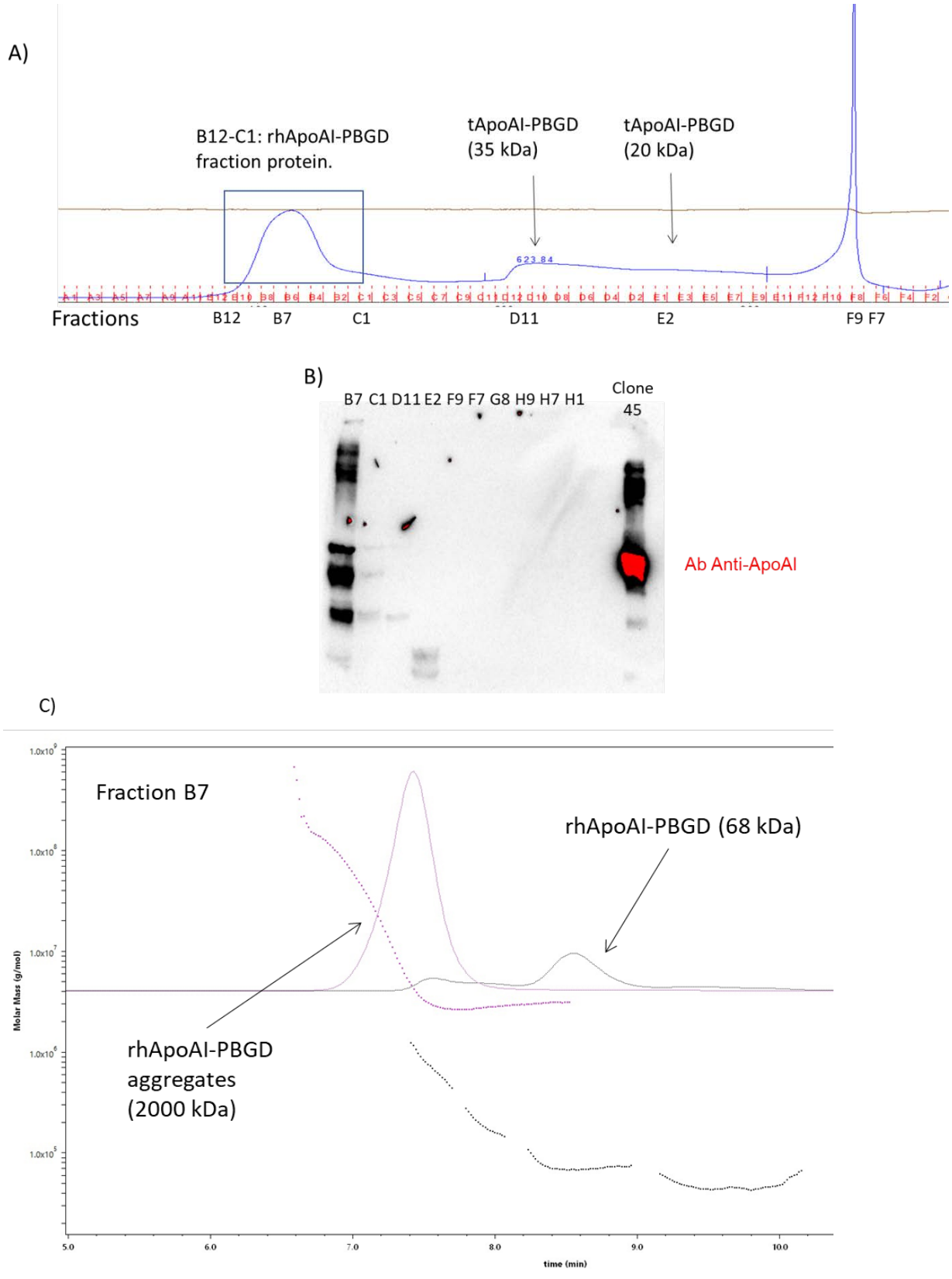

Figure 26. 1 L SEC characterization of the rhApoAI-PBGD proteins from the supernatant of CHO-K1SP clone 45 supernatant and eluted fractions. A) R2 supernatant from ultrafiltration was pre-treated with DTT 20 mM and CHAPS 4 % at RT for 1 h and passed

through a 1 L SEC column. B) Representative image of an anti-ApoAI immunoblot of different fractions obtained after SEC. C) SEC-MALS analysis of B7 eluted fractions.

Enzyme analysis of the different eluted fractions showed that aggregates had very low PBGD activity (approximately 0.1 % of the activity measured in the rhApoAI-PBGD protein from bacteria production). Fractions B7, B8 and B9 increased the catalytic activity an average of 10 times when treated with DTT 20mM and CHAPS 4%. These data suggest that the secreted recombinant protein is in form of aggregates, and only the strong denaturing conditions used to perform the immunoblot (DTT + SDS) are capable of disaggregating them.

3.3. Lack of therapeutic activity of rhApoAI-PBGD aggregates in in vivo assays

In order to analyze protein aggregates behaviour in physiological conditions, 60 nmol/kg of rhApoAI-PBGD protein corresponding to fractions from B5 to B8 were i.v. injected in AIP mice to perform a pharmacodynamic study. Three days after the administration, the recombinant protein was localized inside the serum HDL fraction (Fig. 27). That is, it circulates in the same serum fraction as the non-aggregated protein.

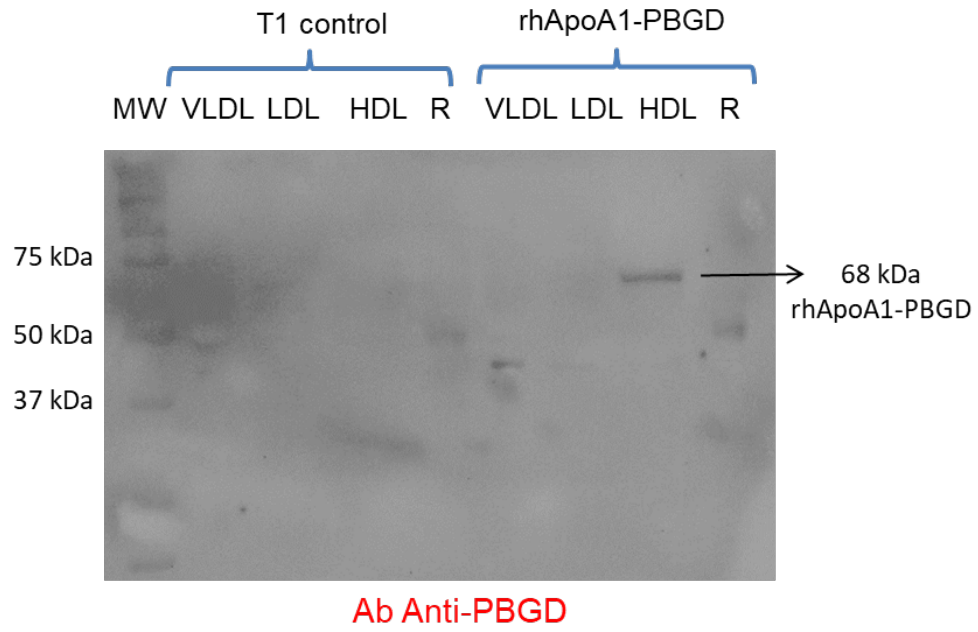

Figure 27. Serum lipoprotein fractions from a T1 mouse and immunoblot detection of PBGD of rhApoAI-PBGD protein produced in CHO-K1SP. WB anti-PBGD image of VLDL, LDL, HDL and R (serum residues) from a female T1 mouse 72 h after i.v. 60 nmol/kg rhApoAI-PBGD administration. MW, molecular weight marker.

In a prevention study using fractions from B5 to B8, a single dose of 60 nmol/kg of rhApoAI-PBGD protein was i.v. administered in AIP mice 24 h before the Pb-induced attack. No differences between the treated group with rhApoAI-PBGD (from CHO-K1SP origin) and the untreated control group were found in the accumulation of heme precursors in urine samples (Fig. 28A-D). The behavioural analysis also showed no differences between groups neither in the pain score (Fig. 28E). At sacrifice, 5 days post-rhApoAI-PBGD administration, hepatic PBGD activity showed a non-significant increase (3.73 ± 0.74 activity units) in the treated group compared to non-injected mice (3.04 ± 0.24 activity units, $p = 0.126$) (Fig. 28F).

On the contrary, AIP mice injected with the rhApoAI-PBGD produced in bacteria significantly increased hepatic PBGD activity and did show a significant therapeutic effect against porphyrin precursors excretion and pain measurement (Fig. 28).

The increase in enzymatic activity of the protein of bacterial origin was similar to that obtained by the protein produced in CHO-K1SP cells (Fig. 28F). However, both proteins did not show the same therapeutic effect. We suggest that could be due to the protein produced in CHO-K1SP cells is present in the form of inactive aggregates in the liver and only the DTT used to quantify the enzymatic activity (lysis and incubation buffer) may disaggregate them and produce the increase in PBGD activity.

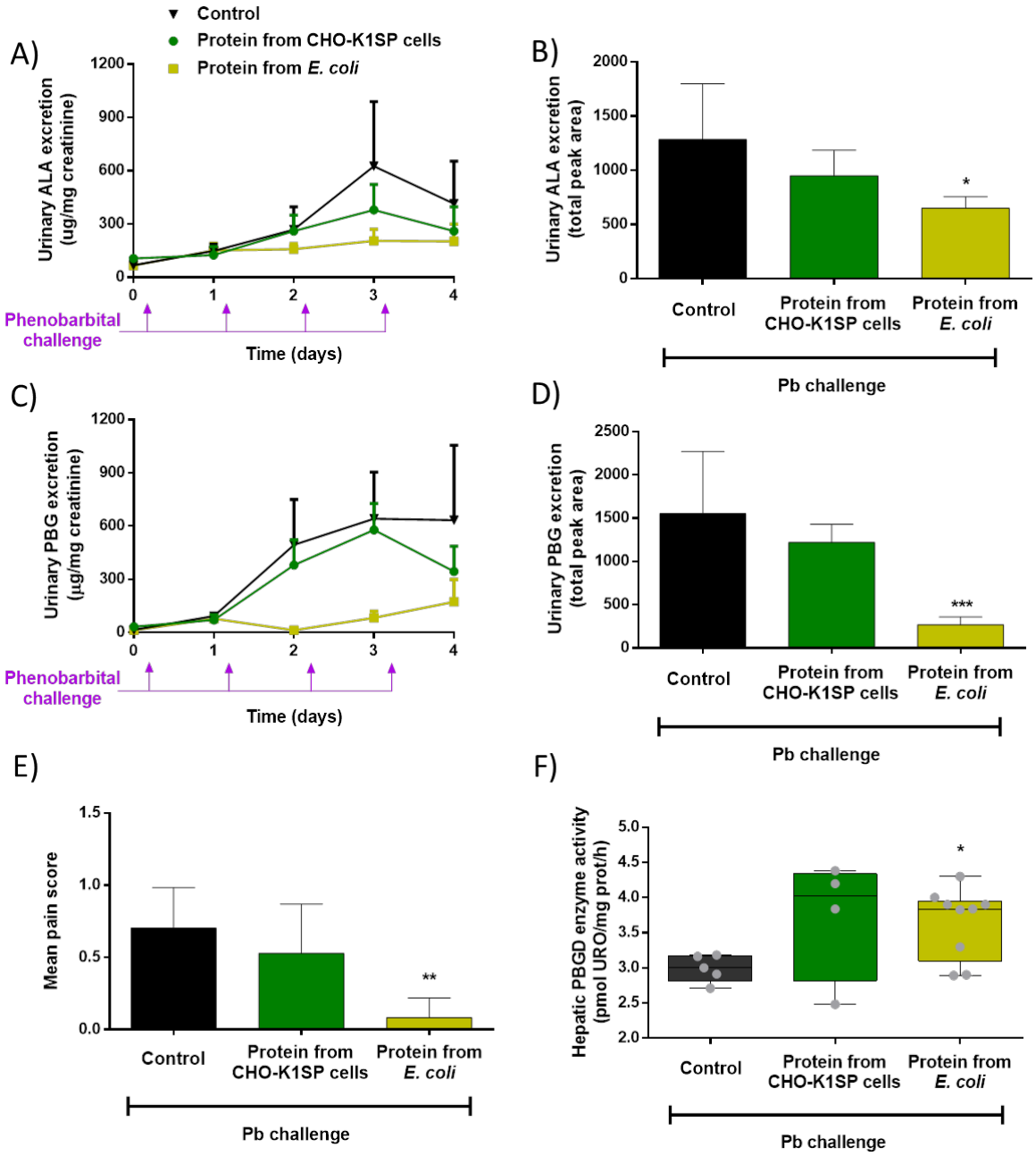

Figure 28. Pharmacodynamic study in AIP mice of rhApoAI-PBGD produced in CHO-K1SP cells. Male AIP mice were i.v. injected with 60 nmol/kg of rhApoAI-PBGD produced in CHO-K1SP cells (n = 4) or produced in bacteria (n = 9). Another uninjected AIP mice (n = 5) constitute the control group. One day after protein administration, all animals were challenged with increased Pb for 4 days to trigger an acute attack. A) Urinary ALA excretion and B) its quantification of the total peak area analysis. C) Urinary PBG excretion and D) its quantification of the total peak area analysis. E) Pain score using the MGS. F) Hepatic PBGD activity 5 days after 60 nmol/kg rhApoAI-PBGD i.v. administration. Data are mean ± SD. *, $p < 0.05$; **, $p < 0.01$; ***, $p < 0.001$ against control group.

Overall these data indicate that although the aggregated protein is detected in the serum HDL fraction, its hepatic delivery is inefficient to protect against the Pb-induced attack.

4. Prolonged therapeutic effect of the rhApoAI-PBGD protein when delivered to the liver of AIP mice using mRNA technology

In order to further study whether conjugated hApoAI-PBGD shows a therapeutic advantage against the unconjugated PBGD protein, a mRNA encoding for hApoAI-PBGD formulated in LNPs was developed. First of all, some animals were sacrificed 24 h after the administration of increased doses of hApoAI-PBGD mRNA to confirm the dose needed to obtain similar protein expression in the liver. As the hApoAI-PBGD sequence is not yet optimized, it is necessary to inject a 5-fold higher dose of the conjugated protein mRNA to obtain a enzymatic activity similar to that of the reference hPBGD mRNA (Fig. 29A).

For the pharmacodynamic study, AIP mice were subjected to two consecutive Pb challenges on days 0 to 3 and between days 12 and 15. The corresponding dose of the

mRNAs was administered 2 h before the second dose of Pb (day 1). During the first challenge, both groups showed very high protection against porphyrin precursors accumulation. However, during the second challenge, a higher protection against urine porphyrin precursor excretion was maintained only in animals treated with rhApoAI-PBGD mRNA (Fig. 29B-E). Furthermore, hApoAI-PBGD mRNA full protected against pain at least up to 14 days after the administration of a single mRNA dose (Fig. 29F).

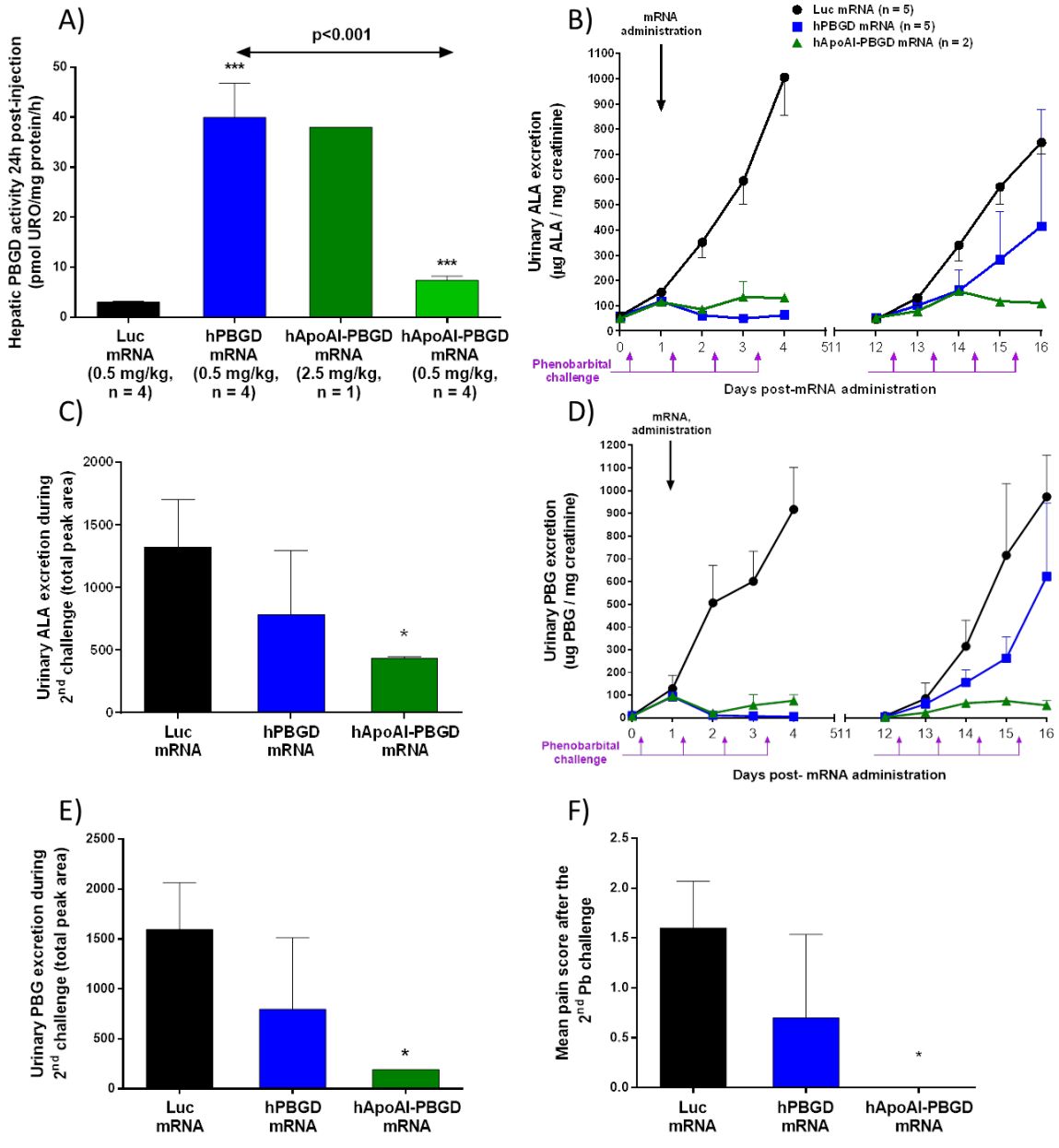

Figure 29. Intracellular stability of rhApoAI-PBGD protein compared to unconjugated PBGD form. Luc is luciferase. A) Hepatic PBGD activity 24 h after a single i.v. administration of 0.5 mg/kg of hApoAI-PBGD mRNA, hPBGD mRNA and Luc mRNA (n = 4, each) or 2.5 mg/kg of hApoAI-PBGD mRNA (n = 1) formulated in LNPs in AIP mice. For the pharmacodynamic study we administered 2 AIP mice with 2.5 mg/kg of hApoAI-PBGD mRNA and 5 animals with 0.5 mg/kg of hPBGD mRNA or Luc mRNA. B) Urinary ALA excretions over two Pb challenges and C) quantification of the total peak area during the second challenge. D) Urinary PBG excretions over two Pb-induced acute attacks and E) quantification of the total peak area during the second challenge. F) Pain score on day 15. Data are mean ± SD. *, $p < 0.05$; ***, $p < 0.001$ vs. control Luc group.

DISCUSSION

AIP has low penetrance, only less than 1 % of the population that inherit a PBGD pathogenic mutation will develop the clinical features of the disease. First acute attack emerges in most of the patients after exposure to precipitating factors such as drugs or other chemicals, alcohol intake, acute illness, infection, stress, physical exhaustion, caloric deprivation and steroid hormones, mainly oestrogens and progesterone, that regulate reproductive cycle in women. After the first attack, the precipitating agent is identified and removed if possible.

Some patients may not develop an acute attack again, although most of them maintain high urinary excretion of ALA and PBG for years. These patients are classified as Asymptomatic High Excretors. Family studies allow identification of asymptomatic mutation carries. Regardless of their biochemical activity, all these individuals are classified as patients with latent porphyria and do not receive any treatment. However, a recent study shows that 46.4 % of them report chronic symptoms associated with porphyria, such as abdominal pain, fatigue, muscle pain and insomnia [118]. All these asymptomatic patients are exposed to the potential toxicity of heme precursors when passing through the kidney, especially ALA which has been identified as responsible for progressive renal failure [119], or also to an increased risk of developing hepatocellular carcinoma [33], the most common long-term complications associated with acute hepatic porphyrias.

Frequency and severity of the acute attacks allows classification of patients into different groups, which may condition their treatment. Patients suffering sporadic acute attacks (1 to 3 per year) can be treated according to their clinical severity. Carbohydrate overload (300 to 500 g/day, based on oral or i.v. glucose infusions) is indicated for mild crises and no paresis, while i.v. administration of hemin is recommended for severe attacks characterized by severe neuropathic abdominal pain, fatigue, muscle pain, and insomnia associated in some cases with peripheral neuropathy. Hemin administration (3-4 mg/kg) is the standard of care for acute hepatic

porphyrias and is more effective than glucose in reducing activation of the heme synthesis pathway by negative retro-inhibition of *Alas1*. Treatment duration ranged from one to eight days during acute attack and biochemical remission of ALA and PBG is not typically produced until two or three days after the beginning of the treatment. The reduction in abdominal pain was most often observed on the third day of treatment [120]. The efficacy of this treatment is very difficult to assess due to significant variability among patients and depends on the early initiation of i.v. administration of this compound [55].

Patients suffering frequent acute attacks represent 5 % of the symptomatic patients, which are mainly women (80 %). Although, there are no reports about the efficacy of hemin administration to prevent acute porphyria attacks, the preventative dose evaluated was i.v. hemin given at 3 mg/kg of body weight administered monthly or bi-monthly [54]. However, repeated administration of hemin therapy can exacerbate side effects, causing thrombophlebitis at the peripheral vein infusion site requiring the administration through a central vein, iron overload (250 mg dose of heme contains 22.7 mg of iron), and reduction of the therapeutic efficacy after recurrent administration due to continued activation of heme catabolism [58].

Recently, ALAS1 iRNA strategy (givosiran) has been approved for the treatment of severely affected patients that suffer recurrent porphyria acute attacks. S.c. givosiran administration has shown promising results preventing ALA/PBG accumulation and reducing the frequency of acute attacks by 74 % in a phase III clinical trial (NCT03338816). However, several adverse events have been associated with its use, as serum ALT levels elevation and kidney issues [61]. Downregulation of *ALAS1* combined with defective heme synthesis in severely affected patients could lower hepatic heme content and reduce the activity of heme-dependent hepatic proteins causing reduced drug metabolization rates [121] and aggravation of the dysregulation of one-carbon metabolism, resembling classic homocystinuria [62,63].

Current approved treatments for acute porphyria do not provide an etiological solution for the disease. Thus, there is a need for a new physiological treatment that covers the full spectrum of the disease, from sporadic to recurrent attacks, regardless of their severity. Increasing hepatic levels of PBGD has shown to be effective for the treatment of acute attacks in a mouse model of AIP in different preclinical studies. This increase of PBGD activity has been firstly experimentally accomplished by administration of an rAAV2/5 encoding for human *PBGD* cDNA [71]. In AIP mice, over-exposure of PBGD protein was safe, and partial recovery of hepatic PBGD levels was sufficient to prevent the occurrence of acute crisis. However, a clinical trial (NTC020082860) failed to reduce levels of porphyrin precursors due to insufficient liver transduction at the doses tested (up to 1.8×10^{13} genome copies/kg). AIP candidates for GT should be only those patients with severe and frequent acute attacks accompanied by neurologic symptoms, requiring repeated administration of hemin or liver transplantation.

I.v. administration of hPBGD mRNA formulated into LNPs [2] or the i.v. or s.c. administration of ApoAI-conjugated PBGD protein showed rapid increase of PBGD activity in hepatocytes [3] and a fast normalization of urine porphyrin precursors in ongoing attacks in AIP mice. Indeed, both products maintained same degree of protection after repeated administrations. A rapid effect is a very important aspect in acute presentations of the disease while sustained efficacy after repeat dosing is necessary for chronic presentations. Proved safety and translatability after multiple administrations allows mRNA formulated in LNPs and rhApoAI-PBGD ERT to treat chronic presentations, where re-administration and individual dosage decisions could be taken according to the clinical and biochemical status of the patient. These features are crucial for a new era of personalized and precision medicine.

The effect of hepatic PBGD augmentation on poorly described disease parameters associated with acute hepatic porphyrias is explored in this thesis (Table 2).

Table 2. Summary of symptoms and features occurring in human patients with severe AIP and experimental acute hepatic porphyria models. Colour code represents the degree of protection against a particular symptom of hepatic augmentation PBGD therapy in experimental models. Green, orange and red colour indicate effective, partial or no protection of the therapy, respectively.

Human patients with severe AIP		**Experimental model**		**Therapy**	
				Augmenting hepatic PBGD (rAAV-mediated GT)	
Central Nervous System	Ventricle enlargement [112]	**AIP mouse**	Present; Exacerbated after recurrent attacks	Effective protection but not reverse alterations previous to therapy	
	Reduced brain perfusion during the acute attack [112]		Present	Effective protection	
				Augmenting hepatic PBGD (mRNA therapy)	**Hemin**
Peripheral Nervous System	Motor impairment [6,7]	**VP rabbit**	Present	Effective protection	Partial protection
Autonomic Nervous System	Chronic hypertension [6,7]		Present	Effective protection	Effective protection
Liver metabolism	Altered glucose homeostasis [122]		Present	Effective protection	No protection
Liver function	Lipid peroxidation [6,7]		Present	Effective protection	Partial protection
	Inflammation [11]		Present	Effective protection	Partial protection
	Cytoplasmic Stress [123]		Present	Effective protection	Exacerbated
	Altered hemoprotein function [2]		Reduced mitochondrial respiratory chain	Effective protection	No protection

Among CNS involvement, structural changes and brain perfusion have been poorly characterized in patients with acute hepatic porphyria. The current neuroanatomical understanding is mainly based on post mortem histology studies [124] and brain MRI analysis of several patients with AIP that showed manifestations compatible with posterior reversible encephalopathy syndrome (PRES) [30,125–133]. In most of these cases, PRES improves after initiation of AIP treatments that decrease ALA and PBG production and excretion. However, given the low blood brain barrier (BBB) permeability of ALA, it has been suggested that PRES manifestations are more related to a transient breakdown of the BBB and concomitant cytotoxic effect of porphyrin precursors of hepatic origin [112]. In patients without PRES but with severe AIP and recurrent acute attacks, neuroradiological studies showed a higher prevalence of BV enlargement. A decreased brain perfusion during acute attacks was also recently reported in two patients in whom perfusion imaging data were acquired [112].

The first aim of this thesis was to study those brain changes in the AIP mouse model and the effect of hepatic PBGD augmentation. AIP mice developed chronic BV dilatation even in the presence of slightly increased porphyrin precursors. Of interest, the BV enlargement was mitigated by the correction of the metabolic PBGD defect using liver-directed GT. In this study, we decided to use a rAAV2/5-*PBGD* vector because of its high tropism towards liver cells and the ability to maintain high levels of PBGD in the liver of AIP mice over several months after a single injection [71]. Other vectors with hepatic tropism or the PBGD protein directed to the liver with ApoAI conjugation, could obtain the same effect as long as an adequate dosage is found.

AIP mice not exposed to Pb challenge also exhibited reduced CBF with normal systolic blood pressure [2]. However, it is possible that small vessels dysfunction is only local. In the brain of our AIP mice, the CA1 region of the hippocampus located adjacent to the enlarged BV space exhibited high expression of *Ednrb*. It seems possible that overexpression of *Ednrb* might be a compensatory mechanism counteracting

vasoconstrictive forces [134–136]. Interestingly, normalization of CBF, and *Ednrb* expression in the CA1 region, occurred in AIP mice that received liver GT.

Repeated Pb challenge exacerbated BV enlargement in AIP mice and liver-directed GT afforded full protection. However, a direct neurotoxic effect of ALA and PBG is an unlikely factor because porphyrin precursors are markedly accumulated in their liver and plasma, but less in the CNS as has been previously reported by Yasuda et. al [137] and in the VP model in rabbits described in this thesis. Our findings suggest that constitutive small vessel dysfunction in association with systemic arterial hypertension occurring during acute porphyria attacks might cause an imbalance in cerebral spinal fluid dynamics resulting in BV enlargement. The imbalance could be due to increased pulse pressure in the BV via choroid plexus pulsation [138], abnormal fluid re-absorption by arachnoid villi [139] or both.

Upon Pb challenge, AIP mice developed arterial hypertension [2] and increased EDN1 plasma levels which may be associated with a further CBF decrease. Of note, augmenting PBGD levels in the liver of AIP mice protects against hypertension [2] and restored CBF. Given that the liver is an important site for circulating EDN1 clearance through the EDNRB [113]; we suggest that the correction of the metabolic defect in the liver of AIP mice after the treatment with rAAV2/5-PBGD, can enhance EDN1 clearance by increasing hepatic *Ednrb* expression. Although downregulation of this receptor has been described in liver disorders [140], further studies are needed to understand the mechanism that regulates the expression of the *Ednrb* receptor in a porphyric liver.

Similarly, a previous report showed increased local vasoconstrictor responses in the mesenteric arteries in this mouse model with significant vasodilatation after hemin administration [141]. In parallel, we reported here that hemin administration protects against increased systolic blood pressure in VP rabbits [142], as well as in AIP mice as

previously reported [2]. Therefore, these data suggest that microcirculation dysfunction and hypertension during porphyria attack might be related to heme availability rather than the accumulation of porphyrins and porphyrin precursors that still persist after hemin therapy in both models mentioned.

Overall, we observed BV enlargement in the brain of AIP mice seemingly as a result of vascular dysfunction, associated with reduced CBF. In AIP mice, correction of the hepatic PBGD deficiency reversed CBF reduction and prevented the progressive BV enlargement occurring in animals subjected to repeated acute porphyric attacks.

In addition to central and autonomic nervous system alterations, motor discoordination and disturbances in nerve conduction velocity associated with acute porphyria attacks have been studied in AIP mice in absence or after treatment with PBGD augmentation therapy [2,71]. However, although this mouse model closely mirrors the characteristics of acute porphyria attack in human, large animal models are needed to facilitate the translation of experimental therapies from the laboratory to patients [117]. Thus, we developed a pharmacological model in rabbits that reproduces the characteristics of acute attacks observed in patients with acute hepatic porphyria.

Previous studies have described that AIA induces *Alas1* expression and disrupts the regulatory hepatic heme pool in female New Zealand rabbits [143]. A single 300-400 mg/kg AIA dose showed moderate ALA and PBG urinary accumulation. However, those levels were normalized in few hours after the drug exposure, and rabbits injected with AIA did not show the clinical features of patients with acute porphyria [143]. In order to increase and maintain ALA and PBG levels and reproduce the classic symptomatology associated with acute porphyrias, AIA was administered in combination with Rif, another well-known porphyrinogenic drug.

AIA has long been known to be a suicide substrate for CYP450s [144], probably caused by a change in its conformation by the binding of an allyl group [145,146]. As

reported, Rif inhibits PPO activity in leucocytes from seven healthy volunteers after daily administration of Rif (600 mg) for a week [147]. This inhibition is supported by the observation that our VP rabbits showed unchanged *Ppo* gene expression but decreased enzyme activity. Rif together with AIA have been described as strong inducers of CYP3A4 and CYP3A5, and moderate inducers of CYP2B6, CYP2C8, CYP2C9, and CYP2C19 [148–150], thereby further increasing heme demand and inducing hepatic *Alas1* transcription. Again, combined administration of AIA and Rif resulted in a strong induction of hepatic *Alas1* gene expression and protein level. As a result, VP rabbits showed increased hepatic heme contents but also high accumulation of both porphyrin and porphyrin precursors. Finally, rabbits also showed fecal porphyrin excretion in a pattern similar to patients with VP [147].

The only described animal model of VP, the $R59W^{+/-}$ mice [151] replicates porphyrin accumulation as human patients with VP, but fails to recapitulate porphyrin precursors accumulation and the symptomatology associated with acute attacks. Thus, VP rabbits represent a perfect model to characterize the induction of acute attacks in a VP context.

Together with porphyrins accumulation, high urine ALA and PBG excretion is a biochemical hallmark of patients with VP, but its cause is not well known. Some authors suggest potential PBGD allosteric inhibition by the low-carboxylated porphyrins, coproporphyrinogen and protoporphyrinogen [44]. However, VP rabbits exhibited normal hepatic PBGD levels when compared to non-injected rabbits, despite high accumulation of these low-carboxylated porphyrins. Besides, VP rabbits treated with hPBGD mRNA also showed high concentrations of low-carboxylated porphyrins on days 17 and 18 with no concomitant accumulation of heme precursors. Indeed, the liver of VP rabbits overexpressing hPBGD disclosed reduced *Alas1* induction and high heme content, indicating that PBGD is the limiting step of hepatic heme synthesis in these chemically induced VP rabbits.

In addition to the hypertension already mentioned, VP rabbits also reproduced some of the signs and symptoms associated with the acute attacks of porphyria, such as motor impairment [152], and altered GTT [153] and glucose metabolism [109,122] (Table 2).

Motor impairment is widely described in severely affected patients with acute porphyrias [152] and AIP mice, as measured by the rotarod test, reduced stride length, and decreased amplitude of the action potentials in the compound muscle after Pb-induced attacks [71,72]. While both hemin and hPBGD mRNA administration protected against gait problems in our VP rabbits, only hPBGD mRNA efficiently restored the compound motor action potential of the sciatic nerve. Thus, the amplitude parameter is probably affected by the accumulation of heme precursors that still persist in hemin-treated VP rabbits. Although motor disturbances have been associated with high ALA accumulation [140], this model also supports the involvement of PBG in these behavioural troubles.

Early studies reported abnormal oral GTT results and hyperinsulinemia in patients with AIP [153–155], which resemble the findings of cellular insulin resistance. More recently, we reported a high prevalence of insulin resistance and hyperinsulinemia in patients with AIP [122]. We also reported serum hyperinsulinemia, delayed GTT, and a different response to fasting between AIP and WT mice [109], which were efficiently normalized after augmenting hepatic PBGD levels [109]. Our rabbit model also reproduced altered GTT and reduced brain glucose uptake. Given that hPBGD mRNA administration, but not hemin, efficiently restored both parameters, these data highlight that porphyrin precursors accumulation, but not porphyrins or reduced heme content, are associated with altered glucose homeostasis.

Liver parenchyma in VP rabbits was normal and without necrotic areas, however, it exhibited a darkness colour probably due to the formation of green pigments after AIA administration, as previously described [144–146]. Besides, a MT-CO1 immunoblot

revealed abnormal mitochondrial distribution on the periphery of hepatocytes. This is probably caused by cytoskeleton restructuring due to an undetermined response to drug administration [156]. Unlike patients with acute hepatic porphyrias, VP rabbits display moderate and transient changes in liver status (ALT, ALP) that could be related to an adaptive response of the hepatocyte metabolism to drug administration, as previously reported [147,157].

AIP mice suffering from recurrent acute attacks and patients with acute porphyria do not usually show alterations in those serum liver function parameters, but oxidative stress has been reported. Disturbances of the redox state and glutathione metabolism was previously reported in rats administered with a large single dose of AIA [158]. In our rabbits, the expression of the biomarkers of oxidative stress was strongly induced after recurrent AIA and Rif challenges. Of note, while the administration of hPBGD mRNA normalized the expression of these genes, hemin treatment maintained high *Hepcidin* expression, and further increased *Ho-1* and *Hsp70* mRNA levels, as similarly reported in AIP mice [11].

The kinetics of lipid peroxidation throughout the study, another measure related to oxidative stress [159], was determined by urinary TBARS levels. A significant increase in TBARS excretion was observed at the end of the D15 challenge, which was associated with an increased in urinary excretion of ALA. The administration of a single dose of hPBGD mRNA normalized the regulatory steps of the synthesis (*Alas1*) and catabolism (*Ho-1*) of the hepatic heme pathways and fully protected against ALA and TBARS accumulation.

Heme availability for important hemoprotein functions was analyzed in the liver of this rabbit model. Four types of heme are described in eukaryotes, that is, protoheme and heme A, B, and C [115,160]. Protoheme is the precursor of the other three different types of heme and constitutes a pool of “free heme”. The mitochondrial respiratory

chain is constituted of 5 multi-enzyme complexes (I, II, III, IV and V or ATP synthase). Mitochondrial complexes II and III use heme B, whereas heme C is used by cytochrome c1 of complex III, and two groups of heme A are part of the MT-CO1 in complex IV. The analysis of complexes I–V protein subunit levels in isolated liver mitochondria showed that the protein content of the complex IV declines after recurrent challenges with AIA and Rif, whereas mitochondrial complexes I–III were much less affected. Given that heme A needs chemical modifications that differ from B and C, we hypothesize that the protein content of mitochondrial complex IV is primarily affected under conditions with reduced heme availability [115]. Although hemin administration partially corrected complex IV content, only rabbits treated with hPBGD mRNA showed normal values.

Although the protein content of the mitochondrial respiratory chain complexes I–III remained unchanged in the liver of VP rabbits, their enzymatic activities were markedly reduced. A previous study using the AIP mouse model also revealed a failure of hepatic mitochondrial energy metabolism and TCA cycle after Pb challenge [161]. Given the close interconnection between TCA cycle and the activity of the respiratory complexes I–III, Homedan et al. suggested that the TCA cycle is unable to supply the reduced cofactors to the mitochondrial respiratory chain due to the high demand for succinyl-coenzyme A (CoA) to form ALA [161]. However, in our rabbits, mitochondrial respiratory chain activities were measured independently of the contribution of the TCA cycle. Another difference with this study was that in the AIP mouse model, the activity of the complexes returned to normal after the administration of hemin, but this effect was not seen in our rabbits. We suggest that the high oxidative stress observed in VP rabbits, especially in those treated with hemin, may affect the iron-sulphur clusters that contain complexes I–III. These clusters contain enzymes that are known to represent critical targets for the oxygen free radicals [162] contributing to the pathophysiology of the acute attack [163]. Of interest, the administration of a single dose of hPBGD mRNA

prevented the induction of oxidative stress and tended to normalize the activity of the respiratory complexes.

In summary, hPBGD mRNA administration is able to counteract symptomatology and biochemical disturbances of the VP model in rabbits. These data suggest that PBGD is a secondary limiting rate enzyme in the heme biosynthesis pathway in VP and possibly in HCP, another mixed hepatic porphyria. Regarding cutaneous symptomatology associated with high serum porphyrin levels in VP and HCP, these rabbits were only exposed to soft indoor light and they did not show any type of skin photosensitivity despite high porphyrin accumulation. Future work should be necessary to study the effect of PPO mRNA therapy in this experimental VP model.

Based on these results, PBGD augmentation seems to be an appropriate treatment for acute attacks of porphyria, regardless of whether it is achieved by administration of cDNA encoded in rAAV2/5 or mRNA encapsulated in LNPs. Recently, the increase of the deficient enzyme obtained after administration of the rhApoAI-PBGD protein has also shown to be an effective treatment in preclinical studies in AIP mice [3]. The proof-of-concept of the rhApoAI-PBGD was performed in AIP mice with recombinant protein produced in *E. coli* [3]. The main advantage of this ERT approach over GT and mRNA-based therapies is that it acts in the three involved compartments of the acute attack, liver, serum and brain. Furthermore, it could be administered by s.c. injection, thereby being less constraining than i.v. administration. As tested, rhApoAI-PBGD did not show any immunological anaphylactic reaction nor antibody formation in preclinical studies [3], which are typical limitations of protein-based ERT. However, recombinant proteins have a high production cost and the design of large-scale production processes is required.

Prokaryotic cell factory was used due to its fast growth, easy manipulation and cost-effectiveness [164]. For this production, a polyhistidine-tag was incorporated at the N-

terminal region of the rhApoAI-PBGD to facilitate purification process. However, bacteria production, antibiotic resistance or the use of the histidine-tag are not recommendable for obtaining GMP labelling requirements. Next, production of rhApoAI-PBGD was also assayed in HEK293 cells as eukaryotic host. The histidine-tag was replaced by a signal sequence that allows the protein of interest to be secreted into the supernatant. This procedure facilitates protein harvest avoiding cell lysing step. Best HEK293 clone was selected by ampicillin antibiotic resistance in DMEM culture medium supplemented 2-10 % with fetal bovine serum and produced 17.65 ng of rhApoAI-PBGD per L of supernatant. Finally, production of the recombinant protein was also performed in CHO-K1SP cell line. To avoid the use of antibiotic resistance genes, best clone was selected by measuring rhApoAI-PBGD levels in the supernatant. This cell line increased the production yield by a factor of 4×10^6 fold (50-60 mg of rhApoAI-PBGD per L of supernatant).

Scaling up process for our CHO-K1SP cells were obtained after incubation in DYNAMIS synthetic culture medium at 8 % CO_2 supplemented with Feed B at 32 ºC for 8 days. Feed B supplementation maintains lactate levels, a subproduct of CHO-K1Sp cells, below toxic concentrations (< 2 g/L). 32 ºC culture condition was selected because previous reports suggest that reduction of the temperature of culture to 30-33 ºC increased recombinant protein production in CHO cells [165,166]. Temperature drop also reduces cell growth but increases cell viability, thus release of impurities from dead cells into the environment is reduced. According to Vergara et al. this temperature was also optimal to increase mRNA stability and to improve protein folding capacity and chaperone expression of endoplasmic reticulum [166]. The supernatant collected on day 8 of clone 45 at 32 ºC was selected for the purification assays because it was the last day before cell viability began to decrease. Also, 32 ºC culture seemed to produce more amount of protein than 37 ºC one according to Fig. 24A.

However, anti-ApoAI and anti-PBGD immunoblot analysis in reducing conditions showed up to three truncated forms of the rhApoAI-PBGD protein. While the complete protein (68 kDa) represented 25% of the total produced protein, truncated fractions with a molecular size of 55, 35 and 20 kDa accounted for 31 %, 35 % and 9 % of the total, respectively.

The 20 kDa protein was only detected by anti-ApoAI antibody, indicating partial or total loss of the PBGD protein (42 KDa). However, the 55 and 35 kDa protein fraction were detected by both anti-ApoAI and anti-PBGD antibodies. Proteome analysis recognized 61 peptides in the complete rhApoAI-PBGD protein, but only 57 and 53 peptides in the 55 kDa and 35 kDa truncated forms, respectively. Regarding PBGD activity, the 55 and 35 kDa protein fractions are unlikely to have protein activity because despite containing the Cys261 (the catalytic centre of the PBGD), they missed peptides of the 3 domain of PBGD that allows the formation of a thioether bond between the PBG substrate and the Cys261 through its sulphur residue [167]. Non-enzymatic hydrolytic protein cleavage is more susceptible to occur in peptide bonds of Aspartate-Glycine (Asp-Gly) and Aspartate-Proline (Asp-Pro) [167]; interestingly, the Asp-Gly bond is present 3 times and the Asp-Pro 2 times in the final region of the PBGD, which corresponds with the location where protein cleavage is likely to happen in the rhApoAI-PBGD produced in CHO-K1SP.

Anti-proteases treatment to cell culture did not improve protein degradation and suggest that the truncated proteins were already produced inside the cells. Of note, cleavage pattern was cell-specific and truncated rhApoAI-PBGD proteins produced in HEK293 cell line showed a different degradation pattern from that obtained in CHO-K1SP cells. In addition, the recombinant protein produced in *E. coli* showed truncated variants. One of them was characterized and showed a deletion of the N-terminal region of ApoAI, instead of the C-terminal region of PBGD described in those truncated proteins obtained in the CHO-K1SP line. Thus, protein sequence optimization to

prevent degradation by intracellular proteases is required to avoid rhApoAI-PBGD degradation in this specific cell line.

Immunoblot analysis under no reducing conditions (without DTT) suggested that the rhApoAI-PBGD was present in form of aggregates, and SEC-MALS analysis confirmed that the recombinant protein was mostly found in the form of aggregates of between 700 and 2000 kDa (aggregates of more than 10-30 proteins).

Despite the presence of aggregates, a screening purification process was performed in MEP, PPA and HEA resins. These resins were selected for binding the rhApoAI-PBGD by hydrophobicity in the case of MEP, or by hydrophobicity and electrostatic interactions for PPA and HEA (also called mix-mode resins). Given that our recombinant protein has an isoelectric point of 6.59, it should interact with the anionic PPA and HEA resins at neutral pH and be released at acidic pH by sodium acetate buffer. However, none of the resins showed interaction with the recombinant protein. The addition of DTT was assayed in case protein aggregates may be formed by non-native disulphide bonds. Nevertheless, pre-incubation process of the supernatant with DTT or DTT in combination with CHAPS detergent or urea did not significantly modify the presence of aggregates, as confirmed by non-reducing immunoblot. Only strong denaturing immunoblots condition under joint action of SDS detergent and DTT were able to cleavage rhApoAI-PBGD aggregates.

Finally, we selected by SEC elution different fractions (from B12 to C1) containing the rhApoAI-PBGD protein, a SEC-MALS analysis confirmed that the protein was still present in form of aggregates. Aggregates showed 0.1 % of the PBGD activity when compared to the protein of prokaryote origin purified using the polyhistidine tag. In AIP mice, the i.v. administration of a single 60 nmol/kg dose of rhApoAI-PBGD did not induce a significant increase in the hepatic PBGD activity [3]. Although the protein was detected in the HDL fraction, necessary condition for an efficient hepatocyte delivery,

this dose was not able to protect against porphyrin precursor accumulation, or improving pain as was the administration of purified protein [3]. Therefore, the aggregate formation is a major impediment to obtain a recombinant protein that allows an effective therapy for AIP in the clinical area.

Further studies are required for the optimization of rhApoAI-PBGD sequence to avoid aggregate formation. In this way, ApoAI has been described to cause amyloidosis due to abnormal protein folding that generates clusters of molecules. Reviewing the literature, we have identified certain hot-spots in the ApoAI sequence which could be related to aggregate formation. We are testing variants of rApoAI in those hot-spots to define best candidate for reducing aggregate formation.

Finally, the use of the hApoAI-PBGD could be a therapeutic option that increase half-life of the PBGD when expressed intracellularly by means of mRNA. However, further studies on mRNA sequence are needed to increase its stability and efficacy in order to reduce the injected dose.

COROLLARY OF RESULTS

Corollary of results

1. Old AIP mice in no-attack situation reproduces the brain ventricle enlargement and reduced brain perfusion observed in patients with chronic AIP. Recurrence of phenobarbital-induced attacks exacerbated ventricle dilation in AIP mice.

2. Brain ventricle enlargement appears to be a result of vascular dysfunction, and it is exacerbated by systemic hypertension during the induced acute attack in mice.

3. In AIP mice, augmenting PBGD in the liver normalized cerebral perfusion, protected against hypertension and prevented the progressive brain ventricle enlargement.

4. A new pharmacological model of variegate porphyria in rabbits was developed and characterized. Recurrent AIA and rifampicin challenge recapitulated biochemical characteristics of the human variegate porphyria and some clinical manifestations associated with severe acute attacks.

5. Although most symptoms of the acute attacks have been generally associated with ALA accumulation, variegate porphyria rabbits supports the involvement of PBG in behavioural disturbances and pathophysiological findings related to acute attacks.

6. Blood pressure and the function of important hepatic hemoproteins were associated with heme availability, as both were restored after hemin and hPBGD mRNA administration.

7. Glucose homeostasis, liver oxidative stress, motor coordination and compound muscle action were only restored in variegate porphyria rabbits treated with a single dose of hPBGD mRNA, suggesting that they were mostly associated with accumulation of porphyrin precursors.

8. Systemic hPBGD mRNA administration provided successful protection against the acute attack, indicating that PBGD, and not Protoporphyrinogen oxidase, was the critical enzyme for hepatic heme synthesis in variegate porphyria rabbits.

9. Production of rhApoAI-PBGD in CHO-K1SP, HEK293 cell line or *E. coli* lead to the synthesis of a truncated protein dependent on the cell type in which is produced.

10. rhApoAI-PBGD production in CHO-K1SP cell line results in rhApoAI-PBGD aggregates that cannot be separated by different purification process. The administration of these protein aggregates was ineffective in protecting against the acute attack in AIP mice.

11. Administration of a single dose of hApoAI-PBGD mRNA formulated in lipid nanoparticles normalized porphyrin precursors excretion during two consecutive phenobarbital-induced attacks in AIP mice and protected against pain for at least 2 weeks. Whereas, unconjugated hPBGD mRNA only showed full protection for one week.

CONCLUSIONS

Conclusions

1. Augmenting PBGD activity in the liver could be an etiological treatment for AIP as it restores regulation of hepatic heme synthesis pathway and protects against disturbances associated with acute attacks on central, peripheral and autonomic nervous systems on mouse and rabbit models.

2. Messenger RNA-based therapy in the variegate porphyria rabbit model showed more efficient protection against the acute attack than hemin, the standard of care for acute hepatic porphyrias, and rapid therapeutic action to treat acute metabolic decompensations. Thus, it is a promising strategy for etiological treatment of acute porphyria attacks.

Future directions

Future perspective would be focused on performing a clinical trial with the hPBGD mRNA therapy that has already proved to be safe in small and large experimental models, for treating the acute attacks, especially in patients with AIP, who has a deficiency in PBGD activity.

Further studies are focus on optimization of the rhApoAI-PBGD sequence that could reduce aggregate formation and the appearance of truncated forms, favouring scalling up industrial processes of the rhApoAI-PBGD protein for its commercial production. An optimized rhApoAI-PBGD sequence could also constitute a second generation of PBGD messengers to expand the therapeutic window during an ongoing acute attack and to space dosage in patients with chronic AIP presentation.

REFERENCES

REFERENCES

1. Córdoba, K.M.; Jericó, D.; Sampedro, A.; Jiang, L.; Iraburu, M.J.; Martini, P.G.V.; Berraondo, P.; Ávila, M.A.; Fontanellas, A. Messenger RNA as a Personalized Therapy: The Moment of Truth for Rare Metabolic Diseases. (In Press). *Int. Rev. Cell Mol. Biol.* **2022**.
2. Jiang, L.; Berraondo, P.; Jericó, D.; Guey, L.T.; Sampedro, A.; Frassetto, A.; Benenato, K.E.; Burke, K.; Santamaría, E.; Alegre, M.; et al. Systemic Messenger RNA as an Etiological Treatment for Acute Intermittent Porphyria. *Nat. Med.* **2018**, *24*, 1899–1909, doi:10.1038/s41591-018-0199-z.
3. Córdoba, K.M.; Serrano-Mendioroz, I.; Jericó, D.; Merino, M.; Jiang, L.; Sampedro, A.; Alegre, M.; Corrales, F.; Garrido, M.J.; Martini, P.G. V; et al. Recombinant Porphobilinogen Deaminase Targeted to the Liver Corrects Enzymopenia in a Mouse Model of Acute Intermittent Porphyria. *Sci. Transl. Med.* **2022**, *14*, eabc0700, doi:10.1126/scitranslmed.abc0700.
4. Manceau, H.; Gouya, L.; Puy, H. Acute Hepatic and Erythropoietic Porphyrias: From ALA Synthases 1 and 2 to New Molecular Bases and Treatments. *Curr Opin Hematol* **2017**, *24(3)*, 198–207.
5. Phillips, J.D. Heme Biosynthesis and Degradation for Clinicians. In Proceedings of the International Conference of Heme Biosynthesis and the Porphyrias. Orlando, Jan 12-14, 2018.
6. Puy, H.; Gouya, L.; Deybach, J.-C. Porphyrias. *Lancet* **2010**, *375*, 924–937, doi:10.1016/S0140-6736(09)61925-5.
7. Bissell, D.M.; Anderson, K.E.; Bonkovsky, H.L. Porphyria. *N. Engl. J. Med.* **2017**, *377*, 862–872, doi:10.1056/NEJMra1608634.
8. Brown, B.L.; Kardon, J.R.; Sauer, R.T.; Baker, T.A. Structure of the Mitochondrial Aminolevulinic Acid Synthase, a Key Heme Biosynthetic Enzyme. *Structure* **2018**, *26*, 580-589.e4, doi:10.1016/j.str.2018.02.012.
9. Chiabrando, D.; Mercurio, S.; Tolosano, E. Heme and Erythropoieis: More than a Structural Role. *Haematologica* **2014**, *99*, 973 LP – 983, doi:10.3324/haematol.2013.091991.
10. Podvinec, M.; Handschin, C.; Looser, R.; Meyer, U.A. Identification of the Xenosensors Regulating Human 5-Aminolevulinate Synthase. *Proc. Natl. Acad. Sci. U. S. A.* **2004**, *101*, 9127–9132, doi:10.1073/pnas.0401845101.
11. Schmitt, C.; Lenglet, H.; Yu, A.; Delaby, C.; Benecke, A.; Lefebvre, T.; Letteron, P.; Paradis, V.; Wahlin, S.; Sandberg, S.; et al. Recurrent Attacks of Acute

Hepatic Porphyria: Major Role of the Chronic Inflammatory Response in the Liver. *J. Intern. Med.* **2018**, *284*, 78–91, doi:10.1111/joim.12750.

12. Yasuda, M.; Erwin, A.L.; Liu, L.U.; Balwani, M.; Chen, B.; Kadirvel, S.; Gan, L.; Fiel, M.I.; Gordon, R.E.; Yu, C.; et al. Liver Transplantation for Acute Intermittent Porphyria: Biochemical and Pathologic Studies of the Explanted Liver. *Mol. Med.* **2015**, *21*, 487–495, doi:10.2119/molmed.2015.00099.
13. Handschin, C.; Lin, J.; Rhee, J.; Peyer, A.-K.; Chin, S.; Wu, P.-H.; Meyer, U.A.; Spiegelman, B.M. Nutritional Regulation of Hepatic Heme Biosynthesis and Porphyria through PGC-1α. *Cell* **2005**, *122*, 505–515, doi:10.1016/J.CELL.2005.06.040.
14. Degenhardt, T.; Väisänen, S.; Rakhshandehroo, M.; Kersten, S.; Carlberg, C. Peroxisome Proliferator-Activated Receptor Alpha Controls Hepatic Heme Biosynthesis through ALAS1. *J. Mol. Biol.* **2009**, *388*, 225–238, doi:10.1016/j.jmb.2009.03.024.
15. Drew, P.D.; Ades, I.Z. Regulation of the Stability of Chicken Embryo Liver Delta-Aminolevulinate Synthase MRNA by Hemin. *Biochem. Biophys. Res. Commun.* **1989**, *162*, 102–107, doi:10.1016/0006-291x(89)91968-2.
16. Lathrop, J.T.; Timko, M.P. Regulation by Heme of Mitochondrial Protein Transport through a Conserved Amino Acid Motif. *Science* **1993**, *259*, 522–525, doi:10.1126/science.8424176.
17. Tian, Q.; Li, T.; Hou, W.; Zheng, J.; Schrum, L.W.; Bonkovsky, H.L. Lon Peptidase 1 (LONP1)-Dependent Breakdown of Mitochondrial 5-Aminolevulinic Acid Synthase Protein by Heme in Human Liver Cells. *J. Biol. Chem.* **2011**, *286*, 26424–26430, doi:10.1074/jbc.M110.215772.
18. Ferreira, G.C. Handbook of Porphyrin Science (Volume 29). *Handb. Porphyr. Sci.* 2012, *Volume 29*, 564.
19. Franken, A.C.W.; Lokman, B.C.; Ram, A.F.J.; Punt, P.J.; van den Hondel, C.A.M.J.J.; de Weert, S. Heme Biosynthesis and Its Regulation: Towards Understanding and Improvement of Heme Biosynthesis in Filamentous Fungi. *Appl. Microbiol. Biotechnol.* **2011**, *91*, 447–460, doi:10.1007/s00253-011-3391-3.
20. Junkins-Hopkins, J.M. Porphyrias. *Clin. Pathol. Asp. Ski. Dis. Endocrine, Metab. Nutr. Depos. Dis.* **2010**, *375*, 83–90, doi:10.1007/978-1-60761-181-3_10.
21. Waza, A.A.; Hamid, Z.; Ali, S.; Bhat, S.A.; Bhat, M.A. A Review on Heme Oxygenase-1 Induction: Is It a Necessary Evil. *Inflamm. Res. Off. J. Eur. Histamine Res. Soc. ... [et al.]* **2018**, *67*, 579–588, doi:10.1007/s00011-018-1151-x.

22. Phillips, J.D. Heme Biosynthesis and the Porphyrias. *Mol. Genet. Metab.* **2019**, doi:10.1016/J.YMGME.2019.04.008.
23. Balwani, M. Erythropoietic Protoporphyria and X-Linked Protoporphyria: Pathophysiology, Genetics, Clinical Manifestations, and Management. *Mol. Genet. Metab.* **2019**, *128*, 298–303, doi:10.1016/j.ymgme.2019.01.020.
24. Schulenburg-Brand, D.; Katugampola, R.; Anstey, A. V.; Badminton, M.N. The Cutaneous Porphyrias. *Dermatol. Clin.* **2014**, *32*, 369–384, doi:10.1016/J.DET.2014.03.001.
25. Stölzel, U.; Doss, M.O.; Schuppan, D. Clinical Guide and Update on Porphyrias. *Gastroenterology* **2019**, *157*, 365-381.e4, doi:10.1053/j.gastro.2019.04.050.
26. Stein, P.E.; Badminton, M.N.; Rees, D.C. Update Review of the Acute Porphyrias. *Br. J. Haematol.* **2017**, *176*, 527–538, doi:10.1111/bjh.14459.
27. Bonkovsky, H.L.; Dixon, N.; Rudnick, S. Pathogenesis and Clinical Features of the Acute Hepatic Porphyrias (AHPs). *Mol. Genet. Metab.* **2019**, *128*, 213–218, doi:10.1016/j.ymgme.2019.03.002.
28. Meyer, U.A.; Schuurmans, M.M.; Lindberg, R.L.P. Acute Porphyrias: Pathogenesis of Neurological Manifestations. *Semin Liver Dis* **1998**, *18*, 43–52, doi:10.1055/s-2007-1007139.
29. Brennan, M.J.; Cantrill, R.C. Delta-Aminolaevulinic Acid Is a Potent Agonist for GABA Autoreceptors. *Nature* **1979**, *280*, 514–515, doi:10.1038/280514a0.
30. Jaramillo-Calle, D.A.; Solano, J.M.; Rabinstein, A.A.; Bonkovsky, H.L. Porphyria-Induced Posterior Reversible Encephalopathy Syndrome and Central Nervous System Dysfunction. *Mol. Genet. Metab.* **2019**, *128*, 242–253, doi:10.1016/J.YMGME.2019.10.011.
31. Marsden, J.T.; Chowdhury, P.; Wang, J.; Deacon, A.; Dutt, N.; Peters, T.J.; Macdougall, I.C. Acute Intermittent Porphyria and Chronic Renal Failure. *Clin. Nephrol.* **2008**, *69*, 339–346, doi:10.5414/cnp69339.
32. Tchernitchko, D.; Tavernier, Q.; Lamoril, J.; Schmitt, C.; Talbi, N.; Lyoumi, S.; Robreau, A.-M.; Karim, Z.; Gouya, L.; Thervet, E.; et al. A Variant of Peptide Transporter 2 Predicts the Severity of Porphyria-Associated Kidney Disease. *J. Am. Soc. Nephrol.* **2017**, *28*, 1924 LP – 1932, doi:10.1681/ASN.2016080918.
33. Peoc'h, K.; Manceau, H.; Karim, Z.; Wahlin, S.; Gouya, L.; Puy, H.; Deybach, J.-C. Hepatocellular Carcinoma in Acute Hepatic Porphyrias: A Damocles Sword. *Mol. Genet. Metab.* **2019**, *128*, 236–241, doi:10.1016/j.ymgme.2018.10.001.
34. Moghe, A.; Anderson, K.E. Expanding Experience With Liver Transplantation in Acute Intermittent Porphyria. *Liver Transplant. Off. Publ. Am. Assoc. Study Liver Dis. Int. Liver Transplant. Soc.* 2021, *27*, 477–478.

35. Stojeba, N.; Meyer, C.; Jeanpierre, C.; Perrot, F.; Hirth, C.; Pottecher, T.; Deybach, J.-C. Recovery from a Variegate Porphyria by a Liver Transplantation. *Liver Transplant. Off. Publ. Am. Assoc. Study Liver Dis. Int. Liver Transplant. Soc.* **2004**, *10*, 935–938, doi:10.1002/lt.20136.
36. Dowman, J.K.; Gunson, B.K.; Bramhall, S.; Badminton, M.N.; Newsome, P.N. Liver Transplantation from Donors with Acute Intermittent Porphyria. *Ann. Intern. Med.* 2011, *154*, 571–572.
37. Innala, E.; Bäckström, T.; Bixo, M.; Andersson, C. Evaluation of Gonadotropin-Releasing Hormone Agonist Treatment for Prevention of Menstrual-Related Attacks in Acute Porphyria. *Acta Obstet. Gynecol. Scand.* **2010**, *89*, 95–100, doi:10.3109/00016340903390729.
38. Neeleman, R.A.; Wagenmakers, M.A.E.M.; Koole-Lesuis, R.H.; Mijnhout, G.S.; Wilson, J.H.P.; Friesema, E.C.H.; Langendonk, J.G. Medical and Financial Burden of Acute Intermittent Porphyria. *J. Inherit. Metab. Dis.* **2018**, *41*, 809–817, doi:10.1007/s10545-018-0178-z.
39. Gouya, L.; Ventura, P.; Balwani, M.; Bissell, D.M.; Rees, D.C.; Stölzel, U.; Phillips, J.D.; Kauppinen, R.; Langendonk, J.G.; Desnick, R.J.; et al. EXPLORE: A Prospective, Multinational, Natural History Study of Patients with Acute Hepatic Porphyria with Recurrent Attacks. *Hepatology* **2020**, *71*, 1546–1558, doi:10.1002/hep.30936.
40. Cardenas, J.L.; Guerrero, C. Acute Intermittent Porphyria: General Aspects with Focus on Pain. *Curr. Med. Res. Opin.* **2018**, *34*, 1309–1315, doi:10.1080/03007995.2018.1435521.
41. Meissner, P.N.; Dailey, T.A.; Hift, R.J.; Ziman, M.; Corrigall, A. V; Roberts, A.G.; Meissner, D.M.; Kirsch, R.E.; Dailey, H.A. A R59W Mutation in Human Protoporphyrinogen Oxidase Results in Decreased Enzyme Activity and Is Prevalent in South Africans with Variegate Porphyria. *Nat. Genet.* **1996**, *13*, 95–97, doi:10.1038/ng0596-95.
42. Singal, A.K.; Anderson, K.E. Variegate Porphyria. In; Adam, M.P., Ardinger, H.H., Pagon, R.A., Wallace, S.E., Bean, L.J.H., Mirzaa, G., Amemiya, A., Eds.; Seattle (WA), 1993.
43. Ramanujam, V.-M.S.; Anderson, K.E. Porphyria Diagnostics-Part 1: A Brief Overview of the Porphyrias. *Curr. Protoc. Hum. Genet.* **2015**, *86*, 17.20.1-17.20.26, doi:10.1002/0471142905.hg1720s86.
44. Meissner, P.; Adams, P.; Kirsch, R. Allosteric Inhibition of Human Lymphoblast and Purified Porphobilinogen Deaminase by Protoporphyrinogen and Coproporphyrinogen: A Possible Mechanism for the Acute Attack of Variegate

Porphyria. *J. Clin. Invest.* **1993**, *91*, 1436–1444, doi:10.1172/JCI116348.

45. Chen, B.; Solis-Villa, C.; Hakenberg, J.; Qiao, W.; Srinivasan, R.R.; Yasuda, M.; Balwani, M.; Doheny, D.; Peter, I.; Chen, R.; et al. Acute Intermittent Porphyria: Predicted Pathogenicity of HMBS Variants Indicates Extremely Low Penetrance of the Autosomal Dominant Disease. *Hum. Mutat.* **2016**, *37*, 1215–1222, doi:10.1002/humu.23067.
46. Song, G.; Li, Y.; Cheng, C.; Zhao, Y.; Gao, A.; Zhang, R.; Joachimiak, A.; Shaw, N.; Liu, Z.-J. Structural Insight into Acute Intermittent Porphyria. *FASEB J. Off. Publ. Fed. Am. Soc. Exp. Biol.* **2009**, *23*, 396–404, doi:10.1096/fj.08-115469.
47. Bustad, H.J.; Kallio, J.P.; Laitaoja, M.; Toska, K.; Kursula, I.; Martinez, A.; Jänis, J. Characterization of Porphobilinogen Deaminase Mutants Reveals That Arginine-173 Is Crucial for Polypyrrole Elongation Mechanism. *iScience* **2021**, *24*, 102152, doi:10.1016/j.isci.2021.102152.
48. Anderson, P.M.; Desnick, R.J. Porphobilinogen Deaminase: Methods and Principles of the Enzymatic Assay. *Enzyme* **1982**, *28*, 146–157, doi:10.1159/000459098.
49. Peoc'h, K.; Nicolas, G.; Schmitt, C.; Mirmiran, A.; Daher, R.; Lefebvre, T.; Gouya, L.; Karim, Z.; Puy, H. Regulation and Tissue-Specific Expression of δ-Aminolevulinic Acid Synthases in Non-Syndromic Sideroblastic Anemias and Porphyrias. *Mol. Genet. Metab.* **2019**, *128*, 190–197, doi:10.1016/j.ymgme.2019.01.015.
50. Di Pierro, E.; Granata, F. Nutrients and Porphyria: An Intriguing Crosstalk. *Int. J. Mol. Sci.* **2020**, *21*, doi:10.3390/ijms21103462.
51. Storjord, E.; Dahl, J.A.; Landsem, A.; Ludviksen, J.K.; Karlsen, M.B.; Karlsen, B.O.; Brekke, O.L. Lifestyle Factors Including Diet and Biochemical Biomarkers in Acute Intermittent Porphyria: Results from a Case-Control Study in Northern Norway. *Mol. Genet. Metab.* **2018**, 0–1, doi:10.1016/j.ymgme.2018.12.006.
52. Balwani, M.; Wang, B.; Anderson, K.E.; Bloomer, J.R.; Bissell, D.M.; Bonkovsky, H.L.; Phillips, J.D.; Desnick, R.J. Acute Hepatic Porphyrias: Recommendations for Evaluation and Long-Term Management. *Hepatology* **2017**, *66*, 1314–1322, doi:10.1002/hep.29313.
53. Solares, I.; Tejedor, M.; Jericó, D.; Morales-Conejo, M.; Enríquez de Salamanca, R.; Fontanellas, A.; Tejedor-Jorge, A. Management of Hyponatremia Associated with Acute Porphyria-Proposal for the Use of Tolvaptan. *Ann. Transl. Med.* **2020**, *8*, 1098, doi:10.21037/atm-20-1529.
54. Marsden, J.T.; Guppy, S.; Stein, P.; Cox, T.M.; Badminton, M.; Gardiner, T.; Barth, J.H.; Stewart, M.F.; Rees, D.C. Audit of the Use of Regular Haem

Arginate Infusions in Patients with Acute Porphyria to Prevent Recurrent Symptoms. *JIMD Rep.* **2015**, *22*, 57–65, doi:10.1007/8904_2015_411.

55. Anderson, K.E.; Bloomer, J.R.; Bonkovsky, H.L.; Kushner, J.P.; Pierach, C.A.; Pimstone, N.R.; Desnick, R.J. Recommendations for the Diagnosis and Treatment of the Acute Porphyrias. *Ann. Intern. Med.* **2005**, *142*, 439–450, doi:10.7326/0003-4819-142-6-200503150-00010.
56. Tenhunen, R.; Mustajoki, P. Acute Porphyria: Treatment with Heme. *Semin. Liver Dis.* **1998**, *18*, 53–55, doi:10.1055/s-2007-1007140.
57. Willandt, B.; Langendonk, J.G.; Biermann, K.; Meersseman, W.; D'Heygere, F.; George, C.; Verslype, C.; Monbaliu, D.; Cassiman, D. Liver Fibrosis Associated with Iron Accumulation Due to Long-Term Heme-Arginate Treatment in Acute Intermittent Porphyria: A Case Series. *JIMD Rep.* **2016**, *25*, 77–81, doi:10.1007/8904_2015_458.
58. Dover, S.B.; Moore, M.R.; Fitzsimmons, E.J.; Graham, A.; McColl, K.E. Tin Protoporphyrin Prolongs the Biochemical Remission Produced by Heme Arginate in Acute Hepatic Porphyria. *Gastroenterology* **1993**, *105*, 500–506, doi:10.1016/0016-5085(93)90726-s.
59. Kauppinen, R.; Mustajoki, P. Prognosis of Acute Porphyria: Occurrence of Acute Attacks, Precipitating Factors, and Associated Diseases. *Medicine (Baltimore).* **1992**, *71*, 1–13.
60. Scott, L.J. Givosiran: First Approval. *Drugs* **2020**, *80*, 335–339, doi:10.1007/s40265-020-01269-0.
61. Balwani, M.; Sardh, E.; Ventura, P.; Peiró, P.A.; Rees, D.C.; Stölzel, U.; Bissell, D.M.; Bonkovsky, H.L.; Windyga, J.; Anderson, K.E.; et al. Phase 3 Trial of RNAi Therapeutic Givosiran for Acute Intermittent Porphyria. *N. Engl. J. Med.* **2020**, *382*, 2289–2301, doi:10.1056/NEJMoa1913147.
62. To-Figueras, J.; Wijngaard, R.; García-Villoria, J.; Aarsand, A.K.; Aguilera, P.; Deulofeu, R.; Brunet, M.; Gómez-Gómez, À.; Pozo, O.J.; Sandberg, S. Dysregulation of Homocysteine Homeostasis in Acute Intermittent Porphyria Patients Receiving Heme Arginate or Givosiran. *J. Inherit. Metab. Dis.* **2021**, *44*, 961–971, doi:10.1002/jimd.12391.
63. Fontanellas, A.; Ávila, M.A.; Arranz, E.; Enríquez de Salamanca, R.; Morales-Conejo, M. Acute Intermittent Porphyria, Givosiran, and Homocysteine. *J. Inherit. Metab. Dis.* 2021, *44*, 790–791.
64. McCully, K.S. Homocysteine, Vitamins, and Vascular Disease Prevention. *Am. J. Clin. Nutr.* **2007**, *86*, 1563S-8S, doi:10.1093/ajcn/86.5.1563S.
65. Poli, A.; Schmitt, C.; Moulouel, B.; Mirmiran, A.; Talbi, N.; Rivière, S.; Cerutti, D.;

Bouchoule, I.; Faivre, A.; Grobost, V.; et al. Givosiran in Acute Intermittent Porphyria: A Personalized Medicine Approach. *Mol. Genet. Metab.* **2022**, doi:https://doi.org/10.1016/j.ymgme.2022.01.002.

66. de Sousa Arantes Ferreira, G.; Claudio de Oliveira, L.; Roberto de Sousa Ulisses, L.; Luis Conde Watanabe, A.; Medeiros, I.N.; Souto Siqueira Cardoso, H.; Creão da Costa Alves, I.; Martins de Almeida, T.; Viana de Lima, L.; Fontoura, R.P.; et al. Combined Liver and Kidney Transplant in Acute Intermittent Porphyria: A Case Report. *Am. J. Case Rep.* **2020**, *21*, e927832, doi:10.12659/AJCR.927832.
67. Dowman, J.K.; Gunson, B.K.; Mirza, D.F.; Bramhall, S.R.; Badminton, M.N.; Newsome, P.N.; Party, on behalf of the U.K.L.S. and A.W. Liver Transplantation for Acute Intermittent Porphyria Is Complicated by a High Rate of Hepatic Artery Thrombosis. *Liver Transplant.* **2012**, *18*, 195–200, doi:10.1002/lt.22345.
68. Yin, Z.; Wahlin, S.; Ellis, E.C.S.; Harper, P.; Ericzon, B.-G.; Nowak, G. Hepatocyte Transplantation Ameliorates the Metabolic Abnormality in a Mouse Model of Acute Intermittent Porphyria. *Cell Transplant.* **2014**, *23*, 1153–1162, doi:10.3727/096368913X666980.
69. Bustad, H.J.; Kallio, J.P.; Vorland, M.; Fiorentino, V.; Sandberg, S.; Schmitt, C.; Aarsand, A.K.; Martinez, A. Acute Intermittent Porphyria: An Overview of Therapy Developments and Future Perspectives Focusing on Stabilisation of HMBS and Proteostasis Regulators. *Int. J. Mol. Sci.* **2021**, *22*, doi:10.3390/ijms22020675.
70. Bustad, H.J.; Toska, K.; Schmitt, C.; Vorland, M.; Skjærven, L.; Kallio, J.P.; Simonin, S.; Letteron, P.; Underhaug, J.; Sandberg, S.; et al. A Pharmacological Chaperone Therapy for Acute Intermittent Porphyria. *Mol. Ther.* **2020**, *28*, 677–689, doi:10.1016/j.ymthe.2019.11.010.
71. Unzu, C.; Sampedro, A.; Mauleón, I.; Alegre, M.; Beattie, S.G.; De Salamanca, R.E.; Snapper, J.; Twisk, J.; Petry, H.; González-Aseguinolaza, G.; et al. Sustained Enzymatic Correction by RAAV-Mediated Liver Gene Therapy Protects against Induced Motor Neuropathy in Acute Porphyria Mice. *Mol. Ther.* **2011**, *19*, 243–250, doi:10.1038/mt.2010.210.
72. Yasuda, M.; Bishop, D.F.; Fowkes, M.; Cheng, S.H.; Gan, L.; Desnick, R.J. AAV8-Mediated Gene Therapy Prevents Induced Biochemical Attacks of Acute Intermittent Porphyria and Improves Neuromotor Function. *Mol. Ther.* **2010**, *18*, 17–22, doi:10.1038/mt.2009.250.
73. Unzu, C.; Melero, I.; Hervás-Stubbs, S.; Sampedro, A.; Mancheño, U.; Morales-Kastresana, A.; Serrano-Mendioroz, I.; de Salamanca, R.E.; Benito, A.;

Fontanellas, A. Helper-Dependent Adenovirus Achieve More Efficient and Persistent Liver Transgene Expression in Non-Human Primates under Immunosuppression. *Gene Ther.* **2015**, *22*, 856–865, doi:10.1038/gt.2015.64.

74. D'Avola, D.; López-Franco, E.; Sangro, B.; Pañeda, A.; Grossios, N.; Gil-Farina, I.; Benito, A.; Twisk, J.; Paz, M.; Ruiz, J.; et al. Phase I Open Label Liver-Directed Gene Therapy Clinical Trial for Acute Intermittent Porphyria. *J. Hepatol.* **2016**, *65*, 776–783, doi:10.1016/j.jhep.2016.05.012.
75. Dalwadi, D.A.; Torrens, L.; Abril-Fornaguera, J.; Pinyol, R.; Willoughby, C.; Posey, J.; Llovet, J.M.; Lanciault, C.; Russell, D.W.; Grompe, M.; et al. Liver Injury Increases the Incidence of HCC Following AAV Gene Therapy in Mice. *Mol. Ther.* **2021**, *29*, 680–690, doi:10.1016/j.ymthe.2020.10.018.
76. Johansson, A.; Möller, C.; Gellerfors, P.; Harper, P. Non-Viral Mediated Gene Transfer of Porphobilinogen Deaminase into Mammalian Cells. *Scand. J. Clin. Lab. Invest.* **2002**, *62*, 105–113, doi:10.1080/003655102753611726.
77. Johansson, A.; Nowak, G.; Möller, C.; Harper, P. Non-Viral Delivery of the Porphobilinogen Deaminase CDNA into a Mouse Model of Acute Intermittent Porphyria. *Mol. Genet. Metab.* **2004**, *82*, 20–26, doi:10.1016/j.ymgme.2004.02.008.
78. Houseley, J.; Tollervey, D. The Many Pathways of RNA Degradation. *Cell* **2009**, *136*, 763–776, doi:10.1016/j.cell.2009.01.019.
79. Akinc, A.; Querbes, W.; De, S.; Qin, J.; Frank-Kamenetsky, M.; Jayaprakash, K.N.; Jayaraman, M.; Rajeev, K.G.; Cantley, W.L.; Dorkin, J.R.; et al. Targeted Delivery of RNAi Therapeutics With Endogenous and Exogenous Ligand-Based Mechanisms. *Mol. Ther.* **2010**, *18*, 1357–1364, doi:https://doi.org/10.1038/mt.2010.85.
80. Sabnis, S.; Kumarasinghe, E.S.; Salerno, T.; Mihai, C.; Ketova, T.; Senn, J.J.; Lynn, A.; Bulychev, A.; McFadyen, I.; Chan, J.; et al. A Novel Amino Lipid Series for MRNA Delivery: Improved Endosomal Escape and Sustained Pharmacology and Safety in Non-Human Primates. *Mol. Ther.* **2018**, *26*, 1509–1519, doi:10.1016/J.YMTHE.2018.03.010.
81. Sahay, G.; Querbes, W.; Alabi, C.; Eltoukhy, A.; Sarkar, S.; Zurenko, C.; Karagiannis, E.; Love, K.; Chen, D.; Zoncu, R.; et al. Efficiency of SiRNA Delivery by Lipid Nanoparticles Is Limited by Endocytic Recycling. *Nat. Biotechnol.* **2013**, *31*, 653–658, doi:10.1038/nbt.2614.
82. Patel, S.; Ashwanikumar, N.; Robinson, E.; DuRoss, A.; Sun, C.; Murphy-Benenato, K.E.; Mihai, C.; Almarsson, Ö.; Sahay, G. Boosting Intracellular Delivery of Lipid Nanoparticle-Encapsulated MRNA. *Nano Lett.* **2017**, *17*, 5711–

5718, doi:10.1021/acs.nanolett.7b02664.

83. Trepotec, Z.; Lichtenegger, E.; Plank, C.; Aneja, M.K.; Rudolph, C. Delivery of MRNA Therapeutics for the Treatment of Hepatic Diseases. *Mol. Ther.* **2019**, *27*, 794–802, doi:https://doi.org/10.1016/j.ymthe.2018.12.012.
84. Martini, P.G. V; Guey, L.T. A New Era for Rare Genetic Diseases: Messenger RNA Therapy. *Hum. Gene Ther.* **2019**, *30*, 1180–1189, doi:10.1089/hum.2019.090.
85. Khurana, A.; Allawadhi, P.; Khurana, I.; Allwadhi, S.; Weiskirchen, R.; Banothu, A.K.; Chhabra, D.; Joshi, K.; Bharani, K.K. Role of Nanotechnology behind the Success of MRNA Vaccines for COVID-19. *Nano Today* **2021**, *38*, 101142, doi:https://doi.org/10.1016/j.nantod.2021.101142.
86. Dammes, N.; Peer, D. Paving the Road for RNA Therapeutics. *Trends Pharmacol. Sci.* **2020**, *41*, 755–775, doi:https://doi.org/10.1016/j.tips.2020.08.004.
87. Berraondo, P.; Martini, P.G. V; Avila, M.A.; Fontanellas, A. Messenger RNA Therapy for Rare Genetic Metabolic Diseases. *Gut* **2019**, gutjnl-2019-318269, doi:10.1136/gutjnl-2019-318269.
88. Johansson, A.; Möller, C.; Fogh, J.; Harper, P. Biochemical Characterization of Porphobilinogen Deaminase-Deficient Mice during Phenobarbital Induction of Heme Synthesis and the Effect of Enzyme Replacement. *Mol. Med.* **2003**, *9*, 193–199, doi:10.2119/2004-00002.johansson.
89. Sardh, E.; Rejkjaer, L.; Andersson, D.E.H.; Harper, P. Safety, Pharmacokinetics and Pharmocodynamics of Recombinant Human Porphobilinogen Deaminase in Healthy Subjects and Asymptomatic Carriers of the Acute Intermittent Porphyria Gene Who Have Increased Porphyrin Precursor Excretion. *Clin. Pharmacokinet.* **2007**, *46*, 335–349, doi:10.2165/00003088-200746040-00006.
90. Glass, C.; Pittman, R.C.; Weinstein, D.B.; Steinberg, D. Dissociation of Tissue Uptake of Cholesterol Ester from That of Apoprotein A-I of Rat Plasma High Density Lipoprotein: Selective Delivery of Cholesterol Ester to Liver, Adrenal, and Gonad. *Proc. Natl. Acad. Sci. U. S. A.* **1983**, *80*, 5435–5439, doi:10.1073/pnas.80.17.5435.
91. Lux, S.E.; Hirz, R.; Shrager, R.I.; Gotto, A.M. The Influence of Lipid on the Conformation of Human Plasma High Density Apolipoproteins. *J. Biol. Chem.* **1972**, *247*, 2598–2606.
92. Fung, K.Y.; Wang, C.; Nyegaard, S.; Heit, B.; Fairn, G.D.; Lee, W.L. SR-BI Mediated Transcytosis of HDL in Brain Microvascular Endothelial Cells Is Independent of Caveolin, Clathrin, and PDZK1. *Front. Physiol.* **2017**, *8*, 841,

doi:10.3389/fphys.2017.00841.

93. Kuwahara, H.; Nishina, K.; Yoshida, K.; Nishina, T.; Yamamoto, M.; Saito, Y.; Piao, W.; Yoshida, M.; Mizusawa, H.; Yokota, T. Efficient in Vivo Delivery of SiRNA into Brain Capillary Endothelial Cells along with Endogenous Lipoprotein. *Mol. Ther.* **2011**, *19*, 2213–2221, doi:10.1038/mt.2011.186.
94. Lindberg, R.L.P.; Porcher, C.; Grandchamp, B.; Ledermann, B.; Bürki, K.; Brandner, S.; Aguzzi, A.; Meyer, U.A. Porphobilinogen Deaminase Deficiency in Mice Causes a Neuropathy Resembling That of Human Hepatic Porphyria. *Nat. Genet.* **1996**, *12*, 195–199, doi:10.1038/ng0296-195.
95. Detre, J.A.; Leigh, J.S.; Williams, D.S.; Koretsky, A.P. Perfusion Imaging. *Magn. Reson. Med.* **1992**, *23*, 37–45, doi:10.1002/mrm.1910230106.
96. Williams, D.S.; Detre, J.A.; Leigh, J.S.; Koretsky, A.P. Magnetic Resonance Imaging of Perfusion Using Spin Inversion of Arterial Water. *Proc. Natl. Acad. Sci. U. S. A.* **1992**, *89*, 212–216, doi:10.1073/pnas.89.1.212.
97. Herscovitch, P.; Raichle, M.E. What Is the Correct Value for the Brain-Blood Partition Coefficient for Water? *J. Cereb. Blood Flow Metab.* **1985**, *5*, 65–69, doi:10.1038/jcbfm.1985.9.
98. Westerlund, J.; Pudek, M.; Schreiber, W.E. A Rapid and Accurate Spectrofluorometric Method for Quantification and Screening of Urinary Porphyrins. *Clin. Chem.* **1988**, *34*, 345–351.
99. Elder, G.H.; Smith, S.G.; Smyth, S.J. Laboratory Investigation of the Porphyrias. *Ann. Clin. Biochem.* **1990**, *27 (Pt 5)*, 395–412, doi:10.1177/000456329002700501.
100. Da Silva, V.; Simonin, S.; Deybach, J.C.; Puy, H.; Nordmann, Y. Variegate Porphyria: Diagnostic Value of Fluorometric Scanning of Plasma Porphyrins. *Clin. Chim. Acta.* **1995**, *238*, 163–168, doi:10.1016/0009-8981(95)06085-r.
101. Lockwood, W.H.; Poulos, V.; Rossi, E.; Curnow, D.H. Rapid Procedure for Fecal Porphyrin Assay. *Clin. Chem.* **1985**, *31*, 1163–1167.
102. Rossi, E.; Curnow, D.H. In HPLC of Small Molecules: A Practical Approach. In *Lim, C.K, Ed. IRL Press: Oxford*; 1986; pp. 261–305.
103. Fujita, H.; Orii, Y.; Sano, S. Evidence of Increased Synthesis of Delta-Aminolevulinic Acid Dehydratase in Experimental Lead-Poisoned Rats. *Biochim. Biophys. Acta* **1981**, *678*, 39–50, doi:10.1016/0304-4165(81)90045-3.
104. Tsai, S.F.; Bishop, D.F.; Desnick, R.J. Coupled-Enzyme and Direct Assays for Uroporphyrinogen III Synthase Activity in Human Erythrocytes and Cultured Lymphoblasts. Enzymatic Diagnosis of Heterozygotes and Homozygotes with Congenital Erythropoietic Porphyria. *Anal. Biochem.* **1987**, *166*, 120–133,

doi:10.1016/0003-2697(87)90554-9.

105. de Verneuil, H.; Grandchamp, B.; Nordmann, Y. Some Kinetic Properties of Human Red Cell Uroporphyrinogen Decarboxylase. *Biochim. Biophys. Acta* **1980**, *611*, 174–186, doi:10.1016/0005-2744(80)90053-4.
106. Lamoril, J.; Martasek, P.; Deybach, J.C.; Da Silva, V.; Grandchamp, B.; Nordmann, Y. A Molecular Defect in Coproporphyrinogen Oxidase Gene Causing Harderoporphyria, a Variant Form of Hereditary Coproporphyria. *Hum. Mol. Genet.* **1995**, *4*, 275–278, doi:10.1093/hmg/4.2.275.
107. Li, F.M.; Lim, C.K.; Peters, T.J. An HPLC Assay for Rat Liver Ferrochelatase Activity. *Biomed. Chromatogr.* **1987**, *2*, 164–168, doi:10.1002/bmc.1130020408.
108. Medja, F.; Allouche, S.; Frachon, P.; Jardel, C.; Malgat, M.; Mousson de Camaret, B.; Slama, A.; Lunardi, J.; Mazat, J.P.; Lombès, A. Development and Implementation of Standardized Respiratory Chain Spectrophotometric Assays for Clinical Diagnosis. *Mitochondrion* **2009**, *9*, 331–339, doi:10.1016/j.mito.2009.05.001.
109. Collantes, M.; Serrano-Mendioroz, I.; Benito, M.; Molinet-Dronda, F.; Delgado, M.; Vinaixa, M.; Sampedro, A.; de Salamanca, R.E.; Prieto, E.; Pozo, M.A.; et al. Glucose Metabolism during Fasting Is Altered in Experimental Porphobilinogen Deaminase Deficiency. *Hum. Mol. Genet.* **2016**, *25*, 1318–1327, doi:10.1093/hmg/ddw013.
110. Langford, D.J.; Bailey, A.L.; Chanda, M.L.; Clarke, S.E.; Drummond, T.E.; Echols, S.; Glick, S.; Ingrao, J.; Klassen-Ross, T.; Lacroix-Fralish, M.L.; et al. Coding of Facial Expressions of Pain in the Laboratory Mouse. *Nat. Methods* **2010**, *7*, 447–449, doi:10.1038/nmeth.1455.
111. Matsumiya, L.C.; Sorge, R.E.; Sotocinal, S.G.; Tabaka, J.M.; Wieskopf, J.S.; Zaloum, A.; King, O.D.; Mogil, J.S. Using the Mouse Grimace Scale to Reevaluate the Efficacy of Postoperative Analgesics in Laboratory Mice. *J. Am. Assoc. Lab. Anim. Sci.* **2012**, *51*, 42–49.
112. Jericó, D.; Luis, E.O.; Cussó, L.; Fernández-Seara, M.A.; Morales, X.; Córdoba, K.M.; Benito, M.; Sampedro, A.; Larriva, M.; Ramírez, M.J.; et al. Brain Ventricular Enlargement in Human and Murine Acute Intermittent Porphyria. *Hum. Mol. Genet.* **2020**, *29*, 3211–3223, doi:10.1093/hmg/ddaa204.
113. Dhaun, N.; Goddard, J.; Kohan, D.; Pollock, D.; Schiffrin, E.; Webb, D. Role of Endothelin-1 in Clinical Hypertension. *Hypertension* **2008**, *52*, 452–459, doi:10.1161/HYPERTENSIONAHA.108.117366.
114. Badminton, M.N.; Whatley, S.D.; Aarsand, A.K. Porphyrins and Porphyrias. In *Tietz fundamentals of clinical chemistry and molecular diagnostics.*; Rifai, N.,

Horvath, A.R., Wittwe, C.T., Eds.; Elsevier: St Louis, Missouri, USA, 2019.

115. Atamna, H.; Liu, J.; Ames, B.N. Heme Deficiency Selectively Interrupts Assembly of Mitochondrial Complex IV in Human Fibroblasts: Revelance to Aging. *J. Biol. Chem.* **2001**, *276*, 48410–48416, doi:10.1074/jbc.M108362200.
116. Pigeon, C.; Ilyin, G.; Courselaud, B.; Leroyer, P.; Turlin, B.; Brissot, P.; Loréal, O. A New Mouse Liver-Specific Gene, Encoding a Protein Homologous to Human Antimicrobial Peptide Hepcidin, Is Overexpressed during Iron Overload. *J. Biol. Chem.* **2001**, *276*, 7811–7819, doi:10.1074/jbc.M008923200.
117. Masopust, D.; Sivula, C.P.; Jameson, S.C. Of Mice, Dirty Mice, and Men: Using Mice To Understand Human Immunology. *J. Immunol.* **2017**, *199*, 383–388, doi:10.4049/jimmunol.1700453.
118. Buendía-Martínez, J.; Barreda-Sánchez, M.; Rodríguez-Peña, L.; Ballesta-Martínez, M.J.; López-González, V.; Sánchez-Soler, M.J.; Serrano-Antón, A.T.; Pérez-Tomás, M.E.; Gil-Ferrer, R.; Avilés-Plaza, F.; et al. Health Impact of Acute Intermittent Porphyria in Latent and Non-Recurrent Attacks Patients. *Orphanet J. Rare Dis.* **2021**, *16*, 106, doi:10.1186/s13023-021-01742-3.
119. Pallet, N.; Mami, I.; Schmitt, C.; Karim, Z.; François, A.; Rabant, M.; Nochy, D.; Gouya, L.; Deybach, J.-C.; Xu-Dubois, Y.; et al. High Prevalence of and Potential Mechanisms for Chronic Kidney Disease in Patients with Acute Intermittent Porphyria. *Kidney Int.* **2015**, *88*, 386–395, doi:https://doi.org/10.1038/ki.2015.97.
120. McColl, K.E.; Moore, M.R.; Thompson, G.G.; Goldberg, A. Treatment with Haematin in Acute Hepatic Porphyria. *Q. J. Med.* **1981**, *50*, 161–174.
121. Bosilkovska, M.; Samer, C.; Déglon, J.; Thomas, A.; Walder, B.; Desmeules, J.; Daali, Y. Evaluation of Mutual Drug-Drug Interaction within Geneva Cocktail for Cytochrome P450 Phenotyping Using Innovative Dried Blood Sampling Method. *Basic Clin. Pharmacol. Toxicol.* **2016**, *119*, 284–290, doi:10.1111/bcpt.12586.
122. Solares, I.; Izquierdo-Sánchez, L.; Morales-Conejo, M.; Jericó, D.; Castelbón, F.J.; Córdoba, K.M.; Sampedro, A.; Lumbreras, C.; Moreno-Aliaga, M.J.; Enríquez de Salamanca, R.; et al. High Prevalence of Insulin Resistance in Asymptomatic Patients with Acute Intermittent Porphyria and Liver-Targeted Insulin as a Novel Therapeutic Approach. *Biomedicines* **2021**, *9*, doi:10.3390/biomedicines9030255.
123. Unzu, C.; Sampedro, A.; Mauleón, I.; González-Aparicio, M.; Enríquez de Salamanca, R.; Prieto, J.; Aragón, T.; Fontanellas, A. Helper-Dependent Adenoviral Liver Gene Therapy Protects against Induced Attacks and Corrects Protein Folding Stress in Acute Intermittent Porphyria Mice. *Hum. Mol. Genet.*

2013, *22*, 2929–2940, doi:10.1093/hmg/ddt148.

124. Lai, C.-W.; Hung, T.; Lin, W.S.J. Blindness of Cerebral Origin in Acute Intermittent Porphyria: Report of a Case and Postmortem Examination. *Arch. Neurol.* **1977**, *34*, 310–312, doi:10.1001/archneur.1977.00500170064013.
125. Dagens, A.; Gilhooley, M.J. Acute Intermittent Porphyria Leading to Posterior Reversible Encephalopathy Syndrome (PRES): A Rare Cause of Abdominal Pain and Seizures. *BMJ Case Rep.* **2016**, *2016*, bcr2016215350, doi:10.1136/bcr-2016-215350.
126. Maramattom, B. V; Zaldivar, R.A.; Glynn, S.M.; Eggers, S.D.; Wijdicks, E.F.M. Acute Intermittent Porphyria Presenting as a Diffuse Encephalopathy. *Ann. Neurol.* **2005**, *57*, 581–584, doi:10.1002/ana.20432.
127. Zhao, B.; Wei, Q.; Wang, Y.; Chen, Y.; Shang, H. Posterior Reversible Encephalopathy Syndrome in Acute Intermittent Porphyria. *Pediatr. Neurol.* **2014**, *51*, 457–460, doi:10.1016/J.PEDIATRNEUROL.2014.05.016.
128. Yang, J.; Yang, H.; Chen, Q.; Hua, B.; Zhu, T.; Zhao, Y.; Yu, X.; Zhu, H.; Zhou, Z. Reversible MRI Findings in a Case of Acute Intermittent Porphyria with a Novel Mutation in the Porphobilinogen Deaminase Gene. *Blood Cells, Mol. Dis.* **2017**, *63*, 21–24, doi:10.1016/J.BCMD.2016.12.005.
129. Zheng, X.; Liu, X.; Wang, Y.; Zhao, R.; Qu, L.; Pei, H.; Tuo, M.; Zhang, Y.; Song, Y.; Ji, X.; et al. Acute Intermittent Porphyria Presenting with Seizures and Posterior Reversible Encephalopathy Syndrome: Two Case Reports and a Literature Review. *Medicine (Baltimore).* **2018**, *97*, e11665–e11665, doi:10.1097/MD.0000000000011665.
130. Yang, Y.; Chen, X.; Wu, H.; Peng, H.; Sun, W.; He, B.; Yuan, Z. A Novel Heterozygous Mutation in the HMBS Gene in a Patient with Acute Intermittent Porphyria and Posterior Reversible Encephalopathy Syndrome. *Mol. Med. Rep.* **2020**, *22*, 516–524, doi:10.3892/mmr.2020.11117.
131. Ni, J.; Zhou, L.-X.; Hao, H.; Liu, Q.; Yao, M.; Li, M.; Peng, B.; Cui, L. The Clinical and Radiological Spectrum of Posterior Reversible Encephalopathy Syndrome: A Retrospective Series of 24 Patients. *J. Neuroimaging* **2011**, *21*, 219–224, doi:10.1111/j.1552-6569.2010.00497.x.
132. Shen, F.-C.; Hsieh, C.-H.; Huang, C.-R.; Lui, C.-C.; Tai, W.-C.; Chuang, Y.-C. Acute Intermittent Porphyria Presenting as Acute Pancreatitis and Posterior Reversible Encephalopathy Syndrome. *Acta Neurol. Taiwan.* **2008**, *17*, 177–183.
133. Olivier, P.; Van Melkebeke, D.; Honoré, P.J.; Defreyne, L.; Hemelsoet, D. Cerebral Vasospasm in Acute Porphyria. *Eur. J. Neurol.* **2017**, *24*, 1183–1187, doi:10.1111/ene.13347.

134. Verhaar, M.C.; Wever, R.M.; Kastelein, J.J.; van Dam, T.; Koomans, H.A.; Rabelink, T.J. 5-Methyltetrahydrofolate, the Active Form of Folic Acid, Restores Endothelial Function in Familial Hypercholesterolemia. *Circulation* **1998**, *97*, 237–241, doi:10.1161/01.CIR.97.3.237.

135. Jaureguiberry, M.S.; di Nunzio, A.S.; Dattilo, M.A.; Bianciotti, L.G.; Vatta, M.S. Endothelin 1 and 3 Enhance Neuronal Nitric Oxide Synthase Activity through ETB Receptors Involving Multiple Signaling Pathways in the Rat Anterior Hypothalamus. *Peptides* **2004**, *25*, 1133–1138, doi:10.1016/J.PEPTIDES.2004.04.005.

136. Mazzuca, M.Q.; Khalil, R.A. Vascular Endothelin Receptor Type B: Structure, Function and Dysregulation in Vascular Disease. *Biochem. Pharmacol.* **2012**, *84*, 147–162, doi:10.1016/J.BCP.2012.03.020.

137. Yasuda, M.; Desnick, R.J. Murine Models of the Human Porphyrias: Contributions toward Understanding Disease Pathogenesis and the Development of New Therapies. *Mol. Genet. Metab.* **2019**, *128*, 332–341, doi:10.1016/J.YMGME.2019.01.007.

138. Graff-Radford, N.R.; Knopman, D.S.; Penman, A.D.; Coker, L.H.; Mosley, T.H. Do Systolic BP and Pulse Pressure Relate to Ventricular Enlargement? *Eur. J. Neurol.* **2013**, *20*, 720–724, doi:10.1111/ene.12067.

139. Bothwell, S.W.; Janigro, D.; Patabendige, A. Cerebrospinal Fluid Dynamics and Intracranial Pressure Elevation in Neurological Diseases. *Fluids Barriers CNS* **2019**, *16*, 9, doi:10.1186/s12987-019-0129-6.

140. Zhang, L.; Luo, B.; Dang, Y.; He, R.; Chen, G.; Peng, Z.; Feng, Z. The Clinical Significance of Endothelin Receptor Type B in Hepatocellular Carcinoma and Its Potential Molecular Mechanism. *Exp. Mol. Pathol.* **2019**, *107*, 141–157, doi:https://doi.org/10.1016/j.yexmp.2019.02.002.

141. Pulgar, V.M.; Yasuda, M.; Gan, L.; Desnick, R.J.; Bonkovsky, H.L. Sex Differences in Vascular Reactivity in Mesenteric Arteries from a Mouse Model of Acute Intermittent Porphyria. *Mol. Genet. Metab.* **2019**, *128*, 376–381, doi:https://doi.org/10.1016/j.ymgme.2019.01.005.

142. Jericó, D.; Córdoba, K.M.; Jiang, L.; Schmitt, C.; Morán, M.; Sampedro, A.; Alegre, M.; Collantes, M.; Santamaría, E.; Alegre, E.; et al. MRNA-Based Therapy in a Rabbit Model of Variegate Porphyria Offers New Insights into the Pathogenesis of Acute Attacks. *Mol. Ther. Nucleic Acids* **2021**, *25*, 207–219, doi:10.1016/j.omtn.2021.05.010.

143. Klinger, W.; Müller, D. *The Influence of Allyl Isopropyl Acetamide on D-Aminolevulinic Acid Synthetase and Cytochrome P-450*; 1980; Vol. 39;.

144. Bonkowsky, H.L.; Healey, J.F.; Sinclair, P.R.; Mayer, Y.P.; Erny, R. Metabolism of Hepatic Haem and “green Pigments” in Rats given 2-Allyl-2-Isopropylacetamide and Ferric Citrate. A New Model for Hepatic Haem Turnover. *Biochem. J.* **1980**, *188*, 289–295, doi:10.1042/bj1880289.

145. De Matteis, F. Loss of Haem in Rat Liver Caused by the Porphyrogenic Agent 2-Allyl-2-Isopropylacetamide. *Biochem. J.* **1971**, *124*, 767–777, doi:10.1042/bj1240767.

146. De Matteis, F. Rapid Loss of Cytochrome P-450 and Haem Caused in the Liver Microsomes by the Porphyrogenic Agent 2-Allyl-2-Isopropylacetamide. *FEBS Lett.* **1970**, *6(4)*, 343–345.

147. McColl, K.E.; Thompson, G.G.; el Omar, E.; Moore, M.R.; Park, B.K.; Brodie, M.J. Effect of Rifampicin on Haem and Bilirubin Metabolism in Man. *Br. J. Clin. Pharmacol.* **1987**, *23*, 553–559, doi:10.1111/j.1365-2125.1987.tb03091.x.

148. Nakamura, T.; Okada, K.; Nagata, K.; Yamazoe, Y. Intestinal Cytochrome P450 and Response to Rifampicin in Rabbits. *Jpn. J. Pharmacol.* **2000**, *82*, 232–239, doi:10.1254/jjp.82.232.

149. Zuber, R.; Anzenbacherová, E.; Anzenbacher, P. Cytochromes P450 and Experimental Models of Drug Metabolism. *J. Cell. Mol. Med.* **2002**, *6*, 189–198, doi:10.1111/j.1582-4934.2002.tb00186.x.

150. Zanger, U.M.; Turpeinen, M.; Klein, K.; Schwab, M. Functional Pharmacogenetics/Genomics of Human Cytochromes P450 Involved in Drug Biotransformation. *Anal. Bioanal. Chem.* **2008**, *392*, 1093–1108, doi:10.1007/s00216-008-2291-6.

151. Medlock, A.E.; Meissner, P.N.; Davidson, B.P.; Corrigall, A. V; Dailey, H.A. A Mouse Model for South African (R59W) Variegate Porphyria: Construction and Initial Characterization. *Cell. Mol. Biol. (Noisy-le-grand).* **2002**, *48*, 71–78.

152. Lindberg, R.L.P.; Martini, R.; Baumgartner, M.; Erne, B.; Borg, J.; Zielasek, J.; Ricker, K.; Steck, A.; Toyka, K. V.; Meyer, U.A. Motor Neuropathy in Porphobilinogen Deaminase-Deficient Mice Imitates the Peripheral Neuropathy of Human Acute Porphyria. *J. Clin. Invest.* **1999**, *103*, 1127–1134, doi:10.1172/JCI5986.

153. Tschudy, D.P.; Valsamis, M.; Magnussen, C.R. Acute Intermittent Porphyria: Clinical and Selected Research Aspects. *Ann. Intern. Med.* **1975**, *83*, 851–864, doi:10.7326/0003-4819-83-6-851.

154. Sixel-Dietrich, F.; Verspohl, F.; Doss, M. Hyperinsulinemia in Acute Intermittent Porphyria. *Horm. Metab. Res. = Horm. und Stoffwechselforsch. = Horm. Metab.* **1985**, *17*, 375–376, doi:10.1055/s-2007-1013547.

155. Stein, J.A.; Tschudy, D.P. Acute Intermittent Porphyria. A Clinical and Biochemical Study of 46 Patients. *Medicine (Baltimore).* **1970**, *49*, 1–16.
156. Bethesda. LiverTox: Clinical and Research Information on Drug-Induced Liver Injury [Internet]. National Institute of Diabetes and Digestive and Kidney. Available online: https://www.ncbi.nlm.nih.gov/books/NBK547852/.
157. Acocella, G. Clinical Pharmacokinetics of Rifampicin. *Clin. Pharmacokinet.* **1978**, *3*, 108–127, doi:10.2165/00003088-197803020-00002.
158. Faut, M.; Paiz, A.; San Martín de Viale, L.C.; Mazzetti, M.B. Alterations of the Redox State, Pentose Pathway and Glutathione Metabolism in an Acute Porphyria Model. Their Impact on Heme Pathway. *Exp. Biol. Med. (Maywood).* **2013**, *238*, 133–143, doi:10.1177/1535370212473702.
159. Pimentel, V.C.; Pinheiro, F. V.; Kaefer, M.; Moresco, R.N.; Moretto, M.B. Assessment of Uric Acid and Lipid Peroxidation in Serum and Urine after Hypoxia-Ischemia Neonatal in Rats. *Neurol. Sci.* **2011**, *32*, 59–65, doi:10.1007/s10072-010-0393-3.
160. Ferreira, G.C.; Franco, R.; Lloyd, S.G.; Pereira, A.S.; Moura, I.; Moura, J.J.; Huynh, B.H. Mammalian Ferrochelatase, a New Addition to the Metalloenzyme Family. *J. Biol. Chem.* **1994**, *269*, 7062–7065.
161. Homedan, C.; Laafi, J.; Schmitt, C.; Gueguen, N.; Lefebvre, T.; Karim, Z.; Desquiret-Dumas, V.; Wetterwald, C.; Deybach, J.C.; Gouya, L.; et al. Acute Intermittent Porphyria Causes Hepatic Mitochondrial Energetic Failure in a Mouse Model. *Int. J. Biochem. Cell Biol.* **2014**, *51*, 93–101, doi:10.1016/j.biocel.2014.03.032.
162. Rötig, A.; Sidi, D.; Munnich, A.; Rustin, P. Molecular Insights into Friedreich's Ataxia and Antioxidant-Based Therapies. *Trends Mol. Med.* **2002**, *8*, 221—224, doi:10.1016/s1471-4914(02)02330-4.
163. Hermes-Lima, M.; Castilho, R.F.; Valle, V.G.R.; Bechara, E.J.H.; Vercesi, A.E. Calcium-Dependent Mitochondrial Oxidative Damage Promoted by 5-Aminolevulinic Acid. *Biochim. Biophys. Acta - Mol. Basis Dis.* **1992**, *1180*, 201–206, doi:https://doi.org/10.1016/0925-4439(92)90069-Y.
164. Rosano, G.L.; Morales, E.S.; Ceccarelli, E.A. New Tools for Recombinant Protein Production in Escherichia Coli: A 5-Year Update. *Protein Sci.* **2019**, *28*, 1412–1422, doi:10.1002/pro.3668.
165. Furukawa, K.; Ohsuye, K. Effect of Culture Temperature on a Recombinant CHO Cell Line Producing a C-Terminal α-Amidating Enzyme. *Cytotechnology* **1998**, *26*, 153–164, doi:10.1023/A:1007934216507.
166. Vergara, M.; Becerra, S.; Berrios, J.; Osses, N.; Reyes, J.; Rodríguez-Moyá, M.;

Gonzalez, R.; Altamirano, C. Differential Effect of Culture Temperature and Specific Growth Rate on CHO Cell Behavior in Chemostat Culture. *PLoS One* **2014**, *9*, e93865, doi:10.1371/journal.pone.0093865.

167. Patel, J.; Kothari, R.; Tunga, R.; Nadine M., R.; Binita S., T. *Overview of Protein and Peptide Degradation Pathways*. 2011, pp. 20–31.

APPENDIX

Video 1. Motor troubles in VP rabbits.

Download : **Download video (17MB)**

Video 2. hPBGD mRNA protection against motor troubles in VP rabbits.

Download : **Download video (19MB)**